Fall 12-18-2020

Atom Transfer Radical Processes: From Catalyst Design to Polymer Synthesis, Characterization, and Application

Michael Novak

ATOM TRANSFER RADICAL PROCESSES: FROM CATALYST DESIGN TO POLYMER SYNTHESIS, CHARACTERIZATION, AND APPLICATION

A Dissertation

Submitted to the Bayer School of Natural and Environmental Sciences

Duquesne University

In partial fulfillment of the requirements for

the degree of Doctor of Philosophy

By

Michael A. Novak

December 2020

ATOM TRANSFER RADICAL PROCESSES: FROM CATALYST DESIGN TO POLYMER SYNTHESIS, CHARACTERIZATION, AND APPLICATION

By

Michael A. Novak

Approved November 12, 2020

_____ Dr. Stephanie J. Wetzel Assistant Professor of Chemistry and Biochemistry (Committee Chair)	_____ Dr. Ellen Gawalt Professor of Chemistry and Biochemistry (Committee Member)
_____ Dr. Jennifer Aitken Professor of Chemistry and Biochemistry (Committee Member)	_____ Dr. John F. Stolz Professor of Environmental Microbiology (External Reviewer)
_____ Dr. Philip Reeder Dean, Bayer School of Natural and Environmental Sciences	_____ Dr. Ellen Gawalt Chair, Department of Chemistry and Biochemistry Professor of Chemistry and Biochemistry

ABSTRACT

ATOM TRANSFER RADICAL PROCESSES: FROM CATALYST DESIGN TO POLYMER SYNTHESIS, CHARACTERIZATION, AND APPLICATION

By

Michael A. Novak

December 2020

Dissertation supervised by Dr. Stephanie J. Wetzel

Due to the toxicity of heavy metals and their prevalence in the environment there exists a need to develop highly active transition metal catalysts ultimately reducing the amount needed for chemical transformations. Additionally, there is interest in the scientific community for creating new materials that can remove these pollutants from industrial wastewater prior to its release into the environment. The work presented here focuses on the reduction and removal of heavy metals from industrial hazardous waste by designing novel highly active catalysts and developing polymeric adsorbents.

Highly active catalyst complexes consisting of novel hybrid ligands, 2-(dimethylamino)ethyl-bis-[2-(pyridylmethyl)amine] (M1-T2), and bis[2-(dimethylamino)ethyl]-2-(pyridylmethyl)amine (M2-T1), were developed for atom transfer radical processes, i.e. atom transfer radical addition and atom transfer radical

polymerization. The catalyst complexes were structurally similar to those containing tris(2-pyridylmethyl)amine (TPMA) or tris[2-(dimethylamino)ethyl]amine (Me_6TREN) ligands. The Cu^{2+} complexes possessed distorted trigonal bipyramidal structures in solution and in the solid state. Electrochemical and kinetic evaluation indicated that the catalyst complexes containing the novel hybrid ligands should be more active in atom transfer radical processes than those containing the TPMA ligand. The novel highly active catalysts developed in this work were more efficient for atom transfer radical addition of monohalogenated alkyl halides to alkenes doubling percent yield of monoadduct in comparison to the TPMA analogue.

Homopolymers, poly(2-hydroxyethyl methacrylate) (PHEMA) and 2-(dimethylamino)ethyl methacrylate (PDMAEMA), and random copolymer, poly(HEMA-*ran*-DMAEMA) were synthesized via atom transfer radical polymerization. Ultimately, fragmentation pattern analysis using multi-stage mass spectrometry was performed to elucidate monomer sequence of the random copolymers. It was determined that the loss of ethylene glycol provides insight regarding the monomer sequence since it can only arise from adjacent HEMA monomers in the polymer backbone.

Two polymeric adsorbents, PHEMA and poly(acrylamide-*co*-acrylic acid), were implemented for the removal of Pb^{2+} from aqueous systems. Inductively coupled plasma mass spectrometry was utilized to quantify Pb^{2+} concentrations pre and post adsorption. Preliminary results indicate that both adsorbents PHEMA and poly(AAm-*co*-AAc), removed 99% and 21% of Pb^{2+}, respectively. This data suggests their potential to be utilized for water remediation applications.

DEDICATION

I dedicate this dissertation to my fiancé and my family for their unconditional love and support. Without them, completing this dissertation would not have been possible.

I love you.

ACKNOWLEDGEMENT

I would first like to acknowledge my advisor, Dr. Stephanie J. Wetzel. I am grateful for her letting me join her group and am appreciative of the advice, insight and support she has provided over the years. I would also like to thank my dissertation committee members: Dr. Jennifer Aitken and Dr. Ellen Gawalt. Their support and constructive feedback are greatly appreciated. I would also like to thank my outside reviewer, Dr. John F. Stolz for his feedback and willingness to take on this role.

I thank my research teammates: Sean Fischer, Gabby Pros, AJ Rupprecht, and Aman Kaur. I appreciate the advice and encouragement they provided. Additionally, I would like to thank graduate students Nick Ferraro and James Henderson for their input regarding mass spectrometer operation. I would also like to thank Liam Dugan and Dr. Mark E. Bier from Carnegie Mellon University for their assistance in collecting mass spectrometry data. I thank Dan Bodnar, Lance Crosby, and Chris Lawson from the instrument shop for their support with instrumentation and equipment. I also thank Scott Boesch for his assistance with computers and software.

Lastly, I would like to thank Duquesne University, the Bayer School of Natural and Environmental Sciences, and the Department of Chemistry and Biochemistry for providing me with the opportunity to study, perform research, and achieve my goals.

TABLE OF CONTENTS

Page

LIST OF FIGURES

Page

LIST OF TABLES

Page

LIST OF SCHEMES

Page

LIST OF ABBREVIATIONS

AAc	Acrylic Acid
AAm	Acrylamide
AC	Activated Carbon
Acetone-d_6	Deuterated Acetone
ACN	Acetonitrile
AIBN	2,2'-Azobis(2-methylpropionitrile)
Al_2O_3	Alumina
AN	Acrylonitrile
APCI	Atmospheric Pressure Chemical Ionization
ARGET	Activators Regenerated By Electron Transfer
ATRA	Atom Transfer Radical Addition
ATRP	Atom Transfer Radical Polymerization
Bpy	2,2'-Bipyridine
BzSCN	Benzyl Thiocyanate
CBr_4	Carbon Tetrabromide
CCl_4	Carbon Tetrachloride
$CDCl_3$	Deuterated Chloroform
CE	Collision Energy
CID	Collision-Induced Dissociation
ClAN	Chloroacetonitrile
ClPN	Chloropropionitrile

CO	Carbon Monoxide
CRP	Controlled Radical Polymerization
$CuBr_2$	Cu(II)bromide
$CuCl_2$	Cu(II)chloride
1,4-DMB	1,4-Dimethoxybenzene
Da	Dalton
DCM	Dichloromethane
DMAEMA	2-(Dimethylamino)ethyl Methacrylate
DMSO	Dimethyl Sulfoxide
DMSO-d_6	Deuterated Dimethyl Sulfoxide
DP	Degree of Polymerization
EBiB	Ethyl-2-bromoisobutyrate
EPA	Environmental Protection Agency
ESI	Electrospray Ionization
Et_3N	Triethylamine
eV	Electron Volt
H_2O	Water
HBr	Hydrobromic Acid
HCl	Hydrochloric Acid
HEMA	2-Hydroxyethyl Methacrylate
HNO_3	Nitric Acid
HPLC	High-Performance Liquid Chromatography
HRMS	High-Resolution Mass Spectrometry

HSAB	Pearson's Hard Soft Acid Base Theory
ICAR	Initiators for Continuous Activation
ICP-MS	Inductively Coupled Plasma Mass Spectrometry
K	Kelvin
KH	Potassium Hydride
LC/MS	Liquid Chromatography Mass Spectrometry
LCST	Lower Critical Solution Temperature
MALDI	Matrix-Assisted Laser Desorption Ionization
M1-T2	2-(dimethylamino)ethyl-bis-[2-(pyridylmethyl)amine]
M2-T1	Bis[2-(dimethylamino)ethyl]-2-(pyridylmethyl)amine
MA	Methyl Acrylate
MCL	Maximum Contaminant Level
Me_6TREN	Tris[2-(dimethylamino)ethyl]amine
MeOH	Methanol
$MgSO_4$	Magnesium Sulfate
MHz	Megahertz
mM	Millimolar
MMA	Methyl Methacrylate
mmol	Millimole
M_n	Number Average Molecular Weight
MΩ	Megaohm
MS/MS	Tandem Mass Spectrometry
MS^n	Multi-Stage Mass Spectrometry

m/z	Mass-to-Charge Ratio
NaBr	Sodium Bromide
$NaHCO_3$	Sodium Bicarbonate
NMP	Nitroxide Mediated Polymerization
NMR	Nuclear Magnetic Resonance
PDI	Polydispersity Index
PMDETA	N,N,N',N",N"-Pentamethyldiethylenetriamine
photoATRP	Photo-Induced Atom Transfer Radical Polymerization
ppb	Parts Per Billion
ppm	Parts Per Million
PTFE	Poly(tetrafluoroethylene)
QTOF	Quadrupole Time-of-Flight
RAFT	Reversible Addition-Fragmentation Chain Transfer
SARA	Supplemental Activators and Reducing Agents
STAB	Sodium Triacetoxyborohydride
TBA-PF_6	Tetrabutylammonium Hexafluorophosphate
TEMPO	2,2,6,6-Tetramethylpiperidine-1-oxyl
TMC	Transition Metal Catalyzed
TPMA	Tris(2-pyridylmethyl)amine
UV/Vis	Ultraviolet/Visible
V-70	2,2'-azobis(2,4-dimethyl-4-methoxyvaleronitrile)
WHO	World Health Organization
XRD	X-Ray Diffraction

Chapter 1

Background

1.1 Introduction: Heavy Metal Pollution and Toxicity

The rapid development of industries such as battery, iron and steel, textile, semi-conductor, and metal plating has led to the wide distribution of heavy metals and is of major environmental concern.[1-3] The World Health Organization (WHO) lists cadmium, mercury, and lead as three of their top ten pollutants of major public health concern due to their increased prevalence and toxicity to living organisms.[4] The term "heavy metal" is ambiguous but generally is applied to the block of elements on the periodic table with Ti, Hf, As, and Bi at its corners as shown in Figure 1.1.[5] They have also been characterized for elements having a specific gravity greater than 5 or atomic weights between 60 and 208.[5-7]

Be											B	C	N	O
Mg											Al	Si	P	S
Ca	Sc	**Ti**	**V**	**Cr**	**Mn**	**Fe**	**Co**	**Ni**	**Cu**	**Zn**	**Ga**	**Ge**	**As**	Se
Sr	Y	**Zr**	**Nb**	**Mo**	**Tc**	**Ru**	**Rh**	**Pd**	**Ag**	**Cd**	**In**	**Sn**	**Sb**	Te
Ba	*	**Hf**	**Ta**	**W**	**Re**	**Os**	**Ir**	**Pt**	**Au**	**Hg**	**Tl**	**Pb**	**Bi**	Po

Figure 1.1 Block of the periodic table used to identify heavy metals (bold symbols).

With the increasing demand for consumer products from the aforementioned industries, the battery sector has experienced steady growth and is a 100 billion dollar industry as of 2020.[8] Additionally, it has been reported that printed circuit board

fabrication wastewater contains 1,200 ppm of Cu^{2+}.[9] Therefore, a need exists for the development of effective adsorbents that can remove heavy metal ions from industrial wastewaters and of highly active catalysts ultimately reducing the amount of hazardous waste produced containing heavy metals.

A primary reason that heavy metal pollution is of concern is that they are highly soluble in aqueous environments, which allows them to easily migrate through the environment as shown in Figure 1.2.[2, 10] Once they reach the environment their removal becomes very difficult i.e., more complex and expensive. Additionally, heavy metals persist in the environment because they are not biodegradable and tend to bioaccumulate in living organisms. In other words, their concentrations increase moving up the food chain (Figure 1.2). Hence, there is a need to remove them from effluent waste prior to its release into the environment.

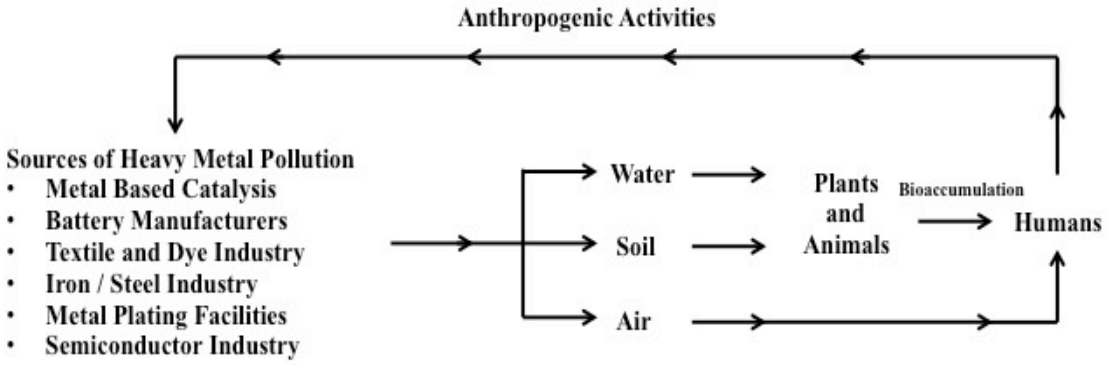

Figure 1.2 Flow chart showing migration of heavy metals through the environment.

Even though some heavy metals e.g., Zn^{2+}, Cr^{3+} are needed by living organisms and are known dietary minerals, they can be toxic at elevated concentrations. Increased levels of heavy metals can produce symptoms ranging from headache and nausea to

organ, nervous, circulatory, and fetal development complications (Table 1.1).[1, 7, 10-12] Due to their toxicity, the Environmental Protection Agency (EPA) has established regulations for their levels in drinking water systems and are known as Maximum Contaminant Levels (MCL).[13] The simplest and most direct route to preventing heavy metals from being introduced into the environment is removing them from effluent hazardous wastewater prior to its release from the industrial site or decreasing the amount present in hazardous waste.[14]

Table 1.1 Hazardous heavy metals, their toxicities,[1, 10] and maximum contaminant level (MCL) standards established by the Environmental Protection Agency.[13, 15]

Heavy Metal	Toxicity	MCL (mg/L)
Cd^{2+}	Kidney damage, carcinogen, gastrointestinal irritant	0.005
Hg^{2+}	Liver, kidney, fetal complications	0.02
Pb^{2+}	Circulatory, nervous system, fetal complications, kidney disease	0.015
Cu^{2+}	Liver damage, Wilson's disease, insomnia	1.3
$Cr^{3+\,(6+)}$	Carcinogenic, headache, nausea	0.1 (0.05)

1.2 Current Approaches for the Reduction and Removal of Heavy Metals in Industrial Wastewater

1.2.1 Development of Highly Active Catalysts

Atom transfer radical processes such as atom transfer radical polymerization (ATRP) and atom transfer radical addition (ATRA) represent fundamental reactions for carbon-carbon bond formation starting from alkyl halides (initiators) and alkenes (monomers).[16-17] Therefore, these processes are very important for the synthesis of polymers, organic molecules, natural products, and pharmaceuticals.[18-20] ATRP and

ATRA typically employ heavy metal based catalysts e.g., Cu, Fe, Ru, Ni, and Pd since they are more effective halogen transfer agents than alkyl halides.[21-24] Traditionally large catalyst loadings were needed (5-30 mol % relative to alkene) to compensate for the accumulation of the deactivator, which is the transition metal complex in it's higher oxidation state.[25] These large catalyst loadings made the process environmentally unfriendly and expensive.[26] Over the past twenty years much effort has been put in to the development of highly active catalysts for these types of reactions and has significantly reduced the amount of transition metal-based catalysts needed. In some cases the amount of catalyst can be reduced to ppm levels (< 0.1 mol % relative to alkene).[27] A primary reason for this sharp decrease in the amount of catalyst required for these processes lies in the fact that the efficiency of the metal-based complex can be modulated by variations in the complexing ligand.[28] Continuing to investigate the development of highly active ligands can pave the way for an even greater reduction in the amount of heavy metal based catalysts needed for atom transfer radical processes ultimately reducing the amount of heavy metal containing hazardous waste produced.

1.2.2 Removal of Heavy Metals From Industrial Wastewater

Over the years, different methods have been utilized for the removal of heavy metals from effluent wastewater prior to its release into the environment. These techniques for their removal from aqueous systems include chemical precipitation, membrane filtration, electrochemical methods, and adsorption.[6, 15, 29-32] Each technique has it's own advantages and disadvantages as shown in Table 1.2.

Chemical precipitation is a conventional and commonly employed method for removing heavy metal ions from industrial wastewater and is considered the workhorse for this process.[2, 7, 32-33] Following precipitation the heavy metal precipitates are removed via sedimentation.[33] Hydroxides are commonly used for this process since they react with most heavy metals forming insoluble species. Chemical precipitation is very effective and has been reported to remove >95% of a given heavy metal from hazardous wastewater.[34-35]

Table 1.2 Advantages and disadvantages of various methods for the removal of heavy metals from industrial wastewater.

Method	Advantages	Disadvantages
Chemical Precipitation	Simple, high removal efficiency	Produces toxic sludge, inefficient for water comprised of different metals, not effective at low metal concentrations
Membrane Filtration	High removal efficiency, efficient at low metal concentrations	Membrane fouling, low permeate flux, high maintenance and operation costs
Electrochemical	Well controlled process, recovery of pure metals	High maintenance and operation costs, costly power supplies
Adsorption	Simple, high removal efficiency, efficient at low metal concentrations, potential for metal recovery	Desorption of metals, occasionally require different adsorbents

Although precipitation is a commonly employed method, it is not without limitations. Wastewater containing a mixture of heavy metals presents a problem since the optimal precipitation pH is specific to each metal. Therefore, metals can be released back into the wastewater as the pH is adjusted.[2, 32-33] Additionally, chemical precipitation creates excessive amounts of toxic sludge, which causes disposal problems and requires further treatment.[33, 36] Furthermore, chemical precipitation makes the recovery of the precipitated metals arduous due to the heterogeneous nature of the residual sludge.[2, 33]

Membrane filtration techniques have received considerable attention and are effective for the removal of heavy metal ions from aqueous systems.[29] Membranes are permeable to water and typically have complex structures such as cross-linked polymers or hollow fiber networks.[37-39] Various types of filtration membranes exist, i.e., nanomembranes, ultrafiltration membranes, and reverse osmosis membranes.[15, 32, 40] The primary advantage of membrane filtration is high separation efficiency.[30] As with other techniques, this process is not without limitations. An intrinsic aspect of membrane filtration is that it is a pressure-driven process and therefore typically requires large amounts of energy hence making it expensive.[30] Additionally, low permeate flux and membrane fouling leads to reduction in removal efficiency and requires high maintenance and operation costs which have limited its use in heavy metal removal.[41]

Electrochemical methods provide a route for the removal of heavy metals from industrial wastewater. Electrodeposition and electrocoagulation systems are comprised of electrodes i.e., anode and cathode in an electrochemical cell.[2, 29, 42] These processes are well controlled and require low amounts of chemicals.[2, 42] A major advantage is that they allow for the recovery of a given metal in it's elemental state.[41] Electrochemical water remediation methods are limited due to their high initial investment, costly power supplies, and high level of maintenance.[41]

Adsorption is one of the simples and most effective methods for removing heavy metal ions from industrial wastewater. It is a mass transfer process in which a substance is transferred from the liquid phase to the surface of the adsorbent via chemical or physical interactions.[7, 10] Types of adsorbents include activated carbon (AC),[7, 10, 32 43] biomass,[3, 44] and polymeric materials,[45-51] all of which have been shown to remove heavy

metals from aqueous systems. Of the various types of adsorbents, polymeric adsorbents possess fundamental advantages such as adjustable surface chemistry and architecture, which can be finely tuned to increase adsorption capacity and enhance selectivity. The concept of selectivity is of interest since industrial wastewaters typically contain a mixture of heavy metals, therefore it would be advantageous to have adsorbents that can selectively remove these toxins prior to their release into the environment. Additionally, polymeric adsorbents allow for feasible regeneration and can be used for multiple adsorption-desorption cycles, unlike other adsorbents.[10, 45, 52] Furthermore, adsorption processes do not create secondary contamination issues such as the production of toxic sludge.

Traditionally, AC has been the most extensively utilized adsorbent for the removal of heavy metals from hazardous wastewater.[43, 53] Compared to AC, synthetic polymers have been shown to possess higher adsorption capacities and therefore have been gaining attention as adsorbents for heavy metals.[45, 49-50, 54-56] Reported adsorption capacities of AC and synthetic polymers for Pb^{2+} were 109 and 253 milligram of metal per gram of adsorbent, respectively.[53, 56] Ceglowski and coworkers used inorganic-organic hybrid polymers containing pyridine-pyrazole moieties as heavy metal chelators and reported an adsorption capacity of 207 mg/g for Cu^{2+}.[52] Whereas activated carbon has shown a capacity of only 29 mg/g for Cu^{2+}.[57] Adsorption capacities for AC and polymeric adsorbents for Cd^{2+} have reported values of 146 and 225 mg/g, respectively.[58-59] Furthermore, synthetic polymers are more effective for Hg^{2+} and Cr^{6+} removal as shown in Table 1.3.[59-62] It is evident that synthetic polymeric adsorbents possess higher adsorption capacities towards numerous heavy metal ions. Lastly, AC is difficult to

regenerate for successive adsorption-desorption cycles.[43, 53, 63] In contrast, it has been shown that polymeric adsorbents can be reused for subsequent cycles, therefore they can be re-implemented for multiple adsorption processes.[64-68] The advent of controlled radical processes, namely ATRP, allows for production of finely tuned polymer architectures and compositions and allows for the production of more effective polymer adsorbents.

Table 1.3 Adsorption capacities of activated carbon and synthetic polymers for various heavy metals.

Adsorbent	**Adsorption Capacity (mg/g)**	**Heavy Metal**
Activated Carbon	109	Pb^{2+}
	29	Cu^{2+}
	53	Cr^{6+}
	146	Cd^{2+}
	65	Hg^{2+}
Synthetic Polymers	253	Pb^{2+}
	207	Cu^{2+}
	138	Cr^{6+}
	225	Cd^{2+}
	160	Hg^{2+}

1.3 Summary

Heavy metal ions are highly toxic on aquatic and terrestrial life, including humans. Three heavy metals i.e., Cd, Hg, and Pb are present on the World Health Organization's top ten list for pollutants of major health concern.[4] Therefore, it is of utmost importance to develop protocols that can reduce the amount of heavy metal hazardous waste produced and to efficiently remove them from industrial wastewater prior to their release into the environment. The aim of this work addresses both of these

aforementioned routes in reducing heavy metal pollution. The focus of Chapter 2 is the development of novel highly active ligands and catalysts for ATRA processes. The novel complexes were structurally characterized and their activities investigated with the goal of reducing the amount of heavy metal catalyst needed ATRA methods. Chapter 3 discusses the ATRP synthesis of hydrophilic polymers, which were fully characterized using high-resolution mass spectrometry and nuclear magnetic resonance (NMR) spectroscopy as primary analytical tools. Chapter 4 is focused on the implementation of tandem mass spectrometry for fragmentation pattern studies of hydrophilic polymers. Lastly, Chapter 5 summarizes the entire body of work, notes key contributions to the scientific community, and discusses future directions.

1.4 References

1. Tchounwou, P. B.; Yedjou, C. G.; Patlolla, A. K.; Sutton, D. J. Heavy Metal Toxicity and the Environment. In *Molecular, Clinical and Environmental Toxicology: Volume 3: Environmental Toxicology*, Luch, A., Ed.; Springer Basel: Basel, 2012, pp 133-164.

2. Fu, F.; Wang, Q. Removal of heavy metal ions from wastewaters: A review. *Journal of Environmental Management* **2011,** *92* (3), 407-418.

3. Bailey, S. E.; Olin, T. J.; Bricka, R. M.; Adrian, D. D. A review of potentially low-cost sorbents for heavy metals. *Water Research* **1999,** *33* (11), 2469-2479.

4. World Health Organization. http://www.who.int/ipcs/assessment/public_health/chemicals_phc/en/ (accessed 01/14/2017).

5. Duffus, J. Heavy Metals-A Meaningless Term? *Pure and Applied Chemsitry* **2002,** *74* (5), 793-807.

6. Srivastava, N. K.; Majumder, C. B. Novel biofiltration methods for the treatment of heavy metals from industrial wastewater. *Journal of Hazardous Materials* **2008,** *151* (1), 1-8.

7. Barakat, M. A. New trends in removing heavy metals from industrial wastewater. *Arabian Journal of Chemistry* **2011,** *4* (4), 361-377.

8. Battery Market http://www.researchandmarkets.com/reports/2762000/the_global_battery_industry_2013 2018_trends (accessed 01/08/2017).

9. Ahmad, A. L.; Ooi, B. S. A study on acid reclamation and copper recovery using low pressure nanofiltration membrane. *Chemical Engineering Journal* **2010,** *156* (2), 257-263.

10. Tripathi A, R. M. Heavy Metal Removal from Wastewater Using Low Cost Adsorbents. *Journal of Bioremediation and Biodegredation* **2015,** *6* (6).

11. Payne, J. C.; ter Horst, M. A.; Godwin, H. A. Lead Fingers: Pb2+ Binding to Structural Zinc-Binding Domains Determined Directly by Monitoring Lead−Thiolate Charge-Transfer Bands. *Journal of the American Chemical Society* **1999,** *121* (29), 6850-6855.

12. Lewis, J. A.; Cohen, S. M. Addressing Lead Toxicity: Complexation of Lead(II) with Thiopyrone and Hydroxypyridinethione O,S Mixed Chelators. *Inorganic Chemistry* **2004,** *43* (21), 6534-6536.

13. Environmental Protection Agency. http://www.epa.gov (accessed 10/10/2016).

14. Moore, J. W. R., S. *Heavy Metals in Natural Waters*; Springer-Verlag New York Inc.: New York, New York, 1984.

15. Kurniawan, T. A.; Chan, G. Y. S.; Lo, W.-H.; Babel, S. Physico–chemical treatment techniques for wastewater laden with heavy metals. *Chemical Engineering Journal* **2006,** *118* (1–2), 83-98.

16. Curran, D. P. The Design and Application of Free Radical Chain Reactions in Organic Synthesis. Part 1. *Synthesis* **1988,** *1988* (06), 417-439.

17. Kharasch, M. S.; Engelmann, H.; Mayo, F. R. The Peroxide Effect In The Addition of Reagents to Unsaturated Compounds. XV. The Addition of Hydrogen Bromide to 1- and 2-Bromo- And Chloropropenes. *The Journal of Organic Chemistry* **1937,** *02* (3), 288-302.

18. Kharasch, M. S.; Jensen, E. V.; Urry, W. H. Addition of Derivatives of Chlorinated Acetic Acids to Olefins. *Science* **1945,** *102* (2640), 128.

19. Matyjaszewski, K.; Xia, J. Atom Transfer Radical Polymerization. *Chemical Reviews* **2001,** *101* (9), 2921-2990.

20. Matyjaszewski, K. Atom Transfer Radical Polymerization (ATRP): Current Status and Future Perspectives. *Macromolecules* **2012,** *45* (10), 4015-4039.

21. Minisci, F. Free-radical additions to olefins in the presence of redox systems. *Accounts of Chemical Research* **1975,** *8* (5), 165-171.

22. Gossage, R. A.; van de Kuil, L. A.; van Koten, G. Diaminoarylnickel(II) "Pincer" Complexes: Mechanistic Considerations in the Kharasch Addition Reaction, Controlled Polymerization, and Dendrimeric Transition Metal Catalysts. *Accounts of Chemical Research* **1998,** *31* (7), 423-431.

23. Wolf, J.; Thommes, K.; Briel, O.; Scopelliti, R.; Severin, K. Dinuclear Ruthenium Ethylene Complexes: Syntheses, Structures, and Catalytic Applications in ATRA and ATRC Reactions. *Organometallics* **2008,** *27* (17), 4464-4474.

24. Kay, S. Ruthenium Catalysts for the Kharasch Reaction. *Current Organic Chemistry* **2006,** *10* (2), 217-224.

25. Clark, A. J. Atom transfer radical cyclisation reactions mediated by copper complexes. *Chemical Society Reviews* **2002,** *31* (1), 1-11.

26. Tsarevsky, N. V.; Matyjaszewski, K. "Green" Atom Transfer Radical Polymerization: From Process Design to Preparation of Well-Defined Environmentally Friendly Polymeric Materials. *Chemical Reviews* **2007,** *107* (6), 2270-2299.

27. Matyjaszewski, K. Controlled Radical Polymerization: State of the Art in 2008. In *Controlled/Living Radical Polymerization: Progress in ATRP*; American Chemical Society, 2009; Vol. 1023, pp 3-13.

28. Tang, W.; Kwak, Y.; Braunecker, W.; Tsarevsky, N. V.; Coote, M. L.; Matyjaszewski, K. Understanding Atom Transfer Radical Polymerization: Effect of Ligand and Initiator Structures on the Equilibrium Constants. *Journal of the American Chemical Society* **2008,** *130* (32), 10702-10713.

29. Vardhan, K. H.; Kumar, P. S.; Panda, R. C. A review on heavy metal pollution, toxicity and remedial measures: Current trends and future perspectives. *Journal of Molecular Liquids* **2019,** *290*, 111197.

30. Carolin, C. F.; Kumar, P. S.; Saravanan, A.; Joshiba, G. J.; Naushad, M. Efficient techniques for the removal of toxic heavy metals from aquatic environment: A review. *Journal of Environmental Chemical Engineering* **2017,** *5* (3), 2782-2799.

31. Wan Ngah, W. S.; Hanafiah, M. A. K. M. Removal of heavy metal ions from wastewater by chemically modified plant wastes as adsorbents: A review. *Bioresource Technology* **2008,** *99* (10), 3935-3948.

32. Zhao, M.; Xu, Y.; Zhang, C.; Rong, H.; Zeng, G. New trends in removing heavy metals from wastewater. *Applied Microbiology and Biotechnology* **2016**, 1-10.

33. Wang, L. K.; Vaccari, D. A.; Li, Y.; Shammas, N. K. Chemical Precipitation. In *Physicochemical Treatment Processes*, Wang, L. K.; Hung, Y.-T.; Shammas, N. K., Eds.; Humana Press: Totowa, NJ, 2005, pp 141-197.

34. Mirbagheri, S. A.; Hosseini, S. N. Pilot plant investigation on petrochemical wastewater treatmentfor the removal of copper and chromium with the objective of reuse. *Desalination* **2005,** *171* (1), 85-93.

35. Chen, Q.; Luo, Z.; Hills, C.; Xue, G.; Tyrer, M. Precipitation of heavy metals from wastewater using simulated flue gas: Sequent additions of fly ash, lime and carbon dioxide. *Water Research* **2009,** *43* (10), 2605-2614.

36. Kongsricharoern, N.; Polprasert, C. Electrochemical precipitation of chromium (Cr6+) from an electroplating wastewater. *Water Science and Technology* **1995,** *31* (9), 109-117.

37. Thong, Z.; Han, G.; Cui, Y.; Gao, J.; Chung, T.-S.; Chan, S. Y.; Wei, S. Novel Nanofiltration Membranes Consisting of a Sulfonated Pentablock Copolymer Rejection Layer for Heavy Metal Removal. *Environmental Science & Technology* **2014,** *48* (23), 13880-13887.

38. Zhu, W.-P.; Sun, S.-P.; Gao, J.; Fu, F.-J.; Chung, T.-S. Dual-layer polybenzimidazole/polyethersulfone (PBI/PES) nanofiltration (NF) hollow fiber membranes for heavy metals removal from wastewater. *Journal of Membrane Science* **2014,** *456*, 117-127.

39. Gao, J.; Sun, S.-P.; Zhu, W.-P.; Chung, T.-S. Polyethyleneimine (PEI) cross-linked P84 nanofiltration (NF) hollow fiber membranes for Pb2+ removal. *Journal of Membrane Science* **2014,** *452*, 300-310.

40. Khedr, M. G. Membrane methods in tailoring simpler, more efficient, and cost effective wastewater treatment alternatives. *Desalination* **2008,** *222* (1), 135-145.

41. Crini, G.; Lichtfouse, E. Advantages and disadvantages of techniques used for wastewater treatment. *Environmental Chemistry Letters* **2019,** *17* (1), 145-155.

42. Bazrafshan, E.; Mohammadi, L.; Ansari-Moghaddam, A.; Mahvi, A. H. Heavy metals removal from aqueous environments by electrocoagulation process– a systematic review. *Journal of Environmental Health Science and Engineering* **2015,** *13*, 74.

43. Babel, S.; Kurniawan, T. A. Low-cost adsorbents for heavy metals uptake from contaminated water: a review. *Journal of Hazardous Materials* **2003,** *97* (1–3), 219-243.

44. Ince, M.; Kaplan İnce, O.; Asam, E.; Onal, A. Using Food Waste Biomass as Effective Adsorbents in Water and Wastewater Treatment for Cu(II) Removal. *Atomic Spectroscopy -Norwalk Connecticut-* **2017,** *38*.

45. Pan, B.; Pan, B.; Zhang, W.; Lv, L.; Zhang, Q.; Zheng, S. Development of polymeric and polymer-based hybrid adsorbents for pollutants removal from waters. *Chemical Engineering Journal* **2009,** *151* (1–3), 19-29.

46. Laus, R.; Costa, T. G.; Szpoganicz, B.; Fávere, V. T. Adsorption and desorption of Cu(II), Cd(II) and Pb(II) ions using chitosan crosslinked with epichlorohydrin-triphosphate as the adsorbent. *Journal of Hazardous Materials* **2010,** *183* (1–3), 233-241.

47. Rivas, B. L.; Pereira, E. D.; Moreno-Villoslada, I. Water-soluble polymer–metal ion interactions. *Progress in Polymer Science* **2003,** *28* (2), 173-208.

48. Kumar, A.; Srivastava, A.; Galaev, I. Y.; Mattiasson, B. Smart polymers: Physical forms and bioengineering applications. *Progress in Polymer Science* **2007,** *32* (10), 1205-1237.

49. Rivas, B. L.; Maureira, A. Poly(2-acrylamido glycolic acid): A water-soluble polymer with ability to interact with metal ions in homogenous phase. *Inorganic Chemistry Communications* **2007,** *10* (2), 151-154.

50. Niu, Y.; Qu, R.; Sun, C.; Wang, C.; Chen, H.; Ji, C.; Zhang, Y.; Shao, X.; Bu, F. Adsorption of Pb(II) from aqueous solution by silica-gel supported hyperbranched polyamidoamine dendrimers. *Journal of Hazardous Materials* **2013,** *244–245*, 276-286.

51. Rahman, M. L.; Sarkar, S. M.; Yusoff, M. M. Efficient removal of heavy metals from electroplating wastewater using polymer ligands. *Frontiers of Environmental Science & Engineering* **2016,** *10* (2), 352-361.

52. Cegłowski, M.; Schroeder, G. Removal of heavy metal ions with the use of chelating polymers obtained by grafting pyridine–pyrazole ligands onto polymethylhydrosiloxane. *Chemical Engineering Journal* **2015,** *259*, 885-893.

53. Al-Malack, M. H.; Basaleh, A. A. Adsorption of heavy metals using activated carbon produced from municipal organic solid waste. *Desalination and Water Treatment* **2016,** *57* (51), 24519-24531.

54. Rivas, B. L.; Maureira, A. Poly(2-acrylamido glycolic acid-co-acryloyl morpholine) and poly(2-acrylamido glycolic acid-co-acrylamide): Synthesis, characterization, and retention properties for environmentally impacting metal ions. *European Polymer Journal* **2008,** *44* (2), 523-533.

55. Sauer, N. N.; Ehler, D. S.; Duran, B. L. Lead Extraction from Contaminated Soil Using Water-Soluble Polymers. *Journal of Environmental Engineering* **2004,** *130* (5), 585-588.

56. Gierczyk, B.; Schroeder, G.; Cegłowski, M. New polymeric metal ion scavengers with polyamine podand moieties. *Reactive and Functional Polymers* **2011,** *71* (4), 463-479.

57. Kongsuwan, A.; Patnukao, P.; Pavasant, P. Binary component sorption of Cu(II) and Pb(II) with activated carbon from Eucalyptus camaldulensis Dehn bark. *Journal of Industrial and Engineering Chemistry* **2009,** *15* (4), 465-470.

58. Rangel-Mendez, J. R.; Streat, M. Adsorption of cadmium by activated carbon cloth: influence of surface oxidation and solution pH. *Water Research* **2002,** *36* (5), 1244-1252.

59. Babić, B. M.; Milonjić, S. K.; Polovina, M. J.; Čupić, S.; Kaludjerović, B. V. Adsorption of zinc, cadmium and mercury ions from aqueous solutions on an activated carbon cloth. *Carbon* **2002,** *40* (7), 1109-1115.

60. Rivas, B. L.; Pooley, S. A.; Maturana, H. A.; Villegas, S. Sorption properties of poly(styrene-co-divinylbenzene) amine functionalized weak resin. *Journal of Applied Polymer Science* **2001,** *80* (12), 2123-2127.

61. Hamadi, N. K.; Chen, X. D.; Farid, M. M.; Lu, M. G. Q. Adsorption kinetics for the removal of chromium(VI) from aqueous solution by adsorbents derived from used tyres and sawdust. *Chemical Engineering Journal* **2001,** *84* (2), 95-105.

62. Pan, Y.; Cai, P.; Farmahini-Farahani, M.; Li, Y.; Hou, X.; Xiao, H. Amino-functionalized alkaline clay with cationic star-shaped polymer as adsorbents for removal of Cr(VI) in aqueous solution. *Applied Surface Science* **2016,** *385*, 333-340.

63. Yuen, F. K.; Hameed, B. H. Recent developments in the preparation and regeneration of activated carbons by microwaves. *Advances in Colloid and Interface Science* **2009,** *149* (1–2), 19-27.

64. Kyzas, G. Z.; Siafaka, P. I.; Lambropoulou, D. A.; Lazaridis, N. K.; Bikiaris, D. N. Poly(itaconic acid)-Grafted Chitosan Adsorbents with Different Cross-Linking for Pb(II) and Cd(II) Uptake. *Langmuir* **2014,** *30* (1), 120-131.

65. Mittal, H.; Maity, A.; Sinha Ray, S. The Adsorption of Pb2+ and Cu2+ onto Gum Ghatti-Grafted Poly(acrylamide-co-acrylonitrile) Biodegradable Hydrogel: Isotherms and Kinetic Models. *The Journal of Physical Chemistry B* **2015,** *119* (5), 2026-2039.

66. Liu, P.; Jiang, L.; Zhu, L.; Wang, A. Attapulgite/Poly(acrylic acid) Nanocomposite (ATP/PAA) Hydrogels with Multifunctionalized Attapulgite (org-ATP) Nanorods as Unique Cross-linker: Preparation Optimization and Selective Adsorption of Pb(II) Ion. *ACS Sustainable Chemistry & Engineering* **2014,** *2* (4), 643-651.

67. Saliba, R.; Gauthier, H.; Gauthier, R.; Petit-Ramel, M. Adsorption of copper(II) and chromium(III) ions onto amidoximated cellulose. *Journal of Applied Polymer Science* **2000,** *75* (13), 1624-1631.

68. Reddy, K. H. R., A. Ravikumar. Removal of Heavy Metal Ions Using the Chelating Polymers Derived by the Condensation of Poly(3-Hydroxy-4-acetylphenyl methacrylate) with different Diamines. *Journal of Applied Polymer Science* **2002,** *88*, 414-421.

Chapter 2

Design of Novel Highly-Active Catalysts for Atom Transfer Radical Processes

2.1 Introduction

Atom transfer radical processes such as atom transfer radical addition (ATRA) and atom transfer radical polymerization (ATRP) are extremely useful synthetic techniques for the production of small organic molecules, polymers, natural products, and pharmaceuticals due to their ability for carbon-carbon bond formation.[1-3] ATRA, also known as Kharasch addition, dates back to 1937 when Kharasch and co-workers discovered the peroxide effect in which an alkyl halide adds across the double bond of an alkene in an anti-Markovnikov fashion as shown in Scheme 1.[4-5] The peroxide serves as the initiator, producing a radical which then homolytically cleaves the R-X bond. Next, during propagation, the halogen radical adds across the double bond of an alkene in an anti-Markovnikov fashion ultimately forming a halogenated monoadduct. Lastly, termination occurs via radical-radical coupling and disproportionation. Kharasch's primary focus was on polyhalogenated alkyl halides such as carbon tetrabromide, bromoform, carbon tetrachloride, and chloroform.[5] This type of addition can be referred to as free-radical initiated ATRA and works well for the production of monoadduct when using simple α-olefins such as 1-octene and 1-hexene. A major disadvantage of free-radical initiated ATRA is that it produces significantly lower yields of monoadduct when monomers that are highly active in free-radical polymerization (e.g., methyl acrylate, methyl methacrylate, acrylonitrile, or styrene) are employed rather than simple α-olefins.[6] The primary reason for this decrease in monoadduct yield is repeating radical addition to

the alkene to form oligomers/polymers and radical-radical termination by either coupling or disproportionation.

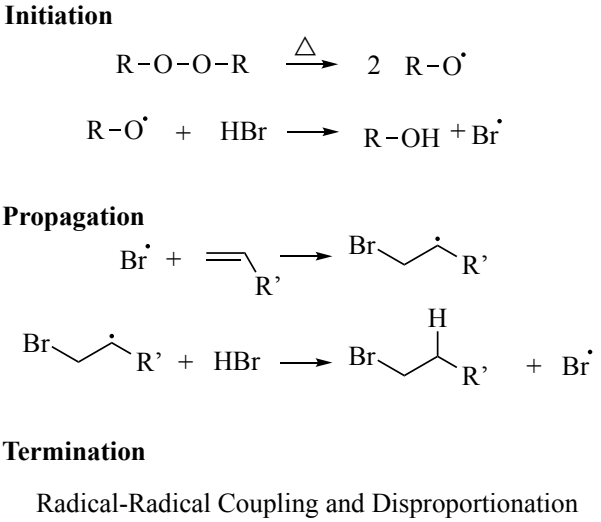

Scheme 2.1 Proposed mechanism for the peroxide effect. The peroxide serves as the initiator for anti-Markovnikov addition of HBr to an unsymmetrical alkene.

Transition-metal catalyzed (TMC) ATRA, discovered by Minisci and co-workers in 1956, overcame this disadvantage and not only works well for simple α-olefins but also for monomers that are highly active in free-radical polymerization.[7] They were attempting the free-radical polymerization of acrylonitrile in a steel autoclave and discovered that a large amount of monoadduct was formed rather than polyacrylonitrile. Ultimately, Minisci and co-workers determined that the inside of the steel autoclave corroded and released iron into the reaction catalyzing the production of monoadduct. They discovered that transition metal complexes are more effective halogen transfer agents allowing for better control over the radical addition. Over the years, transition metals other than iron have been employed for TMC ATRA including copper, nickel, palladium, and ruthenium.[8-12] Traditionally, a major disadvantage of TCM ATRA is that a large excess of transition metal based catalyst is needed, typically 5-30 mol% relative to

alkene, to account for the accumulation of the deactivating complex, i.e. transition metal complex in its higher oxidation state.[6]

The proposed mechanism for copper-catalyzed ATRA and ATRP is shown in Scheme 2.2.[13] The copper complex in its reduced state, Cu^{I}/L_mX, is referred to as the activator and starts the catalytic process by homolytically cleaving the initiator/alkyl halide, R-X, generating a radical and is governed by an activation rate constant, k_{act}. During this step the copper complex is oxidized via one-electron oxidative addition to form Cu^{II}/L_mX_2, known as the deactivator complex. The newly formed radical can proceed in the catalytic cycle by taking two different routes. In one route the activated radical abstracts the transferred halogen from the Cu^{II} complex reforming the alkyl halide, i.e. initiator. This process is governed by the deactivation rate constant, k_{deact}. Hence, a dynamic equilibrium is established via activation and deactivation of the alkyl halide. This equilibrium between the activation and deactivation processes determines the concentration of radicals and is described as $K_{ATRA} = k_{act} / k_{deact}$. In order to minimize radical-radical coupling, which would ultimately terminate the catalytic cycle, the condition of $k_{deact} >> k_{act}$ must exist.[14] The activation/deactivation relationship is critical to performing successful atom transfer radical processes, ATRA and ATRP. In contrast to the first route in which the newly formed radical can proceed, the second route is the addition of this radical across the double bond of an alkene or monomer in an anit-Markovnikov fashion forming a secondary radical. This secondary radical then abstracts a halogen from the deactivator (Cu^{II} complex) forming the monoadduct and regenerating the activator complex (Cu^{I} complex). This catalytic cycle of ATRA and ATRP is nearly identical. When performing ATRA, the production of monoadduct is of interest. To

promote formation of monoadduct and suppress polymer formation, an excess of alkyl halide is used to ensure that the Cu^{I} complex activates the initiator rather than the halogenated monoadduct. When performing ATRP, an excess of monomer, i.e. alkene relative to initiator is used to promote reactivation of the growing polymer chain and has a rate constant, k_p. Similar to the relationship between k_{act} and k_{deact}, the relationship $k_d >> k_p$ must exist in order to form polymer chains rather than oligomers. The initiator-to-monomer ratio is used to dictate the degree of polymerization when performing ATRP. Overtime, the deactivator complex accumulates due to radical-radical coupling or disproportionation in both ATRA and ATRP systems.

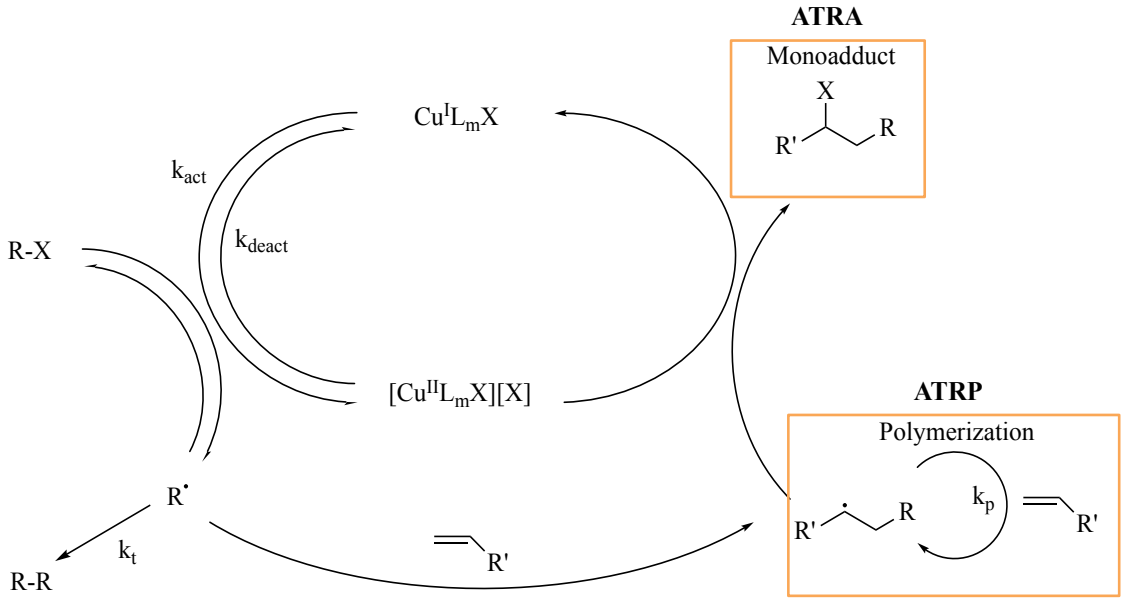

Scheme 2.2 Proposed mechanism for copper-catalyzed ATRA and ATRP showing complexing ligand (L) and alkyl halide (RX, X = Cl or Br).

Over the past few decades much effort has been expended on developing methodologies for decreasing the amount of transition metal catalyst needed to achieve sufficient yield of monoadduct or polymers for ATRA and ATRP, respectively. These

methodologies include the introduction of a reducing agent, such as ascorbic acid or tin (II) 2-ethylhexanoate. This process is termed activators regenerated by electron transfer (ARGET) ATRA.[15] Additionally, 2,2'-Azobis(2-methylpropionitrile) (AIBN) and 2,2'-azobis(2,4-dimethyl-4-methoxyvaleronitrile) (V-70) can be implemented as a radical-based reducing agent. When utilizing AIBN, the reaction must be performed at elevated temperatures since AIBN is a thermally activated reducing agent. The method implementing AIBN or V-70 has been termed initiators for continuous activation (ICAR) ATRA.[16] Other catalyst regeneration methodologies include supplemental activators and reducing agents (SARA)[15] utilizing zero-valent metals, e.g. Cu^0 or Zn^0, and most recently photo-initiated regeneration using light.[17-18] The different catalyst regeneration methods are summarized in Figure 2.1. In addition to greatly reducing the amount of transition metal catalyst need for atom transfer radical processes, another primary advantage of using these reducing agents is that the catalytic process can start from the air-stable Cu^{II} complex in contrast to running reactions under inert conditions, which is needed to prohibit the Cu^{I} complex from being oxidized to the deactivator i.e. the Cu^{II} complex.

The addition of the aforementioned reducing agents work well for activator regeneration but are not without disadvantages. Following the thermal activation of AIBN or ambient temperature activation of V-70, two radicals are produced increasing the radical concentration and hence the probability of radical-radical coupling termination reactions. By utilizing tin (II) 2-ethylhexanoate or zero-valent metals as a reducing agent, the total heavy metal concentration is increased in the system, which is environmentally unfriendly and more expensive. Ascorbic acid is cheap and environmentally benign but forms a strong acid during the reduction of the deactivator

complex, which ultimately degrades the catalyst hindering its efficacy. But, the effect of the strong acid on the catalyst complex can be minimized with the addition of a weak base such as triethylamine.

ARGET

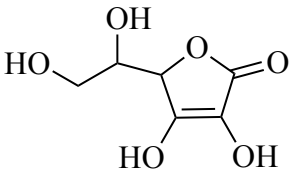

Ascorbic Acid

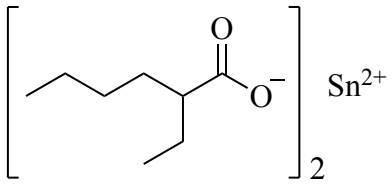

Tin (II) 2-Ethylhexanoate

ICAR

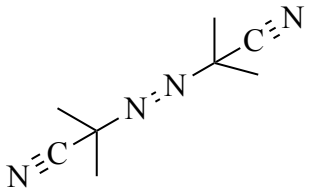

AIBN

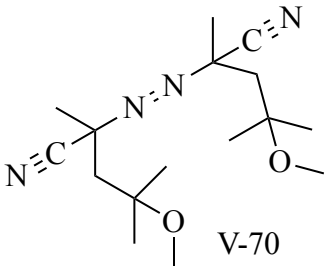

V-70

SARA Cu^0 Zn^0

Photo hv

Figure 2.1 Reducing agents utilized in different catalyst regeneration strategies for atom transfer radical processes, ATRA and ATRP.

In addition to the use of reducing agents for lowering the concentration of the heavy metal catalysts used in ATRA and ATRP systems, the design and development of novel highly active ligands has been shown to assist in lowering the amount of catalyst needed. The efficiency of the metal catalyst can be modulated by variations in the complexing ligand. Denticity of the ligand to the copper center affects the activity of the

catalyst. For example, tetradentate ligand complexes are typically more active than tridentate ligands, which are more active than bidentate ligands. Some of the most active copper complexes reported to date are formed using neutral tetradentate ligands, tris[(2-pyridyl)methyl]amine (TPMA) and tris(2-dimethylaminoethyl)amine (Me_6TREN). Figure 2.1 includes highly active TPMA and Me_6TREN ligands and more traditional, less active ligands such as bidentate 2,2'-bipyridine (bpy) and tridentate N,N,N',N",N"-pentamethyldiethylenetriamine (PMDETA).

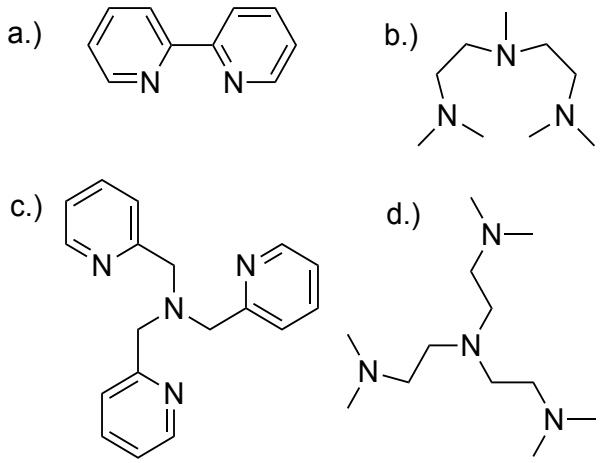

Figure 2.2 Traditional ligands (a) bpy, (b) PMDETA and highly active ligands (c) TPMA, (d) Me_6TREN used for ATRA and ATRP.

Structural differences of ligands can affect the ATRA equilibrium constant (K_{ATRA}) by orders of magnitude as shown in Table 2.1.[15] Although copper complexes coordinated with Me_6TREN have a higher equilibrium constant than that of TPMA complexes, they are not as active in ARGET ATRA systems. TPMA complexes when compared to Me_6TREN complexes are more robust since the pyridine rings of TPMA are less susceptible to protonation than the aliphatic arms of the Me_6TREN when in the presence of a strong acid. Protonation of the complexing ligand degrades the catalyst structure hindering its activity.

Table 2.1 ATRA equilibrium constants (K_{ATRA}) for common ligands. K_{ATRA} was measured using ethyl 2-bromoisobutyrate and $Cu^{I}Br$ in acetonitrile at room temperature.

Ligand	bpy	PMDETA	TPMA	Me_6TREN
$\mathbf{K_{ATRA}}$	10^{-8}	10^{-7}	10^{-5}	10^{-4}

The aim of this work was focused on developing copper catalyst complexes containing hybrid TPMA-Me_6TREN ligands, [Cu^{II}(bis[2-(dimethylamino)ethyl-2-(pyridylmethyl)amine]) and [Cu^{II}([2-(dimethylamino)ethyl-bis-2-(pyridylmethyl)amine]), performing their comprehensive structural characterization, and investigating their activity in ATRA systems.

2.2 Materials

All materials were used as received unless otherwise stated. Ascorbic acid, alumina (Al_2O_3), chloroacetonitrile (ClAN), chloropropionitrile (ClPN), copper (II) bromide ($CuBr_2$), magnesium sulfate ($MgSO_4$), pyridine-2-carboxaldehyde, and triethylamine (Et_3N) were purchased from Alfa Aesar (Fisher Scientific, Tewksbury MA). Benzyl thiocyanate (BzSCN), carbon tetrabromide (CBr_4), carbon tetrachloride (CCl_4) were purchased from TCI America (Fisher Scientific, Tewksbury MA). Copper (II) chloride ($CuCl_2$), 1,4-dimethoxy benzene, ferrocene, N,N-dimethylethane-1,2-diamine, potassium hydride (KH), sodium triacetoxyborohydride (STAB), sodium bicarbonate ($NaHCO_3$), tetrabutylammonium hexafluorophosphate (TBA-PF_6), and 2,2,6,6-tetramethylpiperidine-1-oxyl (TEMPO) were purchased from Sigma-Aldrich (St. Louis MO). Acrylonitrile, methyl acrylate (MA), methyl methacrylate (MMA), and 1-octene were purchased from Acros Organics (Fischer Scientific, Pittsburgh PA) and passed through basic alumina to remove inhibitor and were stored at 4 ^{0}C prior to use.

Acetonitrile, dichloromethane (DCM), diethyl ether, hydrochloric acid (HCl), methanol (MeOH), and n-pentane were purchased from Fischer Scientific. Deuterated chloroform ($CDCl_3$) was purchased from Cambridge Isotope Laboratories (Tewksbury MA). Acetone was supplied by Duquesne University.

2.3 Methods and Instrumentation

2.3.1 Ligand Synthesis and Characterization

Highly active tetradentate ligands, tris(2-pyridylmethyl)amine (TPMA), 2-(dimethylamino)ethyl-bis-[2-(pyridylmethyl)amine] (M1-T2), and bis[2-(dimethylamino)ethyl]-2-(pyridylmethyl)amine (M2-T1) were synthesized by adopting a previously reported method by Britovsek et al.[19] Clean ^{1}H and ^{13}C nuclear magnetic resonance (NMR) spectra were collected on a 400 MHz spectrometer (Bruker, Billerica MA) equipped with TopSpin 3.2 software and obtained without the use of chromatography purification. Deuterated chloroform ($CDCl_3$) was used as solvent. Chemical shifts given in ppm relative to the residual solvent peak ($CDCl_3$ δ7.26 ppm).

2.3.2 Catalyst Complex Synthesis and Characterization

All catalyst complexes $[Cu^{II}(M1\text{-}T2)Br][Br]$, $Cu^{I}(M1\text{-}T2)Br$, $[Cu^{II}(M1\text{-}T2)Cl][Cl]$, $[Cu^{II}(M2\text{-}T1)Br][Br]$, $[Cu^{II}(M2\text{-}T1)Cl][Cl]$ were synthesized using similar methods. Briefly, in a one-pot reaction CuX_2 (X=Cl or Br) (0.28 mmol) and ligand (0.28 mmol) were stirred in 3 mL DCM for 1 hour at ambient temperature. The product was precipitated by the addition of 15 mL pentane and dried under vacuum to yield the catalyst complexes. Slow diffusion of pentane into a concentrated acetone solution of the

complex afforded green (Cu^{II}) or brown (Cu^{I}) crystals suitable for X-ray analysis. The molecular structures of novel catalysts were collected at 150 K using graphite-monochromated Mo Kα radiation (0.71073 Å) with a Smart Apex II CCD diffractometer (Bruker, Billerica MA). The SQUEEZE / PLATON technique was used to account for unspecified electron density located in the lattice for $[Cu^{II}(M2\text{-}T1)Br][Br]$ which was determined to be two molecules of water.[20] Data reduction included absorption corrections by the multi-scan method using SADABS.[21] Structures were solved by direct methods and refined by full matrix least-squares using SHELXTL 6.1 bundled software package.[22] ORTEP-3 for Windows and Crystal Maker 9 were used to generate molecular graphics. To examine the structures of novel catalyst complexes in solution, UV-Vis and variable temperature ^{1}H NMR spectroscopy were utilized. UV-Vis spectra were collected using a Beckman DU-530 spectrometer in a 1.0 cm quartz cuvette and acetonitrile as solvent. Variable temperature NMR spectra were collected on a 400 MHz spectrometer (Bruker, Billerica MA) equipped with TopSpin 3.2 software using acetone-d_6 or $CDCl_3$ as solvent.

2.3.3 Electrochemical Characterization of Novel Catalysts Utilizing Cyclic Voltammetry

Cyclic voltammograms of novel catalyst complexes were collected using an EZstat-Pro (NuVant Systems Inc., Crown Point IN) equipped with a three-electrode system. Copper complexes were dissolved in acetonitrile (5×10^{-3} M) containing supporting electrolyte tetrabutylammonium hexafluorophosphate (TBA-PF_6) (0.1 M). The solution was purged with nitrogen for 30 minutes prior to collecting the

voltammogram. Reported $E_{1/2}$ values are relative to the ferrocene/ferrocinium (Fc/Fc^+) couple.

2.3.4 Kinetic Evaluation of Novel Catalyst Complexes

The observed rate constant (k_{obs}) was determined for ATRA of carbon tetrabromide (CBr_4) to methyl methacrylate (MMA) in the presence of ascorbic acid as the reducing agent. The reaction proceeded at 23°C using methanol (MeOH) as solvent. The catalyst loading was 50 ppm relative to alkene with the following molar ratios: [alkene]:[alkyl halide]:[ascorbic acid] = 1:1.25:0.07, $[alkene]_0$ = 1.34 M. UV-Vis spectra were collected using a Beckman DU-530 spectrometer. Data was collected for 5 hours at λ_{max} of 973 nm and 897 nm for $[Cu^{II}(TPMA)Br][Br]$ and $[Cu^{II}(M1\text{-}T2)Br][Br]$, respectively.

The following method was utilized to determine the activation rate constant (k_a) for catalyst complexes. In a dry box, $Cu^{1}(TPMA)Br$ or $Cu^{1}(M1\text{-}T2)Br$ (5.0 mM), benzyl thiocyanate (BzSCN) (0.098 M), and 2,2,6,6-Tetramethylpiperidine-1-oxyl (TEMPO) (0.1 M) were dissolved in 3 mL acetonitrile. The solution was then transferred to an airtight quartz cuvette and immediately removed from the dry box and placed in the UV-Vis spectrometer. Spectra were collected at 23°C using a Beckman DU-530 spectrometer. Concentration data was collected for 6 hours at 973 nm and 897 nm for independently synthesized $[Cu^{II}(TPMA)NCS]Br]$ and $[Cu^{II}(M1\text{-}T2)NCS]Br]$.

2.3.5 General Procedure for ARGET ATRA of R-X to Various Alkenes

ARGET ATRA experiments using ascorbic acid as the reducing agent were performed in 5 mm NMR tubes. All reactions were performed in MeOH at either 23°C or 60°C for 24 hours with $[alkene]_0$:$[alkyl\ halide]_0$:$[ascorbic\ acid]_0$ = 1:1.25:0.07, $[alkene]_0$ = 1.34 M. The % conversion of alkene and % yield of monoadduct were determined using ^{1}H-NMR spectroscopy collected with a Bruker 400 MHz spectrometer equipped with TopSpin 3.2 software using $CDCl_3$ as solvent and 1,4-dimethoxybenzene as internal standard. When a weak base was introduced into the reaction mixture, it was present in a 5:1 molar ratio relative to ascorbic acid.

2.4 Results and Discussion

2.4.1 Synthetic Methods for Novel, Highly Active Ligands

Two of the most widely utilized ligands for ATRA and ATRP are TPMA and Me_6TREN. They are tripodal ligands which chelate to the copper center in a tetradentate fashion.[23] Both ligands bind tightly to copper and form stable complexes enhancing the activity of the catalyst. Copper complexes involving Me_6TREN provide a higher activation rate constant (k_{act}) compared to TPMA complexes, hence they are more efficient for atom transfer radical processes. When performing ARGET ATRA or ATRP using ascorbic acid as reducing agent, a strong acid (HBr or HCl) is produced as the activator complex is regenerated. Complexes containing Me_6TREN are more easily protonated than TPMA complexes, which decreases their efficiency due to catalyst degradation. Me_6TREN complexes are more active but TPMA complexes are more stable at a lower pH. Therefore, investigations into hybrid ligands are of interest. The

ligands investigated are hybrids of the highly active ligands Me_6TREN and TPMA. Bis[2-(dimethylamino)ethyl-2-(pyridylmethyl)amine] contains 2 Me_6TREN arms and one TPMA arm where as 2-(dimethylamino)ethyl-bis-2-(pyridylmethyl)amine contains one Me_6TREN arm and two TPMA arms as shown in Figure 2.3.

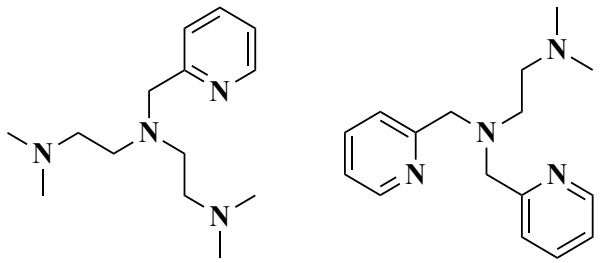

Figure 2.3 Hybrid ligands M2-T1 (left) and M1-T2 (right) investigated in ATRA reactions.

The synthetic scheme for production of the hybrid ligands, shown in Scheme 2.3, were adopted from a method previously reported by Britovsek et al.[19] The synthetic reactions proceed via a reductive amination process using sodium triacetooxyborohydride (STAB) as the reducing agent. This borohydride exhibits good selectivity as a reducing agent, is mild, and safe to handle.[24-26]

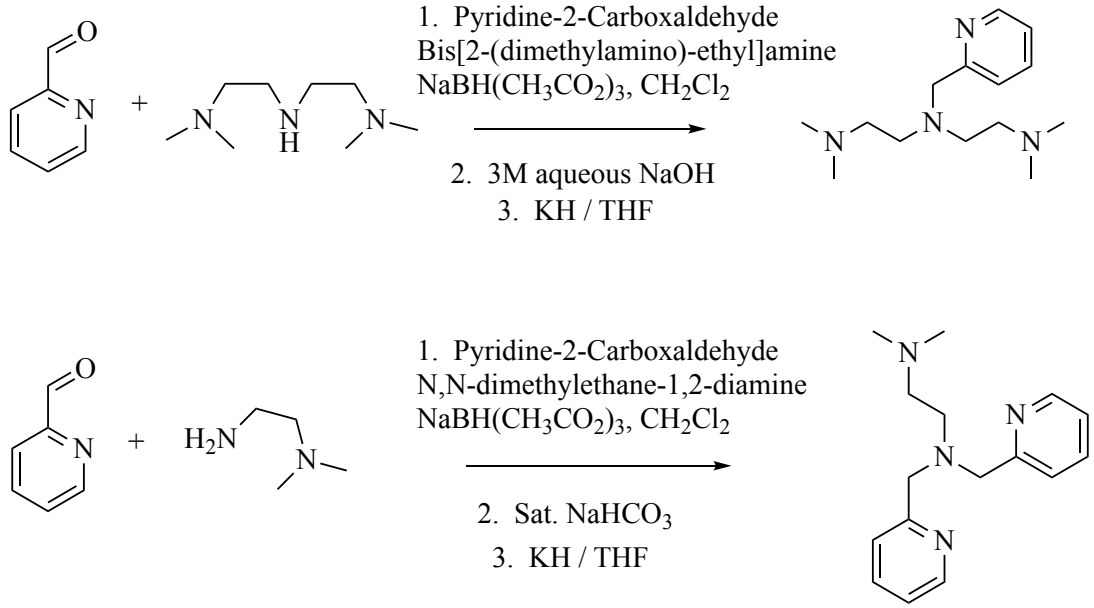

Scheme 2.3 Reaction schemes for hybrid ligands M2-T1 (top) and M1-T2 (bottom).

Results indicated that the protocol adopted from Britovsek et. al. worked efficiently and produced clean NMR spectra without the use of chromatography purification. The ^{1}H NMR spectra are shown in Figures 2.4 and 2.5 including peak assignments. The chemical shifts for the hybrid ligands are in agreement with those reported by Britovsek et al.[19]. Additionally, the ^{13}C NMR spectra are shown in Figure 2.6 and Figure 2.7 supporting the ^{1}H NMR data and confirm the successful synthesis of ligands M1-T2 and M2-T1. The novel hybrid ligands were then complexed to copper, structurally and electrochemically characterized, and their activity evaluated in ATRA reactions.

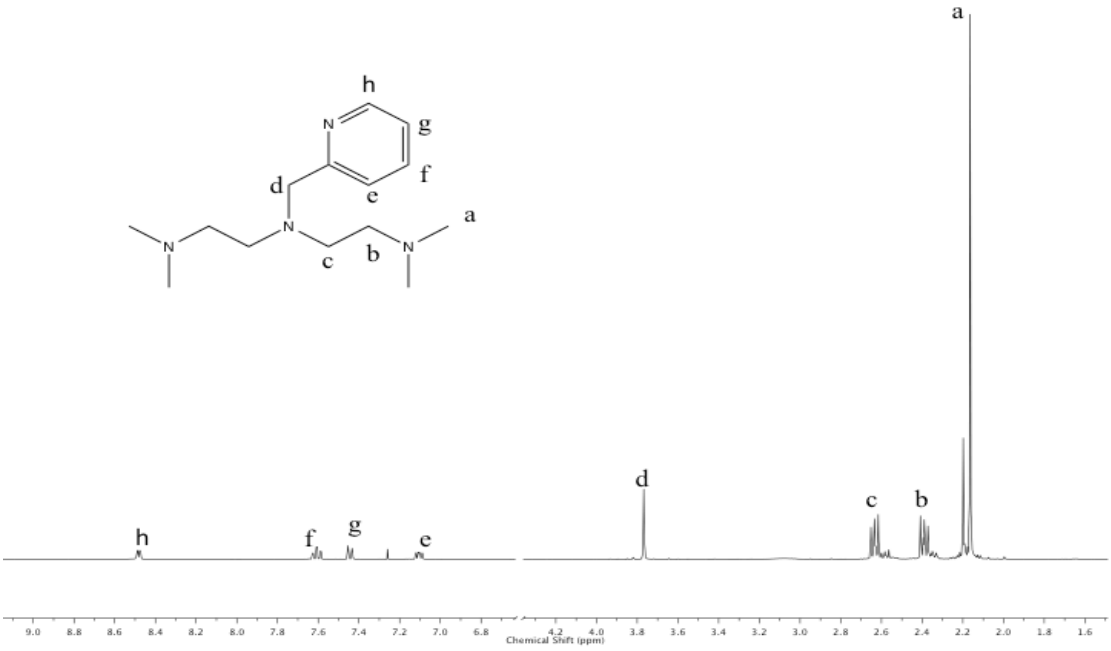

Figure 2.4 ^{1}H NMR spectrum of hybrid ligand M2-T1. (400 MHz, $CDCl_3$, 298 K, 36%)

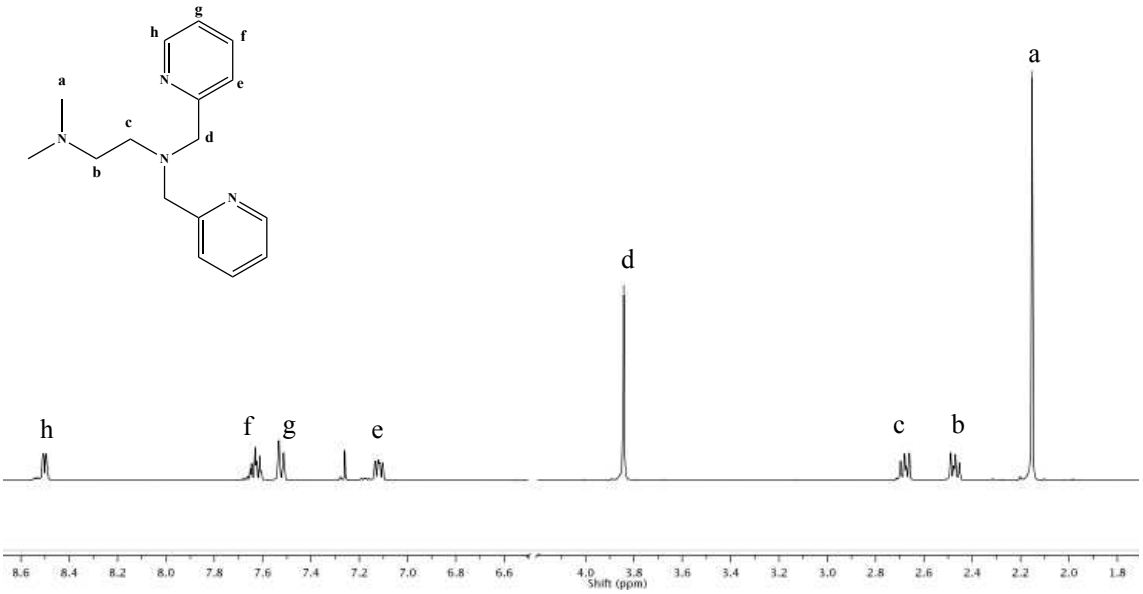

Figure 2.5 ^{1}H NMR spectrum of hybrid ligand M1-T2. (400 MHz, $CDCl_3$, 298 K, 67%)

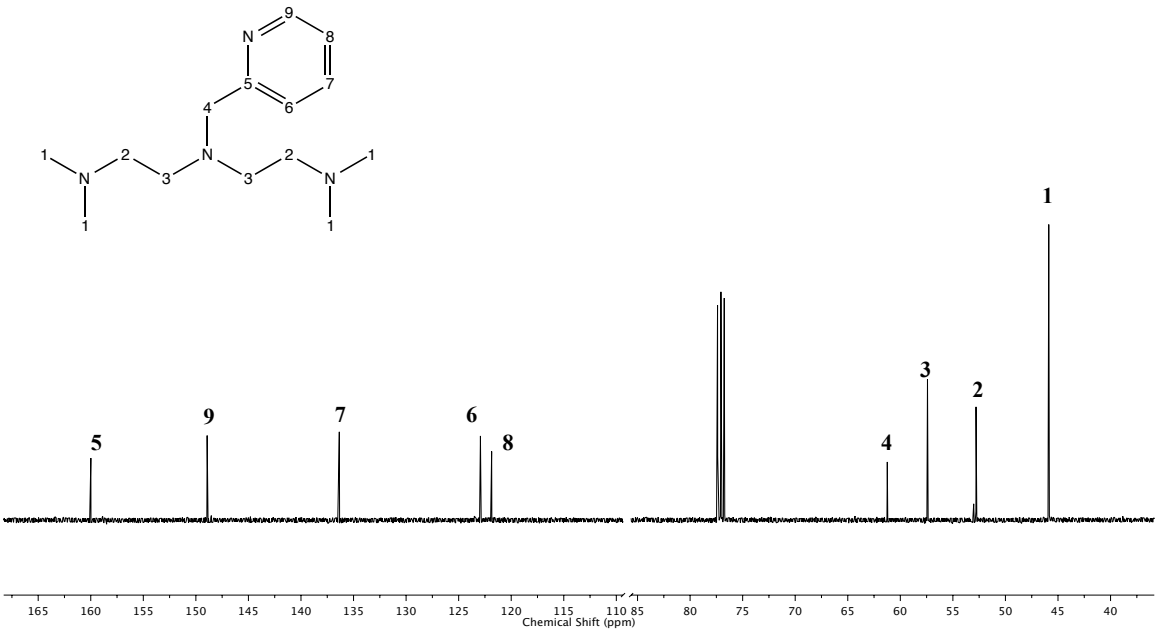

Figure 2.6 ^{13}C NMR spectrum of hybrid ligand M2-T1. (400 MHz, $CDCl_3$, 298 K, 36%)

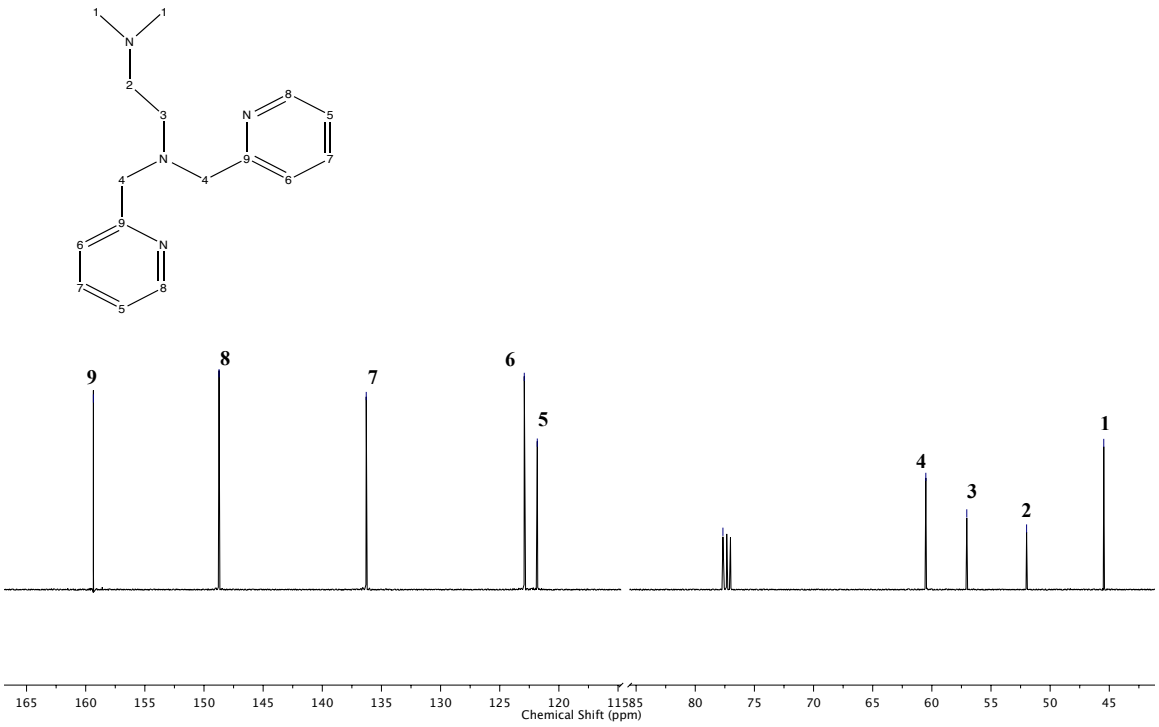

Figure 2.7 ^{13}C NMR spectrum of hybrid ligand M1-T2. (400 MHz, $CDCl_3$, 298 K, 67%)

2.4.2 Structural Characterization of Novel Catalyst Complexes

Structural characterization of catalyst complexes can provide mechanistic information regarding the activation of the alkyl halide and/or monoadduct/polymer formation in ATRA and ATRP. Molecular structures were elucidated using single-crystal X-ray diffraction (XRD) and the structures while in solution were examined using variable temperature ^{1}H-NMR spectroscopy and UV-Vis spectroscopy. Because the copper complexes in the catalytic cycle are constantly being reduced and oxidized, structural characterization of both the Cu^{I} and Cu^{II} species is of interest.

2.4.2.1 Structural Characterization of [Cu^{II}(M1-T2)Br][Br] and Cu^{I}(M1-T2)Br

Crystals suitable for XRD were obtained in acetone via slow diffusion of pentane for Cu^{I}(T2-M1)Br and Cu^{II}(T2-M1)Br_2. Their molecular structures, as shown in Figure 2.7, are similar to previous reported structures for the analogous TPMA and Me_6TREN complexes.[13, 27-28] In the solid state, the Cu^{I} complex has a distorted tetrahedral geometry, which is similar to the previously reported Cu^{I} complexes containing the M1-T2 ligand[29] and the TPMA ligand[13]. Compared to a typical Cu-N bond (2.0-2.1 Å), the Cu1-N1 bond length shown in Figure 2.8 is elongated at approximately 2.5 Å. Therefore, the axial nitrogen can be considered as non-bonding, giving a coordination number of 4 and a distorted tetrahedral geometry. This elongation is in agreement with previously reported crystal structures of copper complexes containing TPMA or its derivative, M1-T2. The angles between Cu(1), Br(1), and the equatorial nitrogen atoms (N4-Cu1-Br1 101.72° (9)) also are indicative of a distorted tetrahedral geometry. A true tetrahedral geometry would have bond angles of 109.5°.[30]

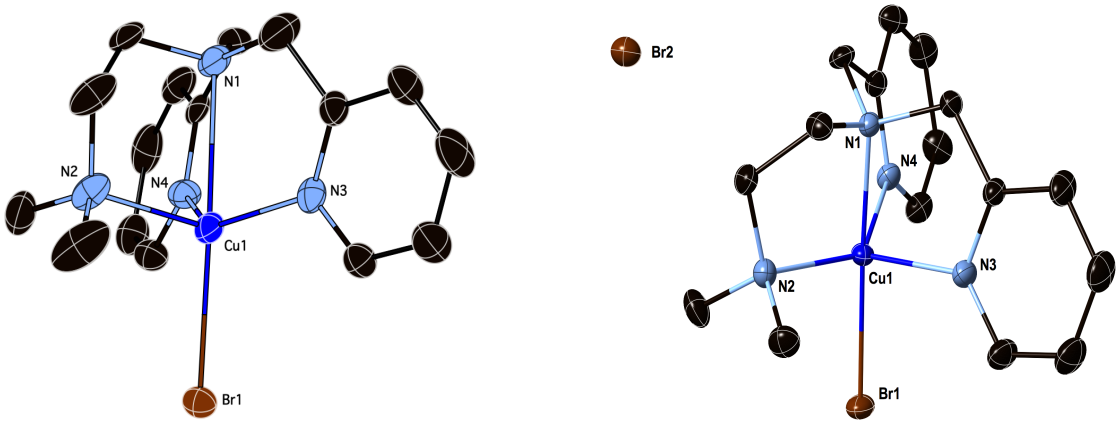

Figure 2.8 Molecular structures of Cu^{I}(M1-T2)Br (left) and [Cu^{II}(M1-T2)Br][Br] (right) collected at 150 K shown with 50% probability ellipsoids. Hydrogen atoms omitted for clarity.

The molecular structure of [Cu^{II}(M1-T2)Br][Br] is considered to have a distorted trigonal bipyramidal structure (Figure 2.8), which is similar to the molecular structures of [Cu^{II}(TPMA)Br][Br] and [Cu^{II}(Me_6TREN)Br][Br].[27-28] If the structure were a true trigonal bipyramidal structure, the bond angle of N1-Cu1-N4 would be 90°. Since the diffraction data indicates that this angle is less than 90° (78.00°) it is concluded that the trigonal bipyramidal structure is slightly distorted because the Cu1 atom lies slightly below the plane of the three equatorial nitrogen atom. Hence the bond angle between N4-Cu1-Br1 is larger than 90° (98.34°). The tau parameter (τ) provides insight into the degree of distortion for 5-coordinate complexes and was calculated to be 0.7 for [Cu^{II}(M1-T2)Br][Br] in contrast to [Cu^{II}(TPMA)Br][Br] and [Cu^{II}(Me_6TREN)Br][Br] which have tau values of 1.0.[13, 27] A value of one represents a true trigonal bipyramidal structure in contrast with a value of zero, which is indicative of a square pyramidal geometry.[31] Crystal and collection data including refinement information are given in the Chapter 2 Appendix.

To examine the structure of the Cu^{I} complex in solution, variable temperature ^{1}H-NMR spectroscopy was utilized, shown in Figure 2.9. This spectrum is indicative of a fluxional system indicative by the singlet from the methylene hydrogens of the TPMA arms (c, 3.7 ppm) becomes 2 doublets at 3.7 and 4.2 ppm giving rise to c and c' peaks, respectively, as the temperature is lowered to 190 K. These hydrogens become nonequivalent, which is caused by one of the TPMA arms dissociating from the copper center. This fluxionality present for Cu^{I} complexes has previously been reported.[23, 32]

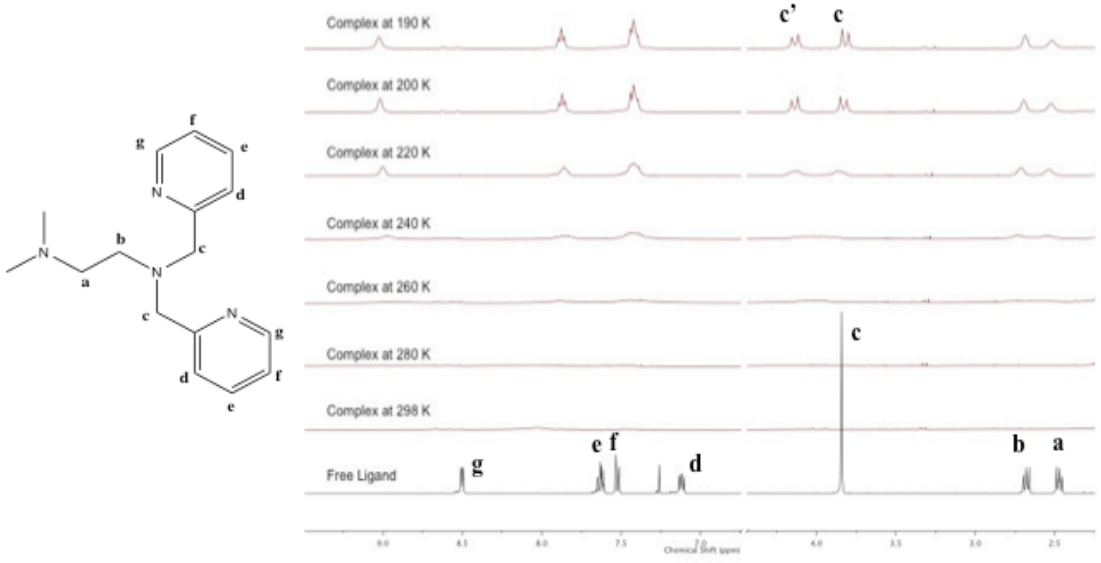

Figure 2.9 Variable temperature NMR spectra of $[Cu^{II}(M1\text{-}T2)Br][Br]$ showing the fluxional characteristic of the ligand-copper complex (400 MHz, acetone-d_6 or $CDCl_3$).

To examine the structure of the Cu^{II} complex in solution, UV-Vis spectroscopy was implemented. The UV-Vis spectra supported the data collected by XRD studies. It is evident in the spectra that there are two strong absorption bands at 914 and 745 nm, shown in Figure 2.10. These two absorption bands in the spectrum are indicative of a

trigonal bipyramidal structure for a d^9 metal due to the allowed d-d transitions shown in Figure 2.11.

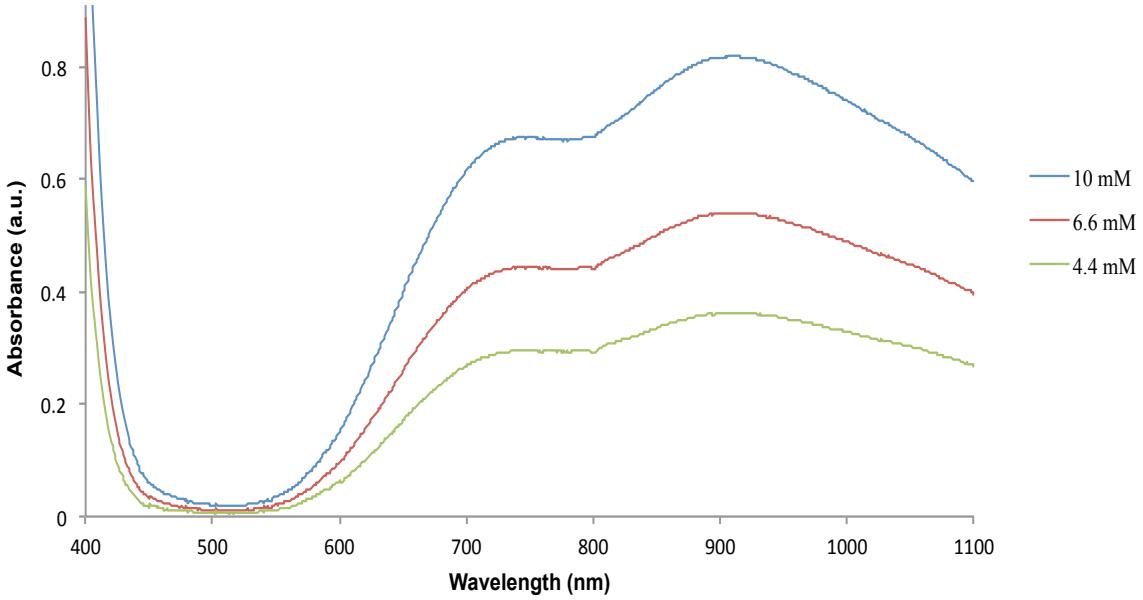

Figure 2.10 UV-Vis spectra of [Cu^{II}(M1-T2)Br][Br] in acetonitrile. Two absorption bands indicate a trigonal bipyramidal structure in solution. λ_{max} = 914 nm, ε = 81.3 L mol^{-1} cm^{-1}.

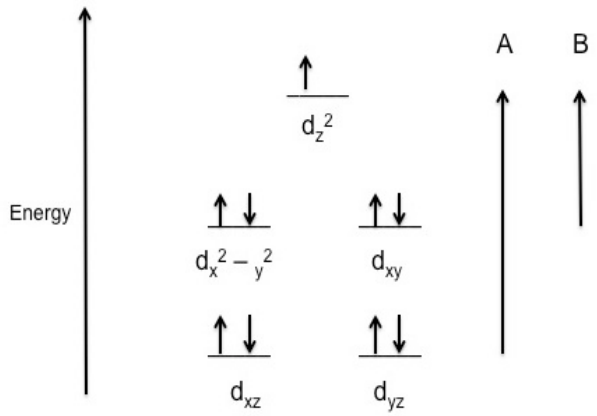

Figure 2.11 The d-orbital splitting for a trigonal bipyramidal complex. The Cu^{II} complex is a d^9 metal allowing for two possible electronic transitions. The labeled transition A is a higher energy transition and correlates to the absorption band at 745 nm in the UV-Vis spectra. In contrast to transition A, a lower energy transition B is observed and correlates to the absorption band at 914 nm in the UV-Vis spectra.

2.4.2.2 Structural Characterization of [Cu^{II}(M2-T1)Br][Br]

Green crystals suitable for XRD were obtained in acetone via slow diffusion of pentane. The molecular structure of the [Cu^{II}(M2-T1)Br][Br] shown in Figure 2.11 indicates a distorted trigonal bipyramidal structure (τ = 0.87). This distortion is in contrast to its analogues, [Cu^{II}(TPMA)Br][Br] and [Cu^{II}(Me_6TREN)Br][Br], which have a perfect trigonal bipyramidal structure (τ = 1). The bond angles of N_{eq}-Cu-N_{eq} range from 126.2(1)° to 109.3(1)° and the deviation of these angles from 120° is indicative of a distorted geometry. Additionally, the N_{ax}-Cu-Br bond angle is 178.50(9)°, which again indicates a slight distortion in geometry.

Another area of interest is the bond length of the axial nitrogen to copper. A bond length of 2.037(3) Å is typical for a copper-nitrogen bond. This length is similar to those of [Cu^{II}(TPMA)Br][Br] and [Cu^{II}(Me_6TREN)Br][Br], which are 2.040(3) Å and 2.046(2) Å, respectively. It has been reported that this bond length increases to approximately 2.4 Å in the Cu^{I} complexes and is considered to be pseudo-coordinated. Crystal and collection data including refinement information are given in the Chapter 2 Appendix.

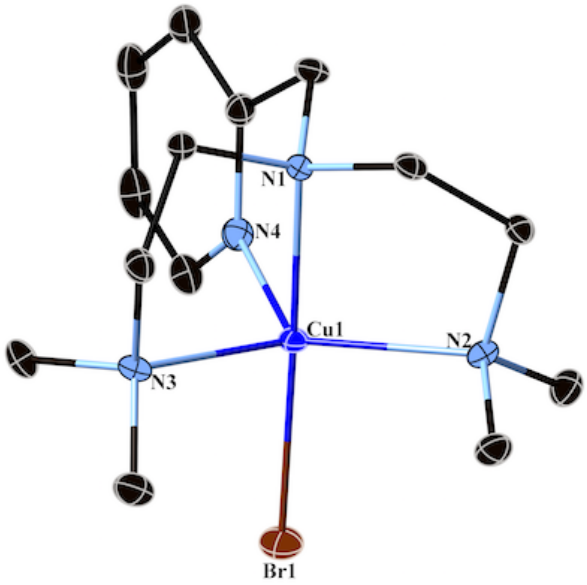

Figure 2.12 Molecular structure of $[Cu^{II}(M2\text{-}T1)Br][Br]*H_2O$ collected at 150 K with 50% probability ellipsoids. Hydrogen atoms, counter atom, and water omitted for clarity.

To examine the structure of $[Cu^{II}(M2\text{-}T1)Br][Br]$ in solution, UV-Vis spectra were collected at various concentrations as shown in Figure 2.13. Similar to the $[Cu^{II}(M1\text{-}T2)Br][Br]$ and $Cu^{I}(M2\text{-}T1)Br$ complexes, two strong absorption bands at 728 nm and 932 nm were observed indicating a trigonal bipyramidal geometry for a d^9 metal and supports the structure elucidated via XRD.

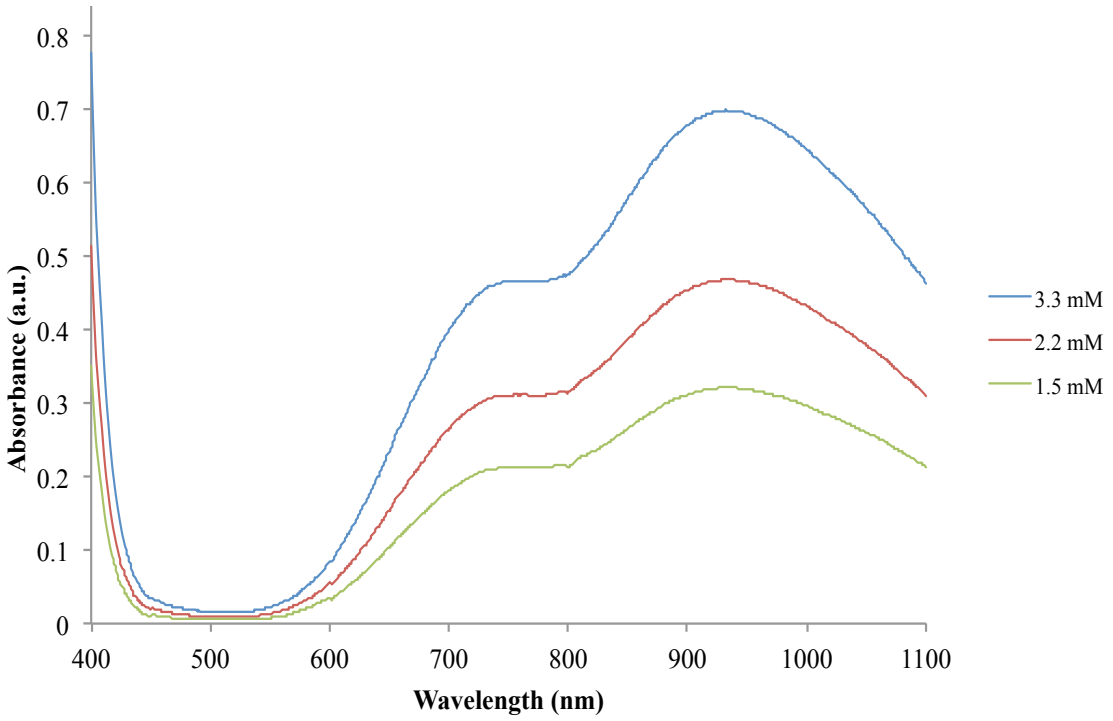

Figure 2.13 UV-Vis spectra of [Cu^{II}(M2-T1)Br][Br] in acetonitrile. Two absorption bands indicate a trigonal bipyramidal structure in solution. λ_{max} = 932 nm, ε = 210 L mol^{-1} cm^{-1}.

2.4.3 Electrochemical Evaluation of Novel Catalysts

Since TMC ATRA is governed by a redox process between lower and higher oxidation states of the copper catalyst, cyclic voltammetry can be an applicable tool for predicting catalytic activity due to the relationship between K_{ATRA} and K_{ET} shown in Figure 2.14. The ATRA equilibrium constant is a product of four component equilibria. K_{ATRA} should correlate with K_{ET} if the halidophilicity remains constant, which is the affinity of the higher oxidation state of the catalyst towards halides. [33-34] Therefore, a more negative reduction potential ($E_{1/2}$) correlates to a more active catalyst complex in these systems.

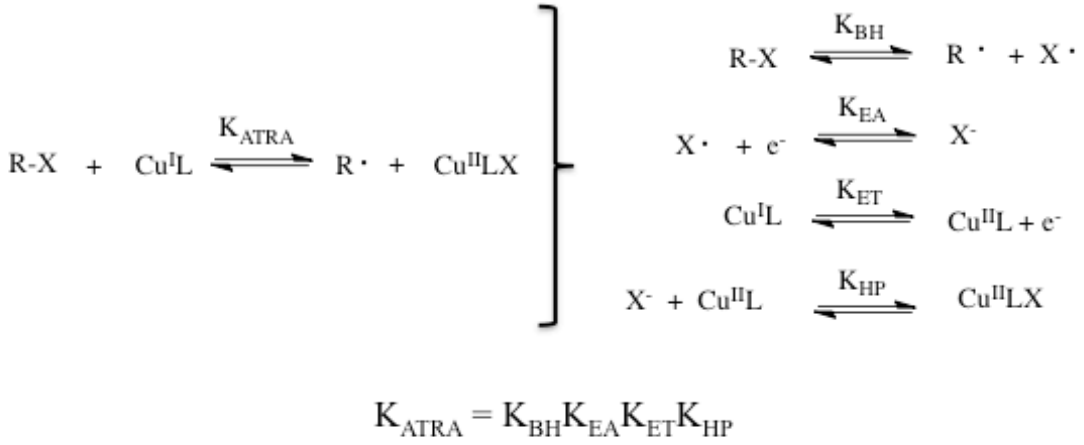

$$K_{ATRA} = K_{BH}K_{EA}K_{ET}K_{HP}$$

Figure 2.14 Components of ATRA equilibrium. BH (Bond Homolysis), EA (Electron Affinity), ET (Electron Transfer), HP (Halidophilicity).

Cyclic voltammetry investigations were performed on the bromide catalyst complexes $CuBr_2$/M1-T2, $CuBr_2$/M2-T1, and compared to the reduction potential of highly active $CuBr_2$/TPMA. The voltammograms shown in Figure 2.15 indicate that the M2-T1 complex has a more negative reduction potential in comparison to the M1-T2 complex, which are -774 mV and -749 mV, respectively. This result was expected since additional aliphatic arms typically provide greater catalytic activity. These hybrid ligand complex half-cell potentials are indicative of having greater catalytic activity to that of the TPMA complex ($E_{1/2}$ = -720 mV).[13] The peak-to-peak separation (ΔE_p) for a one electron, reversible process is 57 mV.[35] The ΔE_p values for all three catalysts $CuBr_2$/M2-T1, $CuBr_2$/M1-T2, and $CuBr_2$/TPMA were calculated to be 109 mV, 83 mV, and 93 mV[13], respectively. Hence, the process is considered quasi-reversible and has been previously reported for similar catalyst complexes.[13] The quasi-reversible nature of these systems was confirmed by the peak anodic current to peak cathodic current ratio (i_{pa}/i_{pc}) values, for which a reversible process i_{pa}/i_{pc} = 1. This ratio was determined to be 1.52,

1.03, and 1.08[13] for $CuBr_2$/M2-T1, $CuBr_2$/M1-T2, and $CuBr_2$/TPMA, respectively. The summarized cyclic voltammetry data is shown in Table 2.1

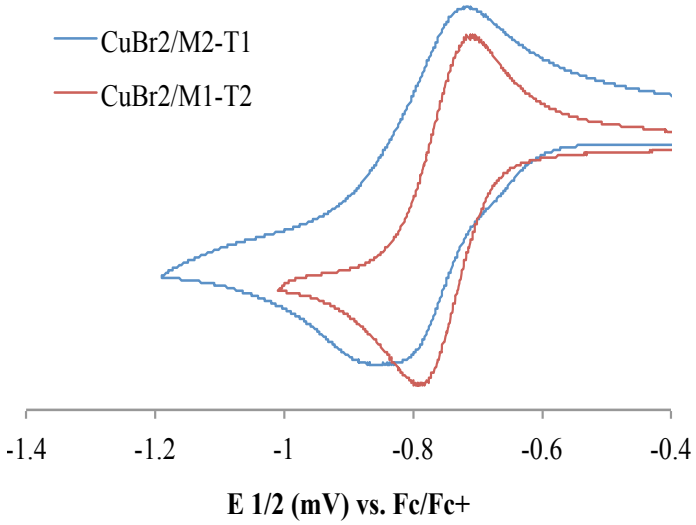

Figure 2.15 Overlaid voltammograms collected in acetonitrile containing the catalyst complex (5 mM) and supporting electrolyte TBA-PF_6 (0.1M). The reported $E_{1/2}$ values are relative to the Fc/Fc^+ couple. The scan rate was set at 50 mV/sec.

Additionally, Cyclic voltammetry investigations were performed on the chloride catalyst complexes $CuCl_2$/M2-T1, $CuCl_2$/M1-T2, and $CuCl_2$/TPMA shown in Figure 2.16. The trend in reduction potentials for the chloride complexes is in agreement with the trend for the bromide complexes: $CuCl_2$/M2-T1 ($E_{1/2}$ = -864 mV) , $CuCl_2$/M1-T2 ($E_{1/2}$ = -835 mV), and $CuCl_2$/TPMA ($E_{1/2}$ = -761 mV). This data again suggests that the M2-T1 complex should be more active in ATRA and ATRP in comparison to the M1-T2 and TPMA complexes. The ΔE_p and i_{pa}/i_{pc} values are indicative of a one electron quasi-reversible process and are summarized in Table 2.2.

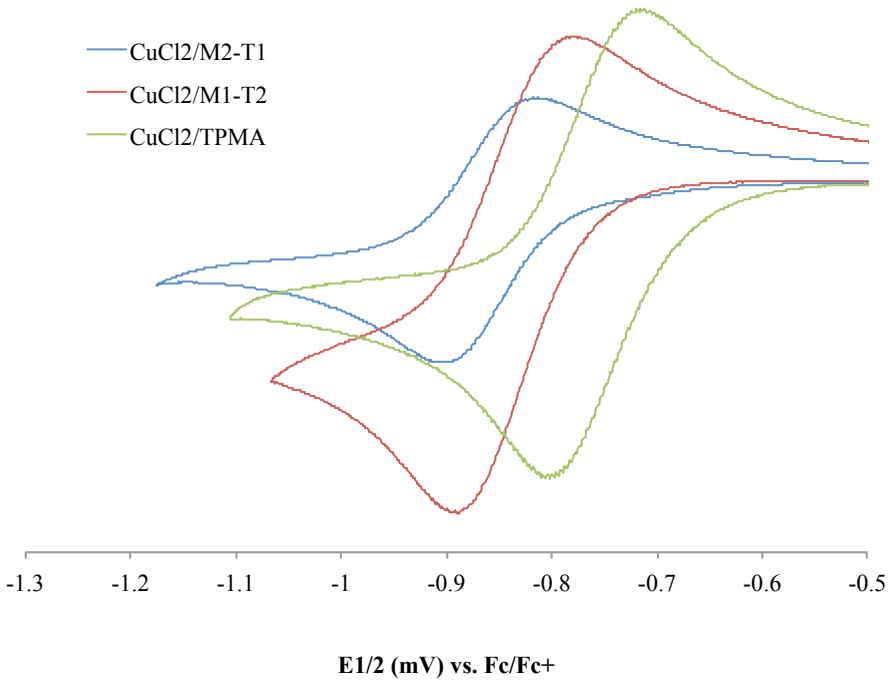

Figure 2.16 Overlaid voltammograms collected in 0.1 M acetonitrile solution containing the catalyst complex and supporting electrolyte (TBA-PF_6). The reported $E_{1/2}$ values are relative to the Fc/Fc^+ couple. The scan rate was set at 50 mV/sec.

Table 2.2 Summary of cyclic voltammetry data for various catalyst complexes.

Complex	**$E_{1/2}$ (mV)**	**ΔE_p (mV)**	**i_{pa} / i_{pc}**
$CuBr_2$/M2-T1	-774	109	1.52
$CuBr_2$/M1-T2	-749	83	1.03
$CuBr_2$/TPMA	-720	93	1.08
$CuCl_2$/M2-T1	-864	97	1.24
$CuCl_2$/M1-T2	-835	110	1.48
$CuCl_2$/TPMA	-761	88	1.31

2.4.4 Kinetic Evaluation of Novel Catalyst Complexes in ATRA Reactions

In order to evaluate the activity of a catalyst in ATRA and ATRP reactions, experiments can be performed to determine the observed rate constant (k_{obs}) and the activation rate constant (k_{act}). For controlled radical processes, the dynamic equilibrium between k_{act} and k_{deact} is a crucial parameter for maintaining a low concentration of radicals allowing for controlled monomer or polymer production. There are various methodologies to determine k_{act} including spectroscopic and chromatographic techniques.[14, 36-38] The method in this report utilizes the radical trapping agent 2,2,6,6-Tetramethylpiperidine-1-oxyl (TEMPO). This spectrophotometric method allows for accurate determination of k_{act} and has been previously implemented for atom transfer radical processes.[14, 39-41] This radical trapping method is shown in Scheme 2.4. TEMPO traps the alkyl radical formed during the activation process allowing for monitoring of the rate of accumulation of the Cu^{II} species. The deactivation process is prohibited due to the trapping of the alky radical.

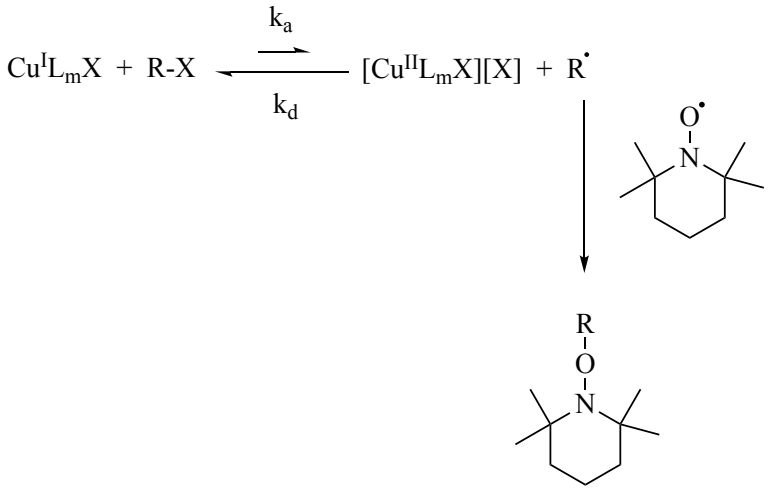

Scheme 2.4 Radical trapping method using TEMPO for determining k_a in atom transfer radical processes.

The activation process in ATRA and ATRP systems follows pseudo first-order kinetics. Protocols implemented for determining k_a must be conducted under oxygen-free, i.e. inert conditions, to prohibit formation of the Cu^{II} species. The reason being that during these experiments, the formation of Cu^{II} is monitored using UV-Vis spectroscopy allowing for calculation of the activation rate constant. This technique was carried out for the reaction between both Cu^{I}(TPMA)Br and Cu^{I}(M1-T2)Br and pseudo alkyl halide benzyl thiocyanate (BzSCN) in the presence of TEMPO and kinetic plots are shown in Figure 2.17. The Cu^{II} concentrations were monitored at 973 nm using $\varepsilon = 221\ M^{-1}\ cm^{-1}$ for independently synthesized [Cu^{II}(TPMA)NCS][Br] and 897 nm using $\varepsilon = 131\ M^{-1}\ cm^{-1}$ for independently synthesized [Cu^{II}(M1-T2)NCS][Br]. There was an order of magnitude difference in the activation rate constants, which were calculated to be $6.8 \times 10^{-3}\ M^{-1}s^{-1}$ and $4.1 \times 10^{-4}\ M^{-1}s^{-1}$ for Cu^{I}(M1-T2)Br and Cu^{I}(TPMA)Br, respectively.

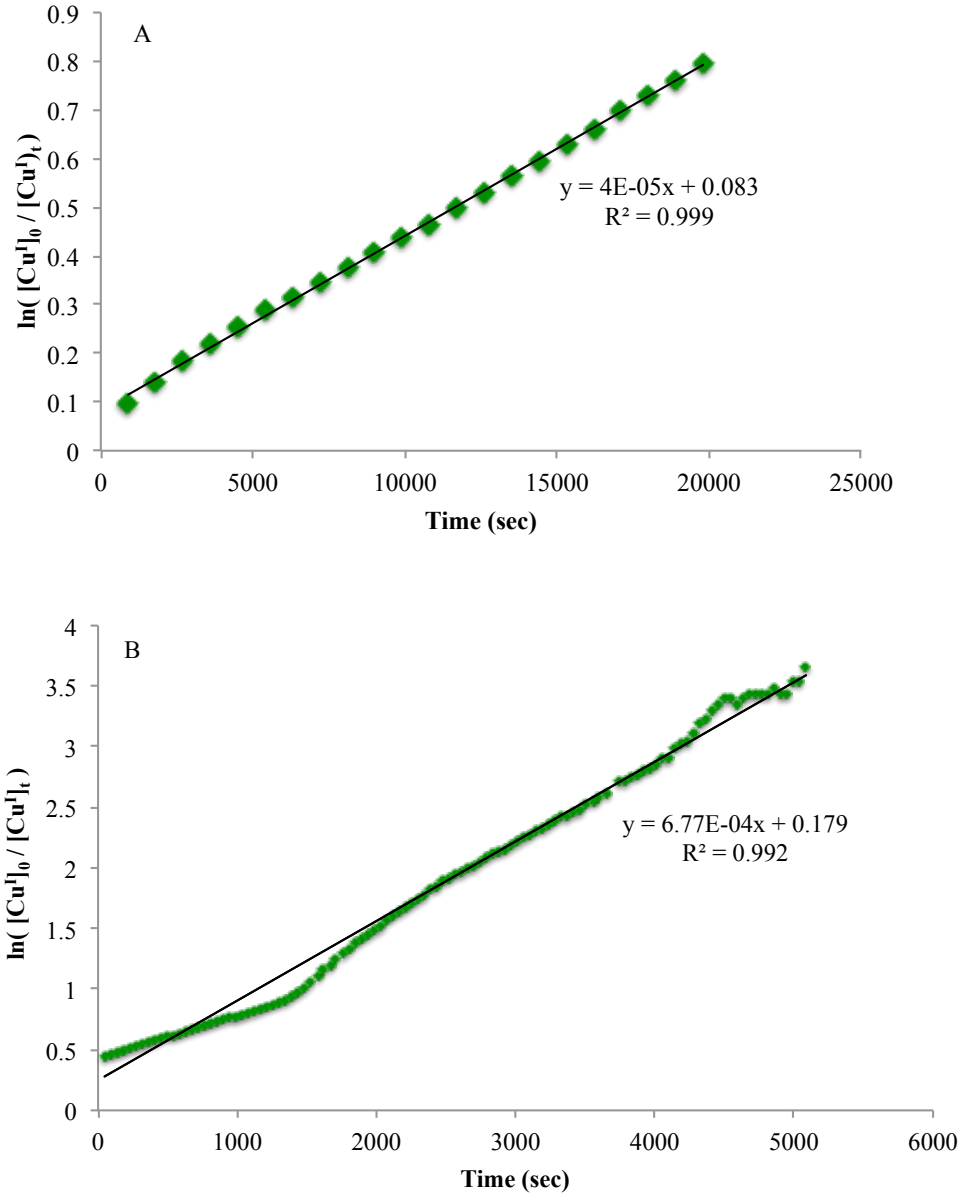

Figure 2.17. Pseudo first-order kinetic plots of the activation rate constant (k_{act}) for the reaction between (A) Cu^{I}(TPMA)Br or (B) Cu^{I}(M1-T2)Br (5.0 x 10^{-3} M) and benzyl thiocyanate (0.098 M) in acetonitrile at 23 °C in the presence of free-radical trapping agent TEMPO (0.1 M) . Cu^{II} concentrations were determined at 973 nm using ε = 221 M^{-1} cm^{-1} for independently synthesized [Cu^{II}(TPMA)NCS][Br] and 897 nm using ε = 131 M^{-1} cm^{-1} for independently synthesized [Cu^{II}(M1-T2)NCS][Br].

Investigations into the observed rate constant (k_{obs}) were also performed. The first order kinetic plots for ATRA of carbon tetrabromide (CBr_4) to methyl methacrylate (MMA) in the presence of ascorbic acid as reducing agent using the TPMA and M1-T2 catalysts are shown in Figure 2.18. The k_{obs} for the M1-T2 complex was approximately double that of the TPMA complex, which were calculated to be 2.8 x 10^{-5} s^{-1} and 1.5 x 10^{-5} s^{-1}, respectively.

The kinetic results for k_{act} and k_{obs} indicate that the M1-T2 complex is more active than the TPMA complex when used in ATRA and ATRP systems. These findings are in agreement with cyclic voltammetry data obtained.

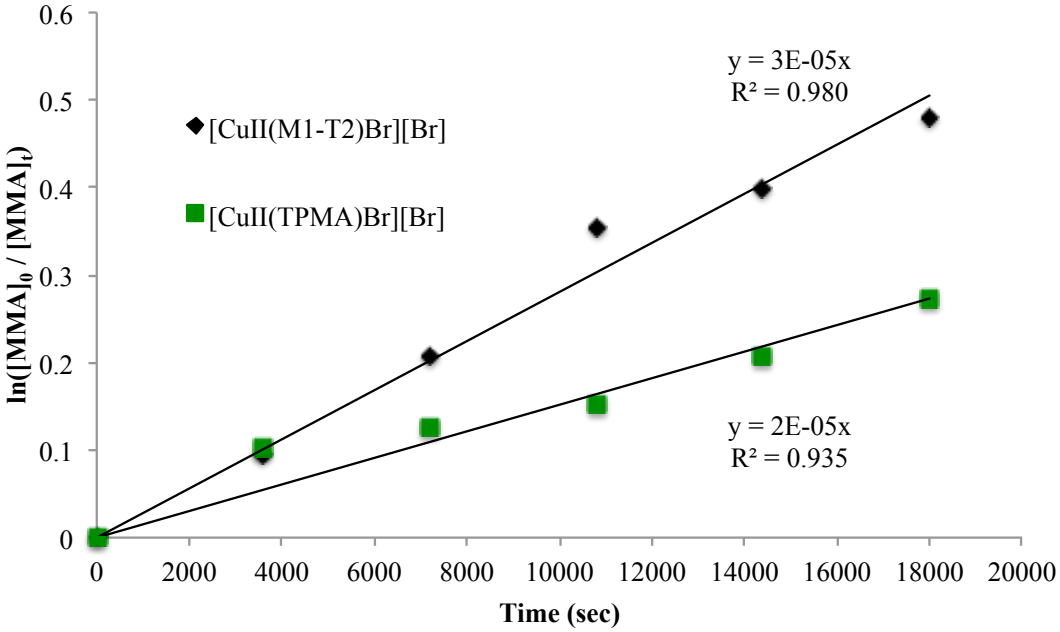

Figure 2.18 First order kinetic plot for ATRA of carbon tetrabromide to methyl methacrylate (MMA) in the presence of ascorbic acid as the reducing agent. [alkene]:[alkyl halide]:[ascorbic acid] = 1:1.25:0.07, $[alkene]_0$ = 1.34 M, Solvent = MeOH, Temp. = 23 °C, Catalyst loading: 50 ppm relative to alkene.

2.4.5 Atom Transfer Racial Addition Using Novel Highly Active Catalysts

One of the most advantageous atom transfer radical strategies is ARGET. The primary reason being that one of the reducing agents that can be employed is ascorbic acid. This reducing agent is environmentally friendly and inexpensive making it an attractive reagent for the reduction of Cu^{II}.[42-43] One of the most active catalysts employed for ARGET is $[Cu^{II}(TPMA)X][X]$ with X = Br or Cl.[6, 23, 44-45] For other ATRA systems i.e. ICAR, SARA, and photo $[Cu^{II}(Me_6TREN)X][X]$ is typically more active than its TPMA analogue. The major drawback with the Me_6TREN catalyst complex when employed in AGRET ATRA utilizing ascorbic acid as reducing agent is that its aliphatic arms become protonated in the presence of strong acid rendering the catalyst inactive. Scheme 2.5 shows the oxidation of ascorbic acid to dehydroascorbic acid.[42] TPMA complexes are not protonated as readily, making it more active in ARGET systems utilizing ascorbic acid. The aim here was to develop Me_6TREN-TPMA hybrid ligands that are less susceptible to protonation but retain the high activity of TPMA complexes. Hybrid ligands were synthesized via a reductive amination protocol adopted from Britovsek and coworkers[19] and their activity evaluated in ATRA reactions using polyhalogenated and monohalogenated alkyl halides.

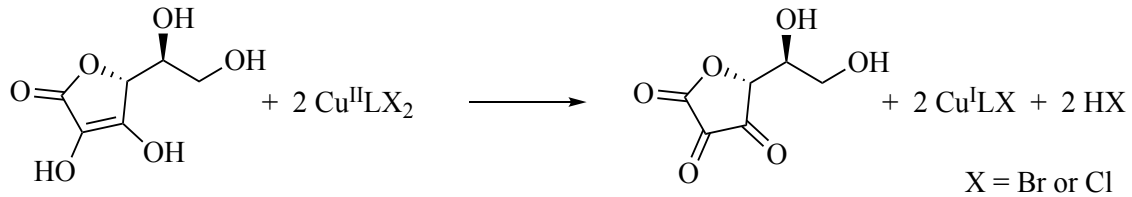

Scheme 2.5 Oxidation of ascorbic acid to dehydroascorbic acid producing strong acid during atom transfer radical processes.

2.4.5.1 ARGET ATRA of Polyhalogenated Alkyl Halides

Initially ARGET ATRA reactions were carried out using polyhalogenated alkyl halides carbon tetrabromide (CBr_4) and carbon tetrachloride (CCl_4) in the presence of weak base triethylamine, which was utilized to neutralize the formation of strong acid during the oxidation of ascorbic acid to dehydroascorbic acid shown in Scheme 2.5. ATRA reactions were performed using a variety of alkenes including simple α-olefins such as 1-octene in addition to alkenes that have a greater tendency to polymerize such as methyl acrylate (MA), methyl methacrylate (MMA), and acrylonitrile.

Based on kinetic and electrochemical evaluations for the bromide and chloride hybrid ligand complexes, $[Cu^{II}(M1\text{-}T2)X][X]$ and $[Cu^{II}(M2\text{-}T1)X][X]$, it was hypothesized these novel catalysts will be more active in ARGET ATRA reactions compared to the TPMA complex. Initially, the reaction temperature was optimized in addition to examining the affect of a weak base in preserving the catalysts structure and hence its efficiency. ARGET ATRA reactions were set up using the novel complex $[Cu^{II}(M1\text{-}T2)Cl][Cl]$ where the reaction consisted of catalyst, alkene (1-octene), and initiator (CCl_4). The reactions were carried out for 24 hours at various temperatures and in the presence and absence of weak base, triethylamine, MeOH as solvent with the following molar ratios: [alkene]:[alkyl halide]:[ascorbic acid] = 1:1.25:0.07, $[alkene]_o$ = 1.34 M. The general reaction is shown in Scheme 2.6. The internal standard used was 1,4-dimethoxy benzene and % Yield was based on the formation of monoadduct and was determined using ^{1}H-NMR spectroscopy.

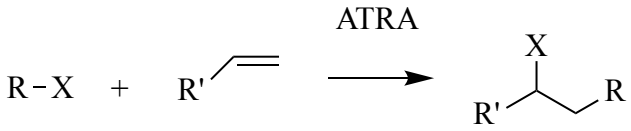

Scheme 2.6. General ARGET ATRA scheme for addition of alkyl halides to alkenes forming monoadduct. Reactions were carried out at various temperatures and in the presence and absence of weak base.

From the data shown in Table 2.3, it is evident that the optimal conditions involve running the reaction at lower temperatures, 23 °C, and in the presence of triethylamine. Evaluating entries 4, 8, and 12 in Table 2.3 for the 10,000-1 [alkene:Cu^{II}] catalyst loading (100 ppm), it is evident that the lowering of the temperature and the addition of triethylamine improve the catalytic efficiency giving 73% conversion of the alkene and 73% yield of monoadduct. Additionally this data indicates good selectivity in that all converted alkene was formed into monoadduct rather than byproducts.

Table 2.3 ARGET ATRA of CCl_4 to 1-octene using $[Cu^{II}(M1\text{-}T2)Cl][Cl]$ and ascorbic acid as the reducing agent in the presence and absence of triethylamine. Reactions were performed in MeOH at 60 °C or 23 °C for 24 h with $[alkene]_0$:$[CCl_4]_0$:[ascorbic acid]$_0$ = 1:1.25:0.07, $[alkene]_0$ = 1.34 M. Ratio of base to ascorbic acid = 5:1. The yield is based on the formation of monoadduct and was determined using ^{1}H NMR spectroscopy (errors ± 10%).

Entry	Alkene	Temp /Base	$[Alkene]_0$:$[Cu^{II}]_0$	% Conv.	% Yield
1	1-Octene	60°C	500:1	71	61
2			1,000:1	60	53
3			5,000:1	30	29
4			10,000:1	33	27
5	1-Octene	60°C / Et_3N	500:1	88	86
6			1,000:1	96	82
7			5,000:1	82	57
8			10,000:1	59	55
9	1-Octene	23°C / Et_3N	500:1	94	94
10			1,000:1	94	94
11			5,000:1	91	91
12			10,000:1	73	73

Following optimization of temperature and investigating the use of a weak base in ARGET ATRA systems, additional experiments were conducted to compare the activity of the novel complexes, $[Cu^{II}(M1\text{-}T2)Cl][Cl]$ and $[Cu^{II}(M1\text{-}T2)Br][Br]$, to that of the TPMA complex using additional alkenes shown in Tables 2.4 and 2.5. It is evident from the data that the M1-T2 hybrid ligand complex is indeed more active than the TPMA complex, which is indicative of the increased % yield of monoadduct and higher turnover numbers.

Table 2.4 ARGET ATRA reactions for $[Cu^{II}(M1\text{-}T2)Cl][Cl]$ and $[Cu^{II}(TPMA)Cl][Cl]$ were performed in MeOH in the presence of triethylamine (ratio of base : ascorbic acid was 5:1) for 24 h with $[alkene]_0$;$[CCl_4]_0$:$[ascorbic\ acid]_0$ = 1:1.25:0.07, $[alkene]_0$ = 1.34 M. The yield is based on the formation of monoadduct and was determined using ^1H NMR spectroscopy (errors ± 10%). Octene and MMA data were collected at 23 °C and MA at 60 °C.

Entry	Alkene	$[Alkene]_0$:$[Cu^{II}]_0$	M1-T2 Complex (% Conv./% Yield)	TPMA Complex (% Conv./% Yield)	TON (M1-T2 / TPMA)
1	1-Octene	1,000-1	94 / 84	90 / 90	822 / 690
2		5,000-1	91 / 76	24 / 24	1467 / 1200
3		10,000-1	73 / 65	14 / 14	2380 / 1400
4	Methyl Methacrylate	250-1	>99 / 77	>99	214 / 193
5		500-1	>99 / 88	98 / 59	432 / 295
6		1,000-1	>99 / 54	94 / 39	531 / 390
7	Methyl Acrylate	250-1	80 / 58	43 / 39	145 / 98
8		500-1	>99 / 38	26 / 22	177 / 110
9		1,000-1	97 / 30	28 / 17	296 / 170

Table 2.5 Reactions for $[Cu^{II}(M1\text{-}T2)Br][Br]$ were performed in MeOH at 23 °C for 24 h with $[alkene]_0$;$[CBr_4]_0$:$[ascorbic\ acid]_0$ = 1:1.25:0.07, $[alkene]_0$ = 1.34 M. The yield is based on the formation of monoadduct and was determined using ^1H NMR spectroscopy (errors ± 10%). All conditions were identical for $[Cu^{II}(TPMA)Br][Br]$ reactions except temperature (60 °C). Catalyst loading of 20,000:1 correlates to 50 ppm.

Entry	Alkene	$[Alkene]_0$:$[Cu^{II}]_0$	M1-T2 Complex (% Conv./% Yield)	TPMA Complex (% Conv./% Yield)
1	1-Octene	20,000 : 1	>99 / 99	>99/76
2	Methyl Methacrylate	20,000 : 1	91 / 40	80 / 31
3	Acrylonitrile	20,000 : 1	71 / 68	80 / 59

2.4.5.2 ARGET ATRA of Monohalogentated Alkyl Halides

Initially, hybrid ligand complexes were evaluated in ARGET ATRA reactions implementing polyhalogenated alkyl halides, CBr_4 and CCl_4. These alkyl halides work well for preliminary investigations but there is greater interest in the synthetic community for utilizing monohalogenated alkyl halides. From a synthetic point of view, the primary reason for increased interest for employing monohalogenated alkyl halides, e.g. chloroacetonitrile (ClAN) or chloropropionitrile (ClPN), is that the monoadduct is synthetically more attractive in comparison to those produced when using polyhalogenated alkyl halides such as CBr_4 or CCl_4. Examples of each monoadduct are shown in Figure 2.18. The monoadduct shown on the right in Figure 2.18 is a more applicable reagent for further synthetic techniques. Additionally, polyhalogenated alkyl halides tend to possess a greater toxicity and are more environmentally unfriendly compare to their monohalogenated counterparts.

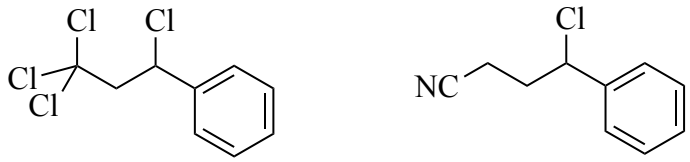

Figure 2.19 Monoadduct formed via ATRA of polyhalogenated CCl_4 (left) and monohalogenated ClAN (right) to styrene.

The activity of the hybrid ligand complex, $[Cu^{II}(M1\text{-}T2)Cl][Cl]$ in ARGET ATRA reactions utilizing monohalogenated alkyl halides was examined. The reactions were carried out in a similar manner to those using polyhalogenated alkyl halides and are shown in Scheme 2.7.

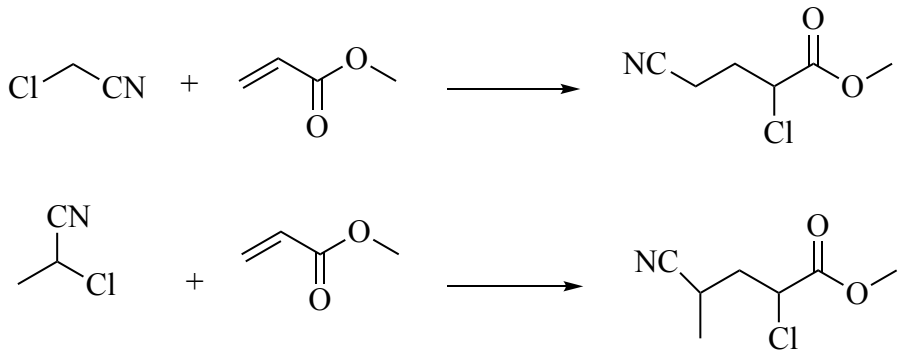

Scheme 2.7 ARGET ATRA reactions schemes for the addition of chloroacetonitrile (top) and chloropropionitrile (bottom) to methyl acrylate.

When implementing monohalogenated alkyl halides in ATRA or ATRP processes, a decrease in % conversion and % yield is typically observed due to their lower activity. Similar to the effects of different ligands on $K_{ATRA/ATRP}$, different initiators also affect the equilibrium constant for atom transfer radical processes. Although polyhalogenated alkyl halides provide a more synthetically useful monoadduct, they decrease K_{ATRA} and therefore decrease the % conversion and % yield. The hybrid ligand complex shows an increased activity for the addition of ClAN to methyl acrylate nearly doubling percent yield as shown in Table 2.6, entries 1 and 2. The M1-T2 and TPMA complexes showed comparable percent yields for the addition of ClPN to methyl acrylate (entries 3 and 4). A possible reason could be due to the decreased initiator efficiency of ClPN compared to that of ClAN.

Table 2.6 ATRA of chloroacetonitrile and chloropropionitrile to methyl acrylate using ascorbic acid as the reducing agent and in the presence of 2,2,6,6-tetramethylpiperidine. Reactions were performed in MeOH at 60 ^{o}C for 24 h with $[alkene]_0$;$[ClAN]_0$:$[ascorbic\ acid]_0$ = 1:1.25:0.07, $[alkene]_0$ = 1.34 M. Ratio of base to ascorbic acid = 5:1. The yield is based on the formation of monoadduct and was determined using ^{1}H NMR spectroscopy (errors ± 10%).

Entry	Alkene	Alkyl Halide	$[Alkene]_0$:$[Cu^{II}]_0$	M1-T2 Complex (% Conv./% Yield)	TPMA Complex (% Conv./% Yield)
1	Methyl Acrylate	Chloroacetonitrile	100 : 1	75 / 65	63 / 50
2			250 : 1	74 / 68	88 / 35
3	Methyl Acrylate	Chloropropionitrile	100 : 1	>99 / 34	95 / 33
4			250 : 1	>99 / 22	95 / 27

2.5 Summary and Conclusions

Novel, highly active novel hybrid ligands, M1-T2 and M2-T1, were successfully synthesized via reductive amination synthetic protocols. When complexed to a copper center, the hybrid ligand complexes, $[Cu^{II}$(M1-T2)Br][Br], Cu^{I}(M1-T2)Br, $[Cu^{II}$(M2-T1)Br][Br] share structural similarities with TPMA and Me_6TREN complexes. Utilizing single-crystal XRD, it was determined that the novel Cu^{II} complexes have a distorted trigonal bipyramidal molecular structure as evident by their tau values: $[Cu^{II}$(M1-T2)Br][Br] (τ = 0.70), $[Cu^{II}$(M2-T1)Br][Br] (τ = 0.87). The TPMA and Me_6TREN Cu^{II} complexes have τ = 1.00 and are considered to have trigonal bipyramidal molecular structures. When probing their structures in solution, the UV-Vis data indicated that both $[Cu^{II}$(M1-T2)Br][Br] and $[Cu^{II}$(M2-T1)Br][Br] retain their trigonal bipyramidal structure indicative by the two strong absorption bands observed in the spectra. Additionally, the $[Cu^{II}$(M1-T2)Br][Br] was shown to be a fluxional system in solution evident by variable

temperature NMR spectroscopy evaluation. While in solution, one of the TPMA arms dissociated from the copper center providing insight into the ATRA/ATRP mechanism.

Electrochemical studies were performed on the hybrid ligand complexes. These studies suggested that the M1-T2 and M2-T1 complexes should be more active in atom transfer radical systems due to their more negative reduction potentials, which were calculated to be -774 mV, -749 mV, and -720 mV for $[Cu^{II}(M2\text{-}T1)Br][Br]$, $[Cu^{II}(M1\text{-}T2)Br][Br]$, and $[Cu^{II}(TPMA)Br][Br]$, respectively. A similar trend was observed for the chloride catalysts with reduction potentials of -864 mV, -835 mV, and -761 mV for $[Cu^{II}(M2\text{-}T1)Cl][Cl]$, $[Cu^{II}(M1\text{-}T2)Cl][Cl]$, and $[Cu^{II}(TPMA)Cl][Cl]$, respectively. Additionally, the cyclic voltammetry data indicated that the oxidation-reduction of the copper center is a quasi-reversible one-electron process.

Kinetic evaluations were performed on $Cu^{I}(M1\text{-}T2)Br$ and $Cu^{I}(TPMA)Br$ utilizing a radical trapping method. The rate constant (k_a) for activation of alkyl halides was calculated by utilizing UV-Vis spectroscopy and monitoring for the formation of the Cu^{II} complex. It was determined that both complexes followed pseudo first-order kinetics and the activation rate constants were calculated to be 6.8×10^{-3} $M^{-1}s^{-1}$ and 4.1×10^{-4} $M^{-1}s^{-1}$ for $Cu^{I}(M1\text{-}T2)Br$ and $Cu^{I}(TPMA)Br$, respectively. Additionally, a first-order kinetic plot was created and the observed rate constant (k_{obs}) was calculated for ATRA of carbon tetrabromide to methyl methacrylate (MMA) in the presence of ascorbic acid as the reducing agent. For $[Cu^{II}(M1\text{-}T2)Br][Br]$ and $[Cu^{II}(TPMA)Br][Br]$ the k_{obs} was calculated to be 2.8×10^{-5} s^{-1} and 1.5×10^{-5} s^{-1}, respectively. The kinetic results support the electrochemical data indicating that the hybrid ligand complexes should be more active than their TPMA analogues in atom transfer radical processes.

As expected, when complexed to a copper center, hybrid ligand, M1-T2 displayed increased activity in ARGET ATRA reactions compared to the well-documented TPMA complex. When performing ATRA of monohalogenated chloroacetonitrile to methyl acrylate, $[Cu^{II}(M1\text{-}T2)Cl][Cl]$ produced a monoadduct % yield = 68, which almost doubles that produced for $[Cu^{II}(TPMA)Cl][Cl]$ (% yield = 35). The ATRA data suggests that hybrid ligand complexes are at minimum comparable and in most cases exceed the activity of TPMA complexes. This increased activity is due to the hybrid ligand containing one or two Me_6TREN arms. Although Me_6TREN complexes are more active than TPMA complexes, they are more easily protonated due to the formation of strong acid when implementing environmentally friendly ascorbic acid as reducing agent. The hybrid ligand complexes reported here preserve the high activity of Me_6TREN complexes but also possess the robustness of TPMA complexes when utilized in ARGET atom transfer radical systems.

From the time this work reported here was performed, ligands with greater activity than M1-T2 and TPMA have been reported. These novel ligands possess electron-donating groups e.g. $–OCH_3$ and $–NMe_2$ on the TPMA scaffold providing equilibrium constants for atom transfer radical processes orders of magnitude greater than that of M1-T2 and TPMA complexes.[46]

2.6 References

1. Curran, D. P. The Design and Application of Free Radical Chain Reactions in Organic Synthesis. Part 1. *Synthesis* **1988,** *1988* (06), 417-439.

2. Bellesia, F.; Clark, A. J.; Felluga, F.; Gennaro, A.; Isse, A. A.; Roncaglia, F.; Ghelfi, F. Efficient and Green Route to γ-Lactams by Copper-Catalysed Reversed Atom

Transfer Radical Cyclisation of α-Polychloro-N-allylamides, using a Low Load of Metal (0.5 mol%). *Advanced Synthesis & Catalysis* **2013,** *355* (8), 1649-1660.

3. Krzysztof, M. From Atom Transfer Radical Addition to Atom Transfer Radical Polymerization. *Current Organic Chemistry* **2002,** *6* (2), 67-82.

4. Kharasch, M. S.; Engelmann, H.; Mayo, F. R. The Peroxide Effect In The Addition of Reagents to Unsaturated Compounds. XV. The Addition of Hydrogen Bromide to 1- and 2-Bromo- And Chloropropenes. *The Journal of Organic Chemistry* **1937,** *02* (3), 288-302.

5. Kharasch, M. S.; Urry, W. H.; Jensen, E. V. Addition of Derivatives of Chlorinated Acetic Acids to Olefins. *Journal of the American Chemical Society* **1945,** *67* (9), 1626-1626.

6. Clark, A. J. Atom transfer radical cyclisation reactions mediated by copper complexes. *Chemical Society Reviews* **2002,** *31* (1), 1-11.

7. Minisci, F. Free-radical additions to olefins in the presence of redox systems. *Accounts of Chemical Research* **1975,** *8* (5), 165-171.

8. Kay, S. Ruthenium Catalysts for the Kharasch Reaction. *Current Organic Chemistry* **2006,** *10* (2), 217-224.

9. Simal, F.; Wlodarczak, L.; Demonceau, A.; Noels, Alfred F. New, Highly Efficient Catalyst Precursors for Kharasch Additions − [RuCl(Cp*)(PPh3)2] and [RuCl(Ind)(PPh3)2]. *European Journal of Organic Chemistry* **2001,** *2001* (14), 2689-2695.

10. Gossage, R. A.; van de Kuil, L. A.; van Koten, G. Diaminoarylnickel(II) "Pincer" Complexes: Mechanistic Considerations in the Kharasch Addition Reaction, Controlled Polymerization, and Dendrimeric Transition Metal Catalysts. *Accounts of Chemical Research* **1998,** *31* (7), 423-431.

11. Xue, G.; Wang, D.; De Hont, R.; Fiedler, A. T.; Shan, X.; Münck, E.; Que, L. A synthetic precedent for the [FeIV2(μ-O)2] diamond core proposed for methane monooxygenase intermediate Q. *Proceedings of the National Academy of Sciences* **2007,** *104* (52), 20713-20718.

12. Quebatte, L.; Thommes, K.; Severin, K. Highly Efficient Atom Transfer Radical Addition Reactions with a RuIII Complex as a Catalyst Precursor. *Journal of the American Chemical Society* **2006,** *128* (23), 7440-7441.

13. Eckenhoff, W. T.; Garrity, S. T.; Pintauer, T. Highly Efficient Copper-Mediated Atom-Transfer Radical Addition (ATRA) in the Presence of Reducing Agent. *European Journal of Inorganic Chemistry* **2008,** *2008* (4), 563-571.

14. Matyjaszewski, K.; Paik, H.-j.; Zhou, P.; Diamanti, S. J. Determination of Activation and Deactivation Rate Constants of Model Compounds in Atom Transfer Radical Polymerization. *Macromolecules* **2001,** *34* (15), 5125-5131.

15. Matyjaszewski, K. Atom Transfer Radical Polymerization (ATRP): Current Status and Future Perspectives. *Macromolecules* **2012,** *45* (10), 4015-4039.

16. Elsen, A. M.; Burdyńska, J.; Park, S.; Matyjaszewski, K. Activators Regenerated by Electron Transfer Atom Transfer Radical Polymerization in Miniemulsion with 50 ppm of Copper Catalyst. *ACS Macro Letters* **2013,** *2* (9), 822-825.

17. Reiser, O. Shining Light on Copper: Unique Opportunities for Visible-Light-Catalyzed Atom Transfer Radical Addition Reactions and Related Processes. *Accounts of Chemical Research* **2016,** *49* (9), 1990-1996.

18. Knorn, M.; Rawner, T.; Czerwieniec, R.; Reiser, O. [Copper(phenanthroline)(bisisonitrile)]+-Complexes for the Visible-Light-Mediated Atom Transfer Radical Addition and Allylation Reactions. *ACS Catalysis* **2015,** *5* (9), 5186-5193.

19. Britovsek, G. J. P.; England, J.; White, A. J. P. Non-heme Iron(II) Complexes Containing Tripodal Tetradentate Nitrogen Ligands and Their Application in Alkane Oxidation Catalysis. *Inorganic Chemistry* **2005,** *44* (22), 8125-8134.

20. Spek, A. Single-crystal structure validation with the program PLATON. *Journal of Applied Crystallography* **2003,** *36* (1), 7-13.

21. Sheldrick, G. M. *SADABS Version 2.03*: University of Gottingen: Gottingen, Germany, 2002.

22. Sheldrick, G. M. *SHELXTL 6.1, Crystallographic Computing System; Bruker Analytical X-Ray System*: Madison, WI, 2000.

23. Kaur, A.; Ribelli, T. G.; Schröder, K.; Matyjaszewski, K.; Pintauer, T. Properties and ATRP Activity of Copper Complexes with Substituted Tris(2-pyridylmethyl)amine-Based Ligands. *Inorganic Chemistry* **2015,** *54* (4), 1474-1486.

24. Abdel-Magid, A. F.; Carson, K. G.; Harris, B. D.; Maryanoff, C. A.; Shah, R. D. Reductive Amination of Aldehydes and Ketones with Sodium Triacetoxyborohydride. Studies on Direct and Indirect Reductive Amination Procedures1. *The Journal of Organic Chemistry* **1996,** *61* (11), 3849-3862.

25. Ahmed, F. A.-M.; Cynthia, A. M. Use of Sodium Triacetoxyborohydride in Reductive Amination of Ketones and Aldehydes. In *Reductions in Organic Synthesis*; American Chemical Society, 1996; Vol. 641, pp 201-216.

26. Ahmed, F. A.-M. *Reductions in Organic Synthesis* [doi:10.1021/bk-1996-0641]; American Chemical Society1996; Vol. 641. p 244.

27. Eckenhoff, W. T.; Pintauer, T. Atom transfer radical addition (ATRA) catalyzed by copper complexes with tris[2-(dimethylamino)ethyl]amine (Me6TREN) ligand in the presence of free-radical diazo initiator AIBN. *Dalton Transactions* **2011,** *40* (18), 4909-4917.

28. Eckenhoff, W. T.; Pintauer, T. Structural Comparison of Copper(I) and Copper(II) Complexes with Tris(2-pyridylmethyl)amine Ligand. *Inorganic Chemistry* **2010,** *49* (22), 10617-10626.

29. Weitzer, M.; Schatz, M.; Hampel, F.; Heinemann, F. W.; Schindler, S. Low temperature stopped-flow studies in inorganic chemistry. *Journal of the Chemical Society, Dalton Transactions* **2002,** (5), 686-694.

30. Kawa, C. J. Finding the bond angle in a tetrahedral shaped molecule. *Journal of Chemical Education* **1988,** *65* (10), 884.

31. Addison, A. W.; Rao, T. N.; Reedijk, J.; van Rijn, J.; Verschoor, G. C. Synthesis, structure, and spectroscopic properties of copper(II) compounds containing nitrogen-sulphur donor ligands; the crystal and molecular structure of aqua[1,7-bis(N-methylbenzimidazol-2[prime or minute]-yl)-2,6-dithiaheptane]copper(II) perchlorate. *Journal of the Chemical Society, Dalton Transactions* **1984,** (7), 1349-1356.

32. Eckenhoff, W. T.; Biernesser, A. B.; Pintauer, T. Kinetic and Mechanistic Aspects of Atom Transfer Radical Addition (ATRA) Catalyzed by Copper Complexes with Tris(2-pyridylmethyl)amine. *Inorganic Chemistry* **2012,** *51* (21), 11917-11929.

33. Tang, W.; Kwak, Y.; Braunecker, W.; Tsarevsky, N. V.; Coote, M. L.; Matyjaszewski, K. Understanding Atom Transfer Radical Polymerization: Effect of Ligand and Initiator Structures on the Equilibrium Constants. *Journal of the American Chemical Society* **2008,** *130* (32), 10702-10713.

34. Nicolay, V. T.; Wade, A. B.; Wei, T.; Krzysztof, M. The Atom Transfer Radical Polymerization Equilibrium: Structural and Medium Effects. In *Controlled/Living Radical Polymerization: Progress in ATRP*; American Chemical Society, 2009; Vol. 1023, pp 85-96.

35. Elgrishi, N.; Rountree, K. J.; McCarthy, B. D.; Rountree, E. S.; Eisenhart, T. T.; Dempsey, J. L. A Practical Beginner's Guide to Cyclic Voltammetry. *Journal of Chemical Education* **2018,** *95* (2), 197-206.

36. Goto, A.; Fukuda, T. Determination of the activation rate constants of alkyl halide initiators for atom transfer radical polymerization. *Macromolecular Rapid Communications* **1999,** *20* (12), 633-636.

37. Ohno, K.; Goto, A.; Fukuda, T.; Xia, J.; Matyjaszewski, K. Kinetic Study on the Activation Process in an Atom Transfer Radical Polymerization. *Macromolecules* **1998,** *31* (8), 2699-2701.

38. Chambard, G.; Klumperman, B.; German, A. L. Effect of Solvent on the Activation Rate Parameters for Polystyrene and Poly(butyl acrylate) Macroinitiators in Atom Transfer Radical Polymerization. *Macromolecules* **2000,** *33* (12), 4417-4421.

39. Horn, M.; Matyjaszewski, K. Solvent Effects on the Activation Rate Constant in Atom Transfer Radical Polymerization. *Macromolecules* **2013,** *46* (9), 3350-3357.

40. Tang, W.; Matyjaszewski, K. Effect of Ligand Structure on Activation Rate Constants in ATRP. *Macromolecules* **2006,** *39* (15), 4953-4959.

41. Balili, M. N. C.; Pintauer, T. Kinetic Studies of the Initiation Step in Copper Catalyzed Atom Transfer Radical Addition (ATRA) in the Presence of Free Radical Diazo Initiators as Reducing Agents. *Inorganic Chemistry* **2010,** *49* (12), 5642-5649.

42. Taylor, M. J. W.; Eckenhoff, W. T.; Pintauer, T. Copper-catalyzed atom transfer radical addition (ATRA) and cyclization (ATRC) reactions in the presence of environmentally benign ascorbic acid as a reducing agent. *Dalton Transactions* **2010,** *39* (47), 11475-11482.

43. Min, K.; Gao, H.; Matyjaszewski, K. Use of Ascorbic Acid as Reducing Agent for Synthesis of Well-Defined Polymers by ARGET ATRP. *Macromolecules* **2007,** *40* (6), 1789-1791.

44. Eckenhoff, W. T.; Pintauer, T. Atom Transfer Radical Addition in the Presence of Catalytic Amounts of Copper(I/II) Complexes with Tris(2-pyridylmethyl)amine. *Inorganic Chemistry* **2007,** *46* (15), 5844-5846.

45. Eckenhoff, W. T.; Pintauer, T. Copper Catalyzed Atom Transfer Radical Addition (ATRA) and Cyclization (ATRC) Reactions in the Presence of Reducing Agents. *Catalysis Reviews* **2010,** *52* (1), 1-59.

46. Ribelli, T. G.; Fantin, M.; Daran, J.-C.; Augustine, K. F.; Poli, R.; Matyjaszewski, K. Synthesis and Characterization of the Most Active Copper ATRP Catalyst Based on Tris[(4-dimethylaminopyridyl)methyl]amine. *Journal of the American Chemical Society* **2018,** *140* (4), 1525-1534.

Chapter 3

Synthesis of Hydrophilic (Co)Polymers Via Atom Transfer Radical Polymerization and Their Characterization Using High Resolution Mass Spectrometry and Nuclear Magnetic Resonance Spectroscopy

3.1 Introduction

Atom transfer radical polymerization (ATRP) has become one of the most advantageous synthetic protocols for polymers. It is considered a controlled/living radical process that allows for the synthesis of polymers with predetermined molecular weights, narrow polydispersity indices (PDI), and high end-group functionality.[1-5] ATRP has been shown to be a robust method and tolerant of various solvents, reaction conditions, and functional groups hence a plethora of architectures and compositions can be realized.[6-8] Additional controlled radical polymerization strategies exist such as nitroxide mediated polymerization (NMP) and reversible addition-fragmentation chain transfer (RAFT) polymerization.[9-13]

ATRP and traditional free-radical polymerizations are similar in that they both proceed via initiation, propagation, and termination reactions involving radicals. Traditional free-radical polymerizations provide broad PDIs and predetermined molecular weights are difficult to achieve. These attributes are primarily due to the lifetime of growing chains is relatively short, the number of growing chains decreases throughout the reaction, and the concentration of initiating species slowly decreases.[14] In contrast to these characteristics, in controlled/living radical polymerizations the lifetime of growing chains is similar to reaction time, the number of growing chains is constant, and the initiator concentration rapidly decreases allowing for narrow PDIs (<1.5) and

predetermined molecular weights. Additionally, controlled/living radical polymerizations allow for the formation of complex architectures due to their high end-group functionality that is retained throughout the polymerization, which is in contrast to polymers formed via traditional free-radical polymerizations.

ATRP is primarily controlled by the dynamic equilibrium between propagating radicals (P_n•) and dormant species (P_n-X) as shown in Scheme 3.1.[15] To provide a low concentration of radicals and maintain a low number of growing polymer chains, the rate of deactivation (k_{deact}) must be larger than the rate of activation (k_{act}),[16] in other words $k_{deact} >> k_{act}$.

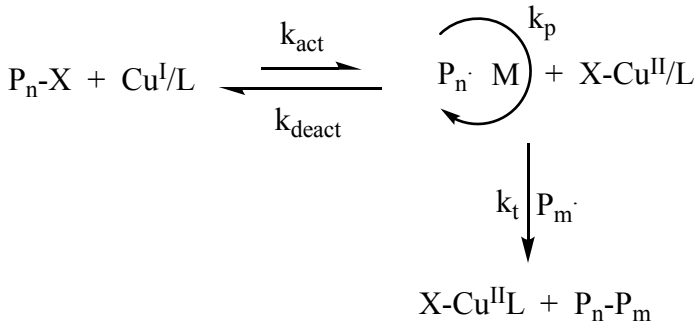

Scheme 3.1 ATRP equilibrium showing magnitudes of the activation and deactivation rates and radical-radical termination. (L = complexing ligand, X = Cl or Br, M = monomer)

There exists a variety of ATRP protocols each utilizing different reducing agents. ARGET implements ascorbic acid or tin (II) 2-ethylhexanoate, ICAR involves radical-based reducing agents, e.g. AIBN or V-70, and SARA utilizes zero-valent metals such as Cu^o and Zn^o.[1, 7] The methodology employed for synthesizing polymers discussed here is known as photo-initiated ATRP (photoATRP), which employs light as a reducing agent for regeneration of the activator, i.e. the copper complex in its lower oxidation state and is shown in Scheme 3.2.[4, 17-18] The use of light for reduction of the deactivator, i.e. copper

complex in its higher oxidation state, is advantageous compared to other catalyst regeneration methods since additional heavy metals are not required as in ARGET and SARA, strong acid is not produced from the oxidation of ascorbic acid (ARGET), and the radical concentration is not increased as in ICAR.

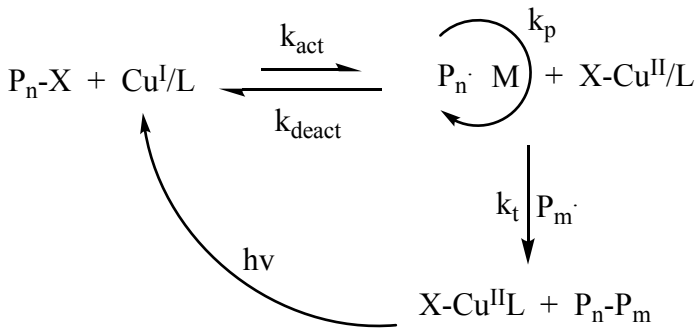

Scheme 3.2 Photo-regeneration of the activator complex in photoATRP.

3.2 Materials

All materials were used as received unless otherwise noted. Alumina, copper (II) bromide ($CuBr_2$), and ethy-2-bromoisobutyrate (EBiB) were purchased from Alfa Aesar (Fisher Scientific, Tewksbury MA). Copper (II) chloride ($CuCl_2$), dimethyl sulfoxide (DMSO), and 1,4-dimethoxybenzene were purchased from Sigma Aldrich (St. Louis MO). 2-Hydroxyethyl methacrylate (HEMA) and 2-(dimethylamino)ethyl methacrylate (DMAEMA) were purchased from Sigma Aldrich and passed through basic alumina to remove inhibitor. The monomers were stored at 4^0C prior to use. Optima grade methanol (MeOH), acetonitrile (ACN), formic acid, HPLC grade water, and reagent grade MeOH, were purchased from Fisher Scientific (Pittsburgh PA). Deuterated chloroform ($CDCl_3$) and deuterated dimethyl sulfoxide (DMSO-d_6) were purchased from

Cambridge Isotope Laboratories (Tewksbury MA). Ligand, tris[2-(dimethylamino)ethyl]amine (Me_6TREN) was synthesized according to a previously reported method.[19]

3.3 Methods and Instrumentation

3.3.1 Catalyst Synthesis

A 0.082 M catalyst solution was prepared with $Cu^{II}Br$ (2.06 x 10^{-5} mol) and Me_6TREN (1.24 x 10^{-4} mol) using MeOH or dimethyl sulfoxide (DMSO) as solvent. The solution was allowed to stir at 23 ^{o}C for 30 minutes.

3.3.2 Polymer Synthesis

The syntheses of poly(2-hydroxyethyl) methacrylate (PHEMA), poly(2-dimethylamino)ethyl methacrylate (PDMAEMA), and poly(2-hydroxyethyl) methacrylate-*ran*-(2-dimethylamino)ethyl methacrylate (poly(HEMA-*ran*-DMAEMA)) were carried out using a modified photoATRP protocol previously reported.[20] For PHEMA and PDMAEMA homopolymers, a solution containing 50% (v/v) solvent was prepared. For the random copolymer a ratio of 1:1:2 (v/v) HEMA:DMAEMA:solvent was used. This ratio was used for all target degrees of polymerization (DP). Solvents utilized were either MeOH or DMSO. Catalyst solution (0.082 M, 500 μL) was added to the reaction vial to give a final ratio of $[M]_0$:$[I]_0$:$[Cu^{II}]_0$:$[Me_6TREN]_0$ = [DP]:[1]:[0.02]:[0.12] for homopolymer synthesis and a ratio of $[M]_0$:$[M]_0$:$[I]_0$:$[Cu^{II}]_0$:$[Me_6TREN]_0$ = [10]:[10]:[1]:[0.02]:[0.12] for copolymer synthesis. A DP of 20 (HEMA = 10, DMAEMA = 10) was targeted for the random copolymer. 1,4

dimethoxybenzene (0.14 mmol) (1,4-DMB) was added as internal standard. Lastly, the initiator, ethyl-2-bromoisobutyrate (EBiB) (30.2 μL, 0.21 mmol) was added and a zero-time aliquot removed for analysis. The reaction vial was capped with a septum, sealed with electrical tape, and purged with nitrogen for 15 minutes. To begin the polymerization, the reaction vial was placed in a UV nail curing lamp ($\lambda_{max} \approx 360$ nm, 4x9 W bulbs), which was set on a magnetic stir plate and allowed to react for a predetermined amount of time.

3.3.3 Mass Spectrometry Characterization

High-resolution mass spectrometry (HRMS) experiments were performed using an Agilent 6530 Accurate Mass QTOF LC/MS (Agilent, Santa Clara CA) equipped with an electrospray ionization source (ESI) and operated in the positive mode. Either MeOH w/0.1% formic acid or ACN:water 50% v/v with 0.1% formic acid was used as mobile phase. The capillary voltage, skimmer voltage, and fragmentor voltage were optimized at 3 kV, 65 V, and 250 V, respectively. Drying and sheath gas temperatures were set at 350 ^{0}C. Crude polymer was dissolved in MeOH or ACN:water (50%, v/v) to a concentration of 1 mg mL^{-1}. The sample was introduced into the ionization source via flow injection analysis at a flow rate of 0.5 mL min^{-1} for PHEMA and 1.0 mL min^{-1} for both PDMAEMA and poly(HEMA-*ran*-DMAEMA). Data processing was carried out using MassHunter (Agilent, Santa Clara CA).

3.3.4 Nuclear Magnetic Resonance Spectroscopy Characterization

To determine percent monomer conversion and the number average molecular weight of polymers (M_n) via end-group analysis, ^{1}H NMR spectroscopy analyses were conducted using a 400 MHz spectrometer (Bruker, Billerica MA) equipped with TopSpin 3.2 software. Either $CDCl_3$ or DMSO-d_6 was used as solvent.

3.4 Results and Discussion

3.4.1 Atom Transfer Radical Polymerization of PHEMA and Characterization Using ^{1}H NMR Spectroscopy and High-Resolution Mass Spectrometry

The synthesis of hydrophilic polymer, PHEMA, was carried out by employing a previously reported photoATRP methodology.[20] The general reaction is shown in Scheme 3.3. A zero-time aliquot of the reaction mixture was taken prior to starting the polymerization for ^{1}H NMR spectroscopy analysis and is shown in Figure 3.1 including peak assignments.

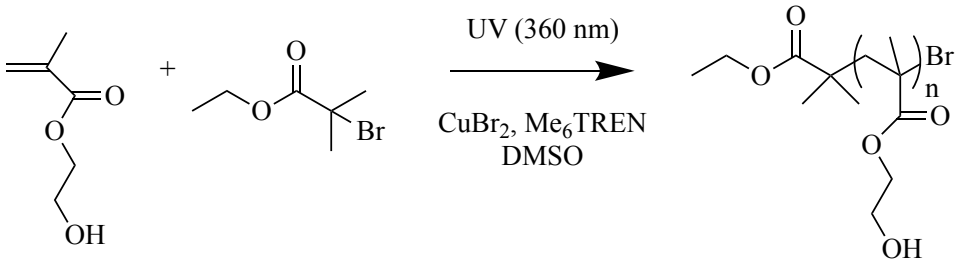

Scheme 3.3 PhotoATRP of HEMA using EBiB as initiator. The ratio of reagents was $[HEMA]_0:[I]_0:[Cu^{II}]_0:[Me_6TREN]_0$ = [20]:[1]:[0.02]:[0.12] in 50% v/v DMSO. $[I]_0:[Cu^{II}]_0$ = 50:1 (2 mol %)

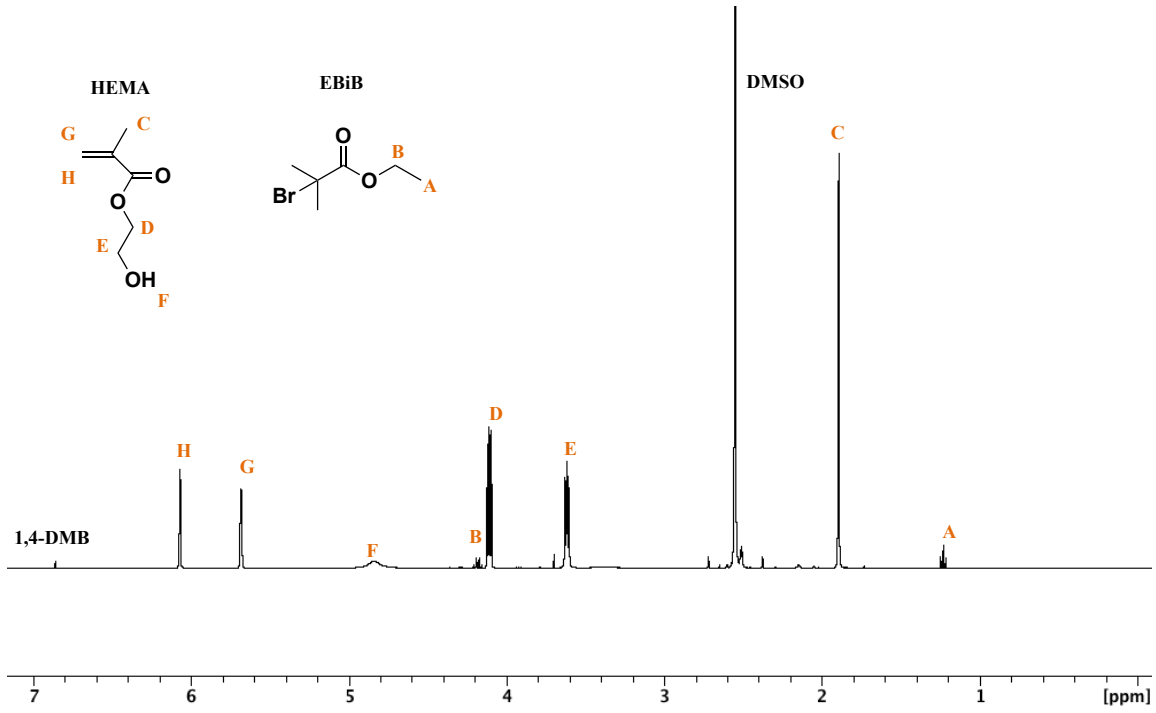

Figure 3.1 ^{1}H NMR spectrum for the zero-time aliquot of PHEMA ATRP reaction mixture including peak assignments. (400 MHz, DMSO-d_6, 298 K)

Following three and six hour reaction times, an aliquot of the reaction mixture was taken to determine percent monomer conversion. End-group analysis was performed to calculate M_n. The ^{1}H NMR spectrum after 3 hours reaction time is shown in Figure 3.2. The data for the three and six hour aliquots indicated a successful polymerization. After three hours reaction time, a 61% monomer conversion was determined. End-group analysis was performed providing an M_n of 2797 g/mol. As expected both monomer conversion (89%) and M_n (3709 g/mol) increased for the six hour reaction time. A summary of the reaction data is shown in Table 3.1.

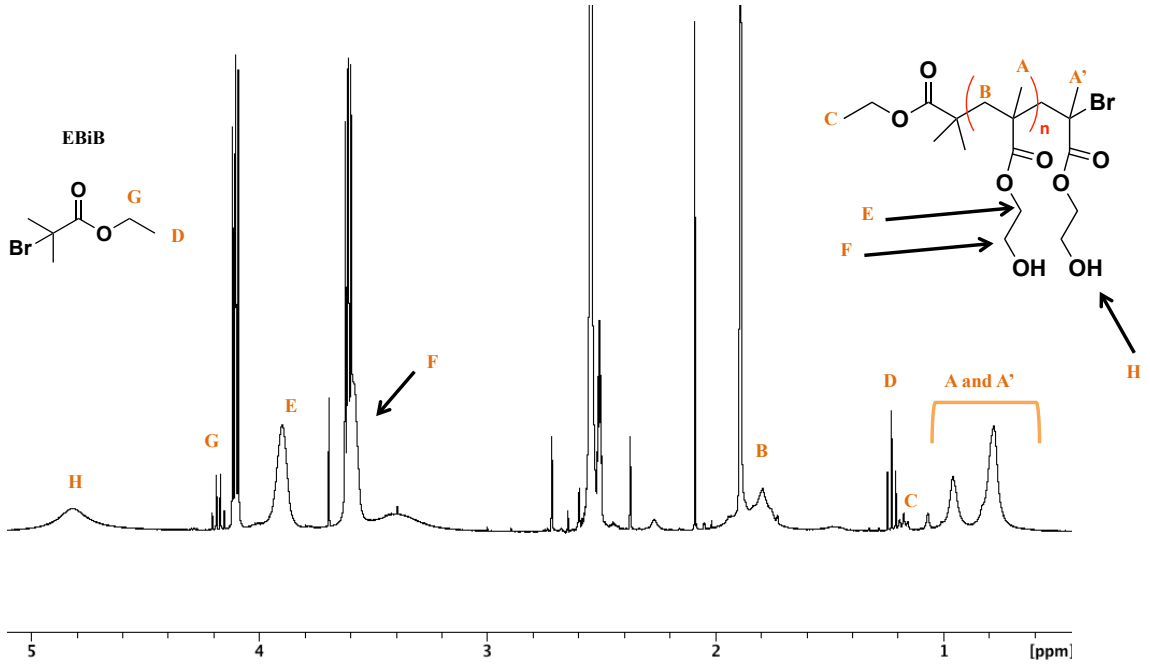

Figure 3.2 ^{1}H NMR spectrum of PHEMA ATRP reaction mixture after 3 hours reaction time including relevant peak assignments. (400 MHz, DMSO-d_6, 298 K)

Table 3.1 Summary of PHEMA reaction conditions, monomer conversions, and calculated M_n values. ^{a} Determined by ^{1}H-NMR analysis (DMSO-D_6).

Entry	Solvent	Target DP	Rxn. Time	Monomer Conv.[a]	M_n [a] (g/mol)
1	DMSO	20	3 hrs.	61 %	2797
2	DMSO	20	6 hrs.	89 %	3709

Following ^{1}H NMR spectroscopy analysis, PHEMA was characterized utilizing ESI-HRMS. The most prominent distribution observed in both the three and six hour reaction time PHEMA spectra (Figure 3.3), is a singly charged sodiated distribution, $[M+Na]^{+}$, which is terminated with bromine at the ω-end of the polymer chain and was expected due to the use of a brominated initiator and the mechanism of ATRP. Additionally, a doubly charged, sodiated distribution was observed containing bromine as the ω-end-group, $[M+2Na]^{2+}$. A third sodiated distribution was detected but possessed a

cyclic or vinyl ω end-group rather than bromine and is thought to arise in the ionization source due to the labile nature of the bromine atom. This observation was confirmed due to the absence of the signature brominated isotopic distribution. All peaks in each singly charged distribution are separated by 130 Da, the mass of the HEMA monomer.

Since a doubly charged, brominated distribution was present, $[M+2Na]^{2+}$, a deconvoluted mass spectrum was used to calculate M_n, which was determined to be 1557 g/mol and 1416 g/mol for the three and six hour reactions, respectively. These values are not in agreement with those calculated from the ^1H NMR spectra. This discrepancy is believed to be due to incomplete initiator activation, volatility, inefficient ionization, and solubility of higher molecular weight polymers when performing ESI-HRMS. The polydispersity index (PDI) for each reaction was calculated to be 1.35.

Due to the high resolution of the mass spectrometer, isotopic distributions were examined to confirm the most dominant distribution in the mass spectrum was indeed brominated. The observed m/z values are in good agreement with the calculated values of the bromine isotopic pattern for the peaks representing a degree of polymerization of 3 (DP = 3) where all have mass accuracies of < 7.4 ppm, shown in Table 3.2.

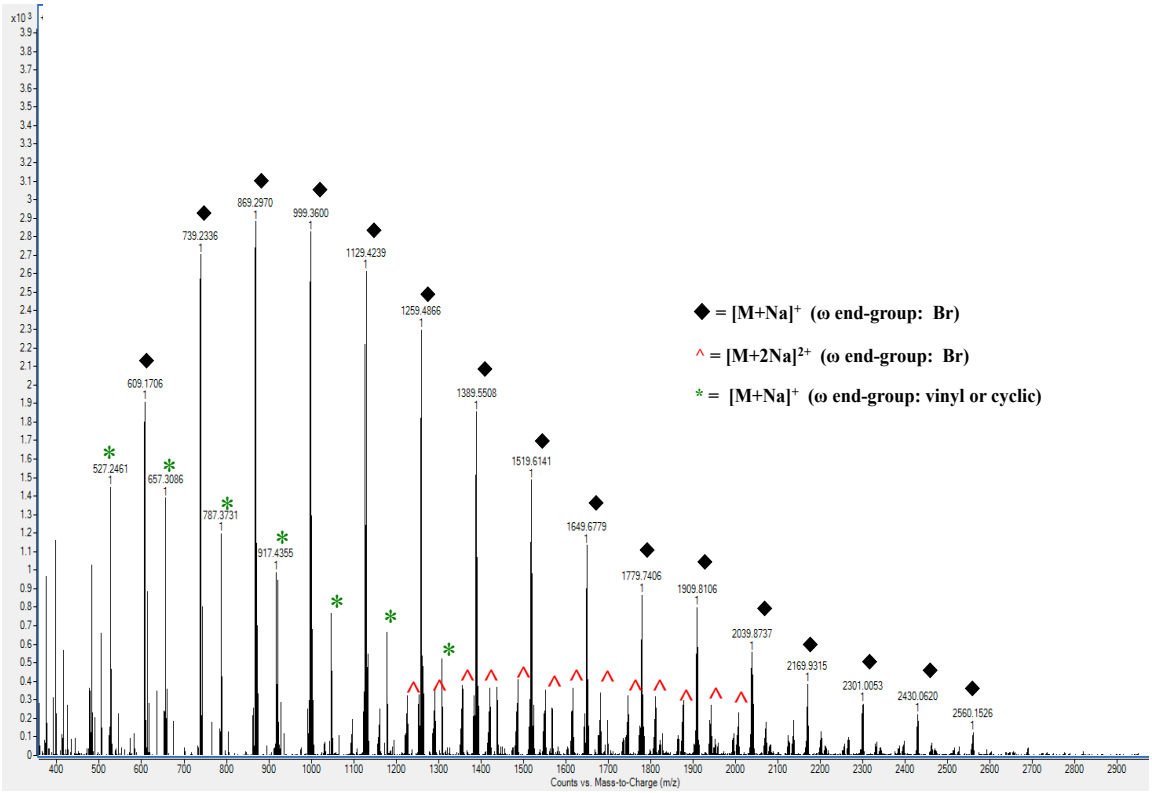

Figure 3.3 ESI-HRMS spectrum of PHEMA (3 hour reaction time) collected in positive mode showing three distributions. The mobile phase was acetonitrile:water 50% v/v with 0.1% formic acid. The flow rate was 0.5 mL min^{-1} and injection volume 2 µL.

Table 3.2 Agreement of observed and calculated m/z values for PHEMA (DP = 3) indicating retention of bromine ω-end group.

Calculated m/z	Observed m/z	Δ ppm
607.1724	607.1717	-1.15
608.1759	608.1759	0.00
609.1708	609.1706	-0.33
610.1741	610.1786	7.37

3.4.2 Atom Transfer Radical Polymerization of PDMAEMA and Characterization Using ^{1}H NMR Spectroscopy and High-Resolution Mass Spectrometry

The reaction for PDMAEMA is shown in Scheme 3.4. Reaction conditions were similar to those of PHEMA except that MeOH was used as solvent. Aliquots of the reaction mixture were taken for ^{1}H NMR spectroscopy analysis prior to polymerization and following predetermined reaction times.

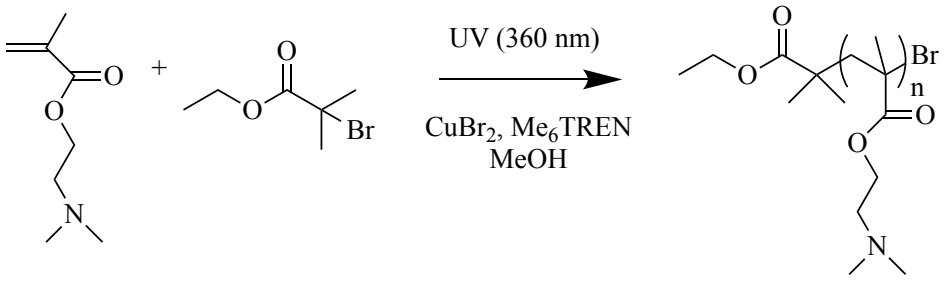

Scheme 3.4 PhotoATRP of DMAEMA using EBiB as initiator. The ratio of reagents was $[DMAEMA]_0:[I]_0:[Cu^{II}]_0:[Me_6TREN]_0$ = [20]:[1]:[0.02]:[0.12] in 50% v/v MeOH. $[I]_0:[Cu^{II}]_0$ = 50:1 (2 mol %)

Zero-time and 1.5-hour reaction time ^{1}H NMR spectra are shown in Figure 3.4 and Figure 3.5, respectively. The NMR spectra indicate a successful photoATRP for the production of PDMAEMA indicated by the presence of broad peaks at 4.01 ppm, 2.54 ppm, and 0.80-1.00 ppm. After 1.5 hours reaction time, percent monomer conversion was determined to be 23% and an M_n of 2080 g/mol was calculated utilizing end-group analysis. As shown in Table 3.3, for entries 2 and 3, monomer conversion and M_n increased as reaction time was increased to 3 and 4.5 hours.

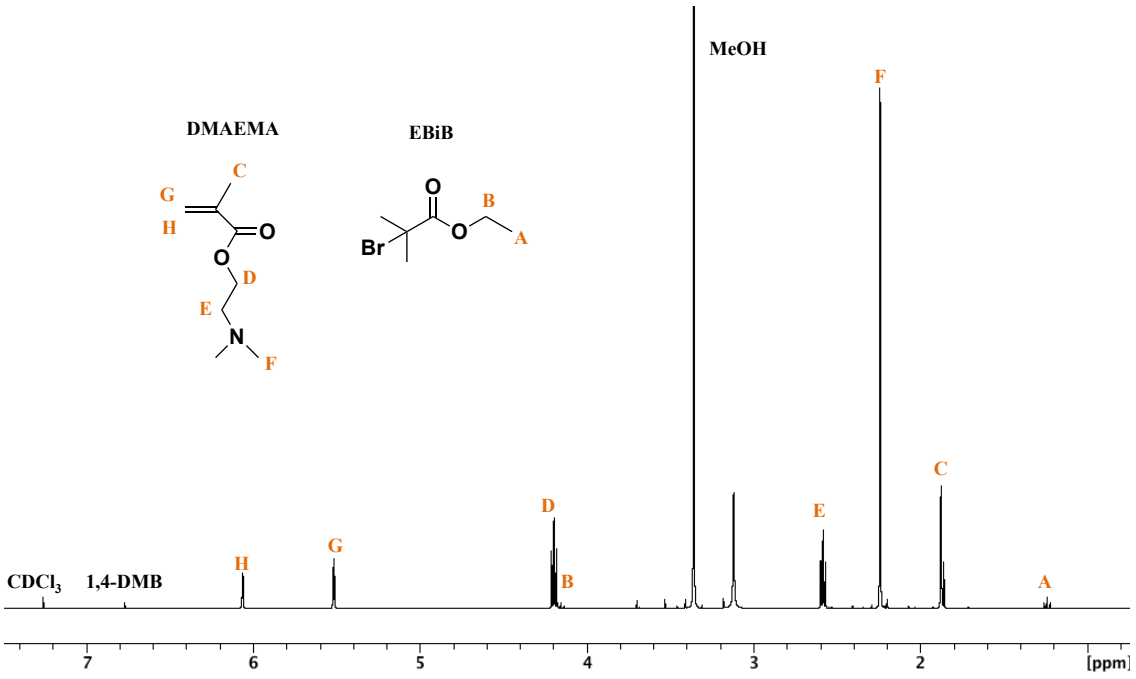

Figure 3.4 ^{1}H NMR spectrum of the zero-time aliquot from DMAEMA ATRP reaction mixture including peak assignments. (400 MHz, $CDCl_3$, 298 K)

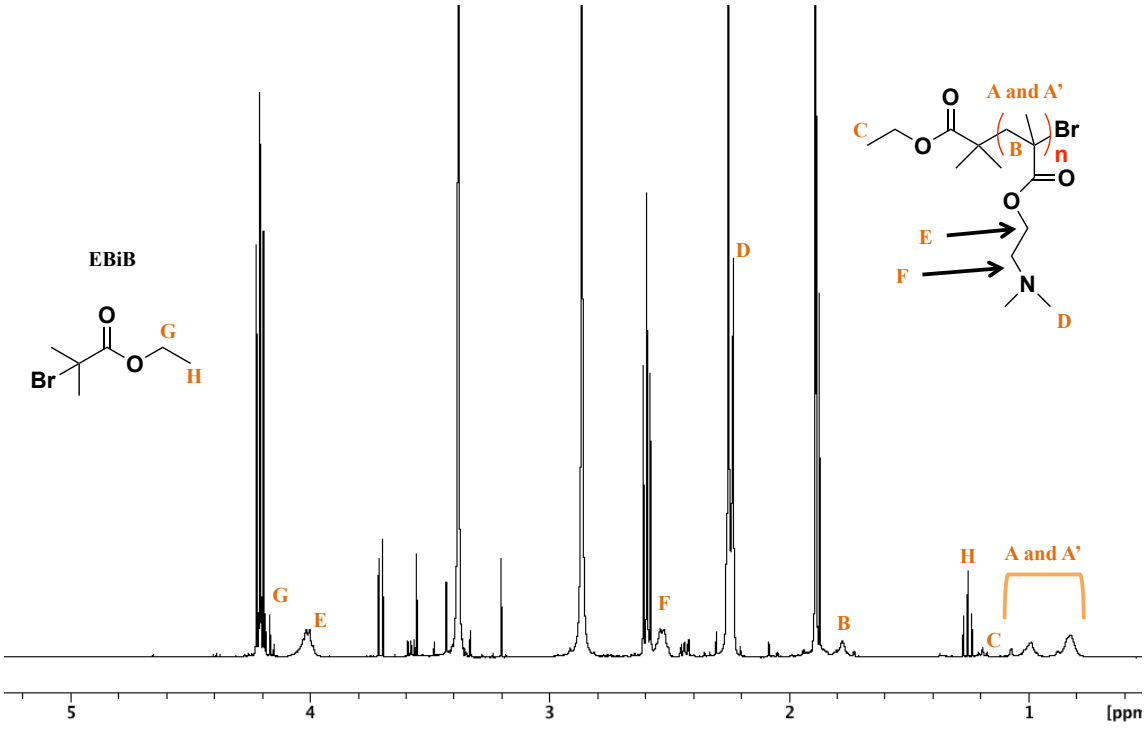

Figure 3.5 ^{1}H NMR spectrum of PDMAEMA ATRP reaction mixture after 1.5 hours reaction time including relevant peak assignments. (400 MHz, $CDCl_3$, 298 K)

Table 3.3 Summary of PDMAEMA reaction conditions, monomer conversions, and calculated M_n values. [a] Determined by ^1H NMR analysis ($CDCl_3$).

Entry	Solvent	Target DP	Rxn. Time	Monomer Conv.[a]	M_n[a] (g/mol)
1	MeOH	20	1.5 hrs.	23 %	2080
2	MeOH	20	3 hrs.	44 %	2395
3	MeOH	20	4.5 hrs.	62 %	2709

Similar to PHEMA mass spectra, three distributions were observed in PDMAEMA spectra, shown in Figure 3.6. The primary difference is that PDMAEMA distributions were protonated where as PHEMA distributions were sodiated and is due to the affinity of the tertiary amine for protons over sodium. There are singly charged and doubly charged bromine ω end-group distributions, $[M+H]^+$ and $[M+2H]^{2+}$, respectively. Additionally, there is a third distribution present, which is singly charged but possesses a vinyl or cyclic ω end-group analogous to PHEMA. All peaks in each singly charged distribution are separated by 157 Da, the mass of the DMAEMA monomer.

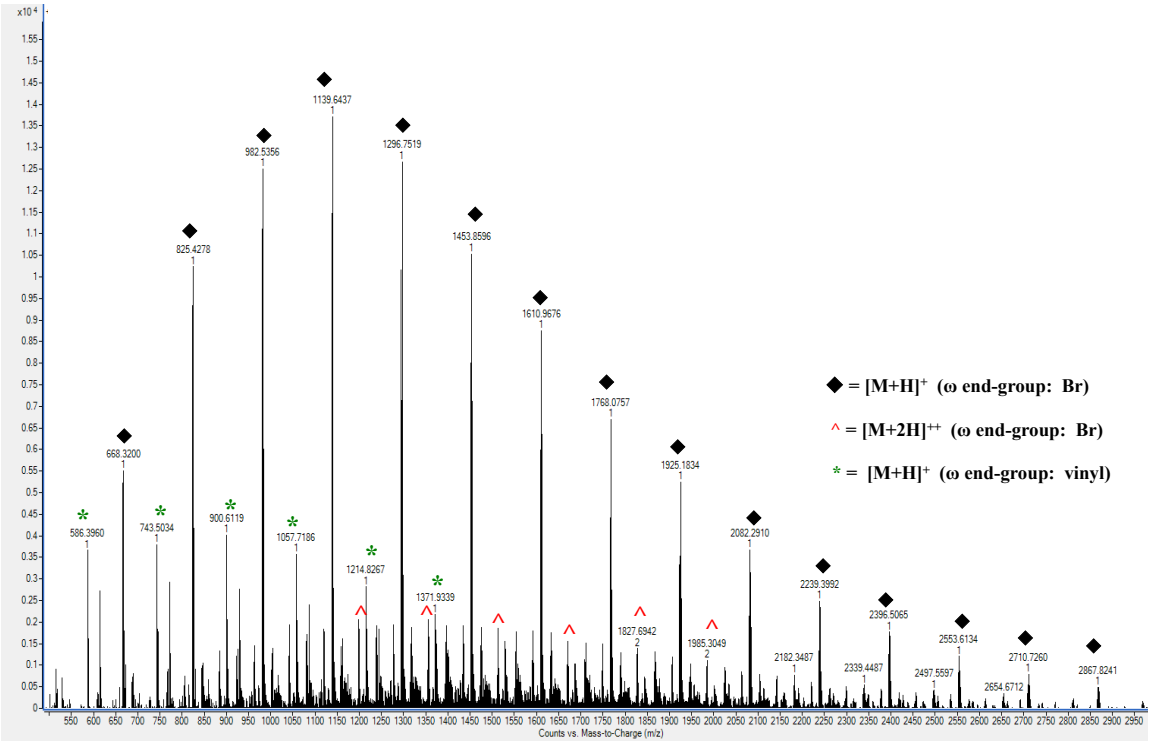

Figure 3.6 ESI-HRMS spectrum of PDMAEMA (1.5 hour reaction time) collected in positive mode showing three distributions. The mobile phase was MeOH with 0.1% formic acid. The flow rate was 1.0 mL min^{-1} and injection volume 2 µL.

Following deconvolution of the 1.5 hour PDMAEMA mass spectrum, M_n was calculated to be 1131 g/mol and the PDI was determined to be 1.22 indicating a relatively well-controlled polymerization. Similar to PHEMA, M_n calculated from the mass spectrum was lower than that calculated using end-group analysis.

To confirm the most intense polymer distribution contained bromine as the ω end-group, isotopic distributions were examined and shown in Table 3.3. The observed m/z values are in good agreement with the calculated values for the bromine isotopic pattern representing a degree of polymerization of 4 (DP = 4) where all have mass accuracies of < 2.0 ppm.

Table 3.4 Agreement of observed and calculated m/z values for PDMAEMA (DP = 4) indicating retention of bromine ω-end group.

Calculated m/z	Observed m/z	Δ ppm
823.4432	823.4434	0.2429
824.4466	824.4473	0.8491
825.4412	825.4428	1.9384
826.4446	826.826.4455	1.0890

3.4.3 Atom Transfer Radical Polymerization of poly(HEMA-ran-DMAEMA) and Characterization Using ^{1}H NMR Spectroscopy and High-Resolution Mass Spectrometry

Following the successful syntheses of PHEMA and PDMAEMA, photoATRP was utilized for the production of the random copolymer poly(HEMA-*ran*-DMAEMA). The general reaction is shown in Scheme 3.5 and the ^{1}H NMR spectrum after 2 hours reaction time in Figure 3.7. Using ^{1}H NMR spectroscopy monomer conversions were calculated to be 50% and 45% for HEMA and DMAEMA, respectively. Additionally, M_n was calculated using end-group analysis and determined to be 2730 g/mol.

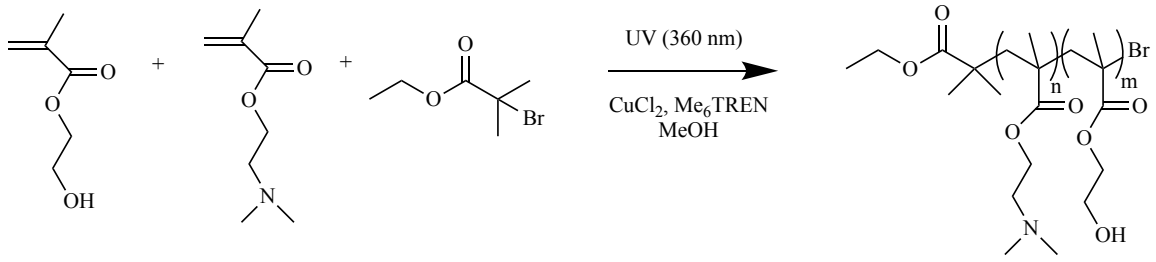

Scheme 3.5. PhotoATRP of poly(HEMA-*ran*-DMAEMA) using EBiB as initiator. The ratio of reagents was $[HEMA]_0:[DMAEMA]_0:[I]_0:[Cu^{II}]_0:[Me_6TREN]_0$ = [10]:[10]:[1]:[0.02]:[0.12] in MeOH. HEMA:DMAEMA: MeOH 1:1:2 v/v. $[I]_0:[Cu^{II}]_0$ = 50:1 (2 mol %)

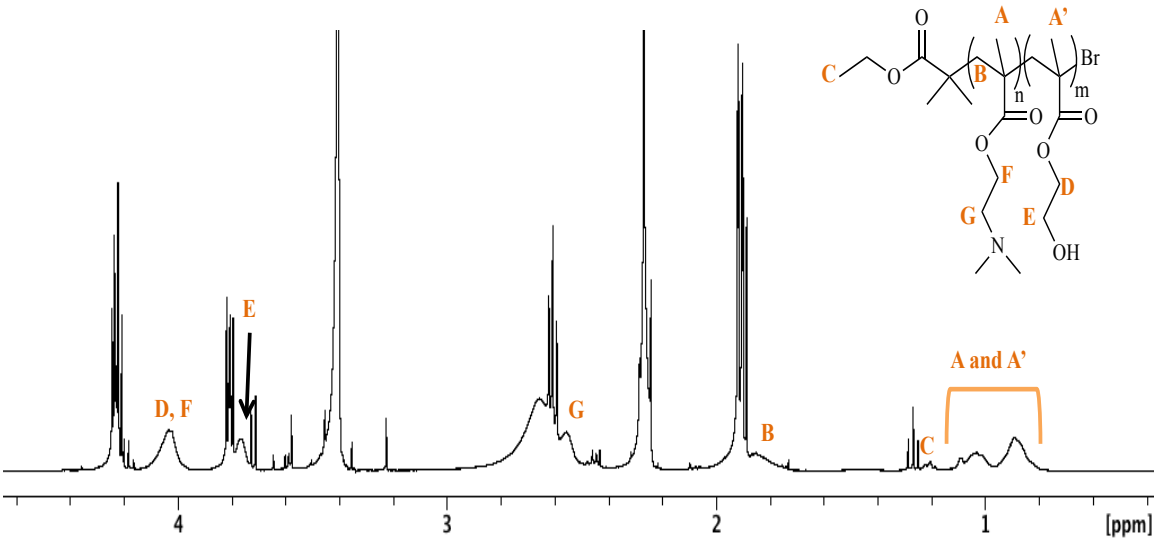

Figure 3.7 ^{1}H NMR spectrum of poly(HEMA-*ran*-DMAEMA) ATRP reaction mixture after two hours reaction time including relevant peak assignments. (400 MHz, $CDCl_3$, 298 K)

The random copolymer, poly(HEMA-*ran*-DMAEMA), was characterized utilizing ESI-HRMS providing a protonated spectrum, similar to the PDMAEMA homopolymer. The spectra of random copolymers are much more convoluted than their homopolymer counterparts. This attribute is evident in Figure 3.8 and is primarily due to the numerous combinations in which the two types of monomer can add to the growing end of a polymer chain. The critical parameters that dictate the order of monomer addition are reactivity ratios, which are solvent dependent, and the concentration of each respective monomer. If monomer reactivity ratios are near unity, the average polymer composition should be that of the initial concentration of each respective monomer.[21-22] It has been previously reported that in polar solvents the reactivity ratios of HEMA and DMAEMA are close to unity hence there is approximately equal probability for the addition of HEMA or PDMEAMA to the growing polymer chain if their initial

concentrations are equivalent.[21-22] Therefore, the analysis of poly(HEMA-*ran*-DMAEMA) spectra is not as direct as that of the respective homopolymers and attention must be paid to the addition sequence provided in the mass spectrometry data by considering the mass of each monomer used in the synthetic protocol.

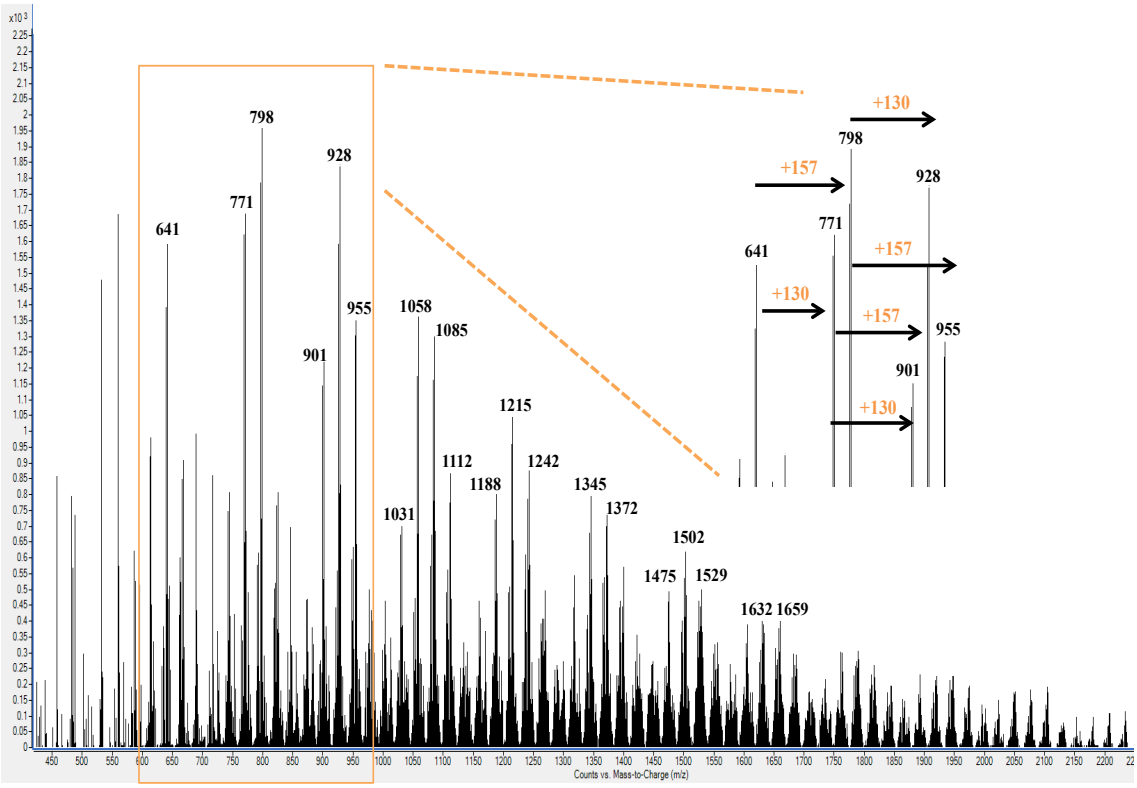

Figure 3.8 ESI-HRMS spectrum of poly(HEMA-*ran*-DMAEMA) (2 hours reaction time) collected in positive mode showing m/z values. The mobile phase was MeOH with 0.1% formic acid. The flow rate was 1.0 mL min^{-1} and injection volume 2 µL. The inset shows various monomer additions to the corresponding m/z values (+130 = HEMA, +157 = DMAEMA).

A structural identification chart of the most prominent distributions in the mass spectrum of poly(HEMA-*ran*-DMAEMA) was prepared, shown in Figure 3.9. Two DMAEMA monomers and one HEMA monomer represent the structure at m/z 641. The

addition of either a HEMA or DMAEMA monomer can occur giving rise to peaks at m/z 771 or 798, respectively. Hence, HEMA or DMAEMA can add to any preceding m/z value allowing for a plethora of monomer sequences having identical molecular weights. The analysis of the specific monomer sequences is the subject of Chapter 4.

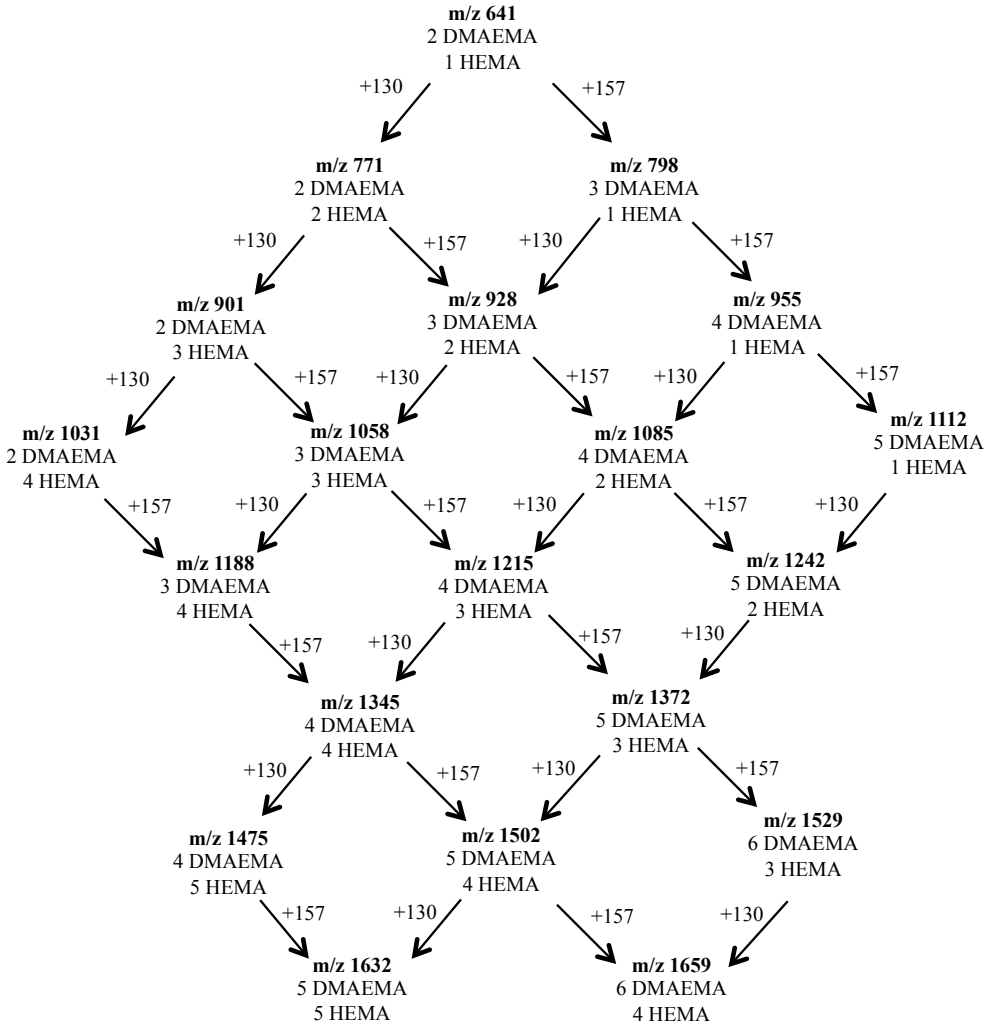

Figure 3.9 Structural identification chart for poly(HEMA-*ran*-DMAEMA) showing various monomer combinations present in the polymer backbone giving rise to specific m/z values where +130 and +157 indicate the addition of a HEMA or DMAEMA monomer, respectively.

3.5 Summary and Conclusions

The syntheses of homopolymers, PHEMA and PDMAEMA, and random copolymer poly(HEMA-*ran*-DMAEMA) were successfully carried out using photoATRP methodology. Each polymer was characterized using ^{1}H-NMR spectroscopy and ESI-HRMS.

The synthesis of PHEMA proceeded efficiently with monomer conversions of 61% and 89% after three and six hours, respectively. The calculation of M_n was performed utilizing ^{1}H NMR spectroscopy and was determined to be 2797 g/mol (3 hr. reaction) and 3709 g/mol (6 hr. reaction). These values are in contrast to those calculated using ESI-HRMS, which were 1557 g/mol and 1416 g/mol for the three and six hour reactions, respectively. The theoretical M_n values for each reaction time were calculated and fall between those determined from the ^{1}H NMR and ESI-HRMS spectra shown in Table 3.3. The elevated M_n values calculated using ^{1}H NMR spectroscopy are due to incomplete initiator activation. In contrast, the decreased M_n values calculated using ESI-HRMS are thought to be related to volatility, inefficient ionization, and decreased solubility of higher molecular weight polymers. Each reaction was relatively well controlled indicated by PDIs of 1.35. Additionally, the retention of the bromine as the ω end-group for the primary distribution in the mass spectra was confirmed using the signature isotopic distribution of bromine with Δppm values < 7.4 as shown previously in Table 3.2.

The synthesis of PDMAEMA proceeded efficiently and after 1.5 hours reaction time, percent monomer conversion was determined to be 23% and an M_n of 2080 g/mol was calculated via end-group analysis. Similar to PHEMA, M_n calculated via ^{1}H NMR

spectroscopy was greater than that calculated using ESI-HRMS, which was 1131 g/mol. Reasons for this discrepancy are the same as those for PHEMA. Similarly to PHEMA, M_n values and % monomer conversions for PDMAEMA increased as reaction time increased. This trend was in contrast to that of M_n calculated via HRMS. The PDIs were calculated to range from 1.22 to 1.38 indicating a relatively well-controlled polymerization. A summary of PHEMA and PDMAEMA data is shown in Table 3.5.

Table 3.5 Summary of PHEMA and PDMAEMA data collected using ^{1}H-NMR spectroscopy and ESI-HRMS. [a]^{1}H NMR spectroscopy, [b]Theoretical, [c]ESI-HRMS, [d]Calculated using deconvoluted mass spectra.

Entry	Polymer	Rxn. Time	Monomer Conv.[a]	M_n [a]	M_n [b]	M_n [c]	PDI[c,d]
1	PHEMA	3 hrs.	61 %	2797	1783	1557	1.35
2	PHEMA	6 hrs.	89 %	3709	2512	1416	1.35
3	PDMAEMA	1.5 hrs.	23 %	2080	825	1131	1.22
4	PDMAEMA	3 hrs.	44 %	2395	1450	1374	1.31
5	PDMAEMA	4.5 hrs.	62 %	2709	2080	1298	1.38

PhotoATRP was utilized for the synthesis of the random copolymer poly(HEMA-*ran*-DMAEMA). After two hours reaction time, monomer conversions were calculated to be 50% and 45% for HEMA and DMAEMA, respectively. End-group analysis was utilized to calculate M_n and was determined to be 2730 g/mol. Similar to PHEMA and PDMAEMA, the M_n value calculated using end-group analysis was larger than the theoretical value (1565 g/mol) due to incomplete initiator activation. Fragmentation pattern analysis of PHEMA, PDMAEMA, and poly(HEMA-*ran*-DMAEMA) was performed to elucidate fragments produced and monomer sequence of the copolymer.

3.6 References

1. Anastasaki, A.; Nikolaou, V.; Nurumbetov, G.; Wilson, P.; Kempe, K.; Quinn, J. F.; Davis, T. P.; Whittaker, M. R.; Haddleton, D. M. Cu(0)-Mediated Living Radical Polymerization: A Versatile Tool for Materials Synthesis. *Chemical Reviews* **2016,** *116* (3), 835-877.

2. Patten, T. E.; Matyjaszewski, K. Copper(I)-Catalyzed Atom Transfer Radical Polymerization. *Accounts of Chemical Research* **1999,** *32* (10), 895-903.

3. Matyjaszewski, K.; Tsarevsky, N. V. Macromolecular Engineering by Atom Transfer Radical Polymerization. *Journal of the American Chemical Society* **2014,** *136* (18), 6513-6533.

4. Anastasaki, A.; Nikolaou, V.; Zhang, Q.; Burns, J.; Samanta, S. R.; Waldron, C.; Haddleton, A. J.; McHale, R.; Fox, D.; Percec, V.; Wilson, P.; Haddleton, D. M. Copper(II)/Tertiary Amine Synergy in Photoinduced Living Radical Polymerization: Accelerated Synthesis of ω-Functional and α,ω-Heterofunctional Poly(acrylates). *Journal of the American Chemical Society* **2014,** *136* (3), 1141-1149.

5. Matyjaszewski, K. Atom Transfer Radical Polymerization (ATRP): Current Status and Future Perspectives. *Macromolecules* **2012,** *45* (10), 4015-4039.

6. Matyjaszewski, K.; Tsarevsky, N. V. Nanostructured functional materials prepared by atom transfer radical polymerization. *Nat Chem* **2009,** *1* (4), 276-288.

7. Woodruff, S. R.; Davis, B. J.; Tsarevsky, N. V. Selecting the Optimal Reaction Conditions for Copper-Mediated Atom Transfer Radical Polymerization at Low Catalyst Concentration. In *Progress in Controlled Radical Polymerization: Mechanisms and Techniques*; American Chemical Society, 2012; Vol. 1100, pp 99-113.

8. Konkolewicz, D.; Matyjaszewski, K. Catalyst Activity in ATRP, Determining Conditions for Well-Controlled Polymerizations. In *Controlled Radical Polymerization: Mechanisms*; American Chemical Society, 2015; Vol. 1187, pp 87-103.

9. Asteasuain, M. Deterministic Approaches for Simulation of Nitroxide-Mediated Radical Polymerization. *International Journal of Polymer Science* **2018,** *2018*, 7803702.

10. Moad, G.; Rizzardo, E.; Thang, S. H. Living Radical Polymerization by the RAFT Process A Second Update. *Australian Journal of Chemistry* **2009,** *62* (11), 1402-1472.

11. Perrier, S.; Takolpuckdee, P.; Mars, C. A. Reversible Addition−Fragmentation Chain Transfer Polymerization: End Group Modification for Functionalized Polymers and Chain Transfer Agent Recovery. *Macromolecules* **2005,** *38* (6), 2033-2036.

12. Perrier, S.; Takolpuckdee, P. Macromolecular design via reversible addition–fragmentation chain transfer (RAFT)/xanthates (MADIX) polymerization. *Journal of Polymer Science Part A: Polymer Chemistry* **2005,** *43* (22), 5347-5393.

13. Junkers, T.; Barner-Kowollik, C.; Lalevée, J. Chapter 6 Recent Developments in Nitroxide Mediated Polymerization. In *Nitroxide Mediated Polymerization: From Fundamentals to Applications in Materials Science*; The Royal Society of Chemistry, 2016, pp 264-304.

14. Gadhave, R. RAFT in living radical emulsion polymerization: What makes it different? *Paintindia* **2016,** *66* (11), 51-57.

15. Kwak, Y.; Magenau, A. J. D.; Matyjaszewski, K. ARGET ATRP of Methyl Acrylate with Inexpensive Ligands and ppm Concentrations of Catalyst. *Macromolecules* **2011,** *44* (4), 811-819.

16. Matyjaszewski, K.; Paik, H.-j.; Zhou, P.; Diamanti, S. J. Determination of Activation and Deactivation Rate Constants of Model Compounds in Atom Transfer Radical Polymerization. *Macromolecules* **2001,** *34* (15), 5125-5131.

17. Reiser, O. Shining Light on Copper: Unique Opportunities for Visible-Light-Catalyzed Atom Transfer Radical Addition Reactions and Related Processes. *Accounts of Chemical Research* **2016,** *49* (9), 1990-1996.

18. Knorn, M.; Rawner, T.; Czerwieniec, R.; Reiser, O. [Copper(phenanthroline)(bisisonitrile)]+-Complexes for the Visible-Light-Mediated Atom Transfer Radical Addition and Allylation Reactions. *ACS Catalysis* **2015,** *5* (9), 5186-5193.

19. Ciampolini, M.; Nardi, N. Five-Coordinated High-Spin Complexes of Bivalent Cobalt, Nickel, andCopper with Tris(2-dimethylaminoethyl)amine. *Inorganic Chemistry* **1966,** *5* (1), 41-44.

20. Anastasaki, A.; Nikolaou, V.; Simula, A.; Godfrey, J.; Li, M.; Nurumbetov, G.; Wilson, P.; Haddleton, D. M. Expanding the Scope of the Photoinduced Living Radical Polymerization of Acrylates in the Presence of CuBr2 and Me6-Tren. *Macromolecules* **2014,** *47* (12), 3852-3859.

21. Teoh, R. L.; Guice, K. B.; Loo, Y.-L. Atom Transfer Radical Copolymerization of Hydroxyethyl Methacrylate and Dimethylaminoethyl Methacrylate in Polar Solvents. *Macromolecules* **2006,** *39* (25), 8609-8615.

22. Ni, H.; Yang, Y.; Chen, Y.; Liu, J.; Zhang, L.; Wu, M. Preparation of a poly(DMAEMA-co-HEMA) self-supporting microfiltration membrane with high anionic permselectivity by electrospinning. *e-Polymers* **2016,** *17*.

Chapter 4

Fragmentation Pattern Analysis of (Co)Polymers Using Multi-Stage Mass Spectrometry

4.1 Introduction

Due to advancement of controlled radical polymerization methodologies, i.e., atom transfer radical polymerization (ATRP), reversible addition-fragmentation chain transfer polymerization (RAFT), and nitroxide-mediated polymerization (NMP), various polymer compositions and architectures can be realized in addition to predetermined molecular weights and narrow PDIs.[1-3] For example, the composition of copolymers can include random, block, gradient, or graph as shown in Figure 4.1. Additionally, polymers can be designed to have different architectures/topologies such as linear, graft/comb, star, or network/gel (Figure 4.1). The advancement of CRP techniques allows for the fine-tuning of these (co)polymer attributes.

Similar to the relationship between structure and function when dealing with biopolymers such as proteins, there exists a similar relationship for synthetic polymers, specifically copolymers.[4] The chemical and physical properties of copolymers are determined by the composition and sequence distribution of monomer units.[5] For instance, changing the ratio of monomers in a copolymer, characteristics such as their thermo-sensitivity can be modulated. Fournier and coworkers synthesized poly(PEGMA-stat-DMAEMA) via RAFT polymerization. They concluded that the higher PEGMA content in the copolymer, the greater the lower critical solution temperature (LCST).[6] Han and coworkers synthesized block copolymers poly(DMAEMA-b-tBuA) via ATRP in which they performed post-polymerization modification to obtain poly(DMAEMA-

block-AAc) via hydrolysis in acidic media. Higher DMAEMA composition showed a decreased LCST for the copolymer.[7]

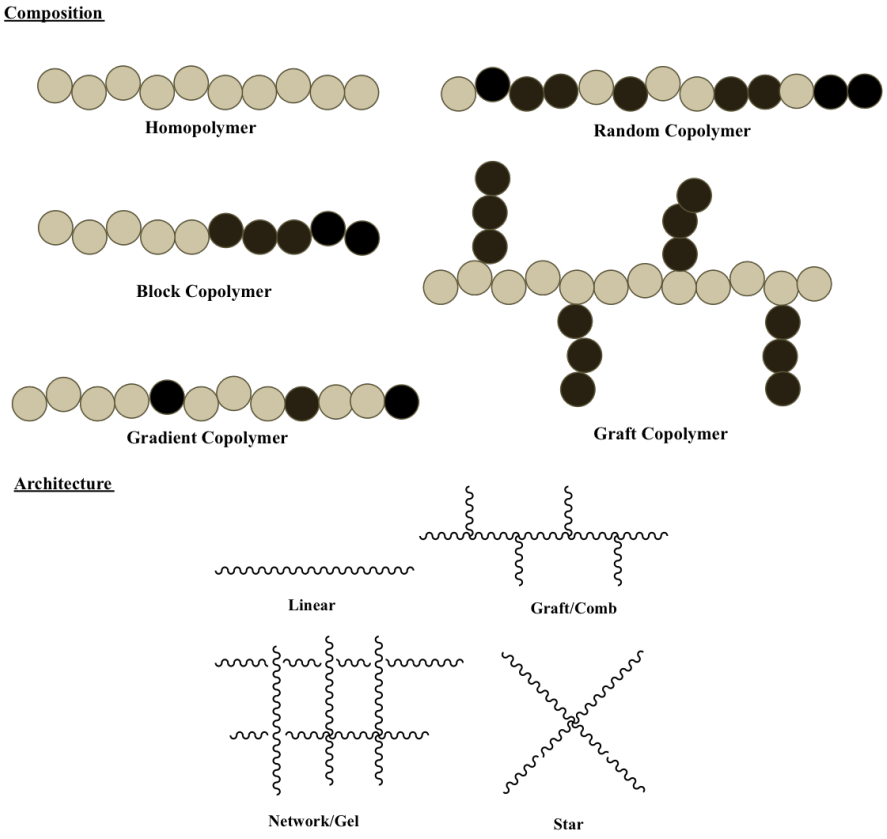

Figure 4.1 Various compositions (top) and architectures (bottom) of (co)polymers achievable due to the advancements of controlled radical polymerization methodologies.

The efficiency of (co)polymers for the removal of various toxins from aqueous systems can be optimized by fine-tuning the composition and/or architecture. For example, it has been reported that the size of a given block of a copolymer affects its efficiency for the removal of toxins from aqueous systems.[8-9] Choi and coworkers reported that the size of the polystyrene block affects the capacity for the removal of organic pollutants from water.[8] It has also been reported that molecular weight and architecture can also play a role in removal efficiency.[10-11]

Due to the advancement of synthetic methodologies for polymers giving rise to more complex polymer compositions and architectures, analytical methods must also advance in order to investigate these aspects of (co)polymers. After the introduction of soft ionization sources, e.g., ESI, MALDI, APCI,[12] mass spectrometry has emerged as a primary tool for characterizing complex polymer systems. In contrast to single-stage mass spectrometry, which measures the m/z ratio of intact ions, tandem mass spectrometry (MS/MS or MS^n) allows for further characterization of synthetic polymers by fragmenting a selected precursor ion into product ions providing detailed information regarding the composition and/or sequence of (co)polymers. The ability to preform sequential isolation-fragmentation steps allows for the reconstruction of the precursor ion.[13] There are numerous fragmentation methods used for multi-stage mass spectrometry experiments including electron capture dissociation (ECD), electron transfer dissociation (ETD), surface-induced dissociation (SID), photo dissociation, and post-source decay (PSD). But the most common ion fragmentation technique is collision-induced dissociation (CID), also known as collisionally activated dissociation (CAD).[14-16] With this process, an inert collision gas is used to induce fragmentation of the selected ion. CID tandem mass spectrometry experiments can be performed on trap or beam mass spectrometers. Beam instruments implement two mass analyzers separated by a collision cell in which an inert gas collides with a mass selected precursor ion. Trap instruments store all ions generated during the ionization process in a trap and the ions can be ejected sequentially for fragmentation.[15] In either case, the selected ion sequentially fragments into representative product ions giving insight into the composition of the respective copolymer. An advantage of trap-based instruments is that more stages of isolation

followed by fragmentation can be performed if signal intensity remains sufficient. Miladinovic et. al. reported that they could differentiate between random and block copolymers using Fourier transform tandem mass spectrometry (FT MS/MS).[17] Altuntas and coworkers implemented MS/MS to analyze (co)poly(methacrylates) and showed how the fragmentation pattern is dependent on the synthetic methodology. For example, copolymers synthesized via RAFT polymerization produced different fragmentation patterns than those synthesized via NMP or ATRP.[12] These results were expected since α and ω-end groups are dictated by the initiator and synthetic methodology used, respectively (Figure 4.2). Since fragments containing the end groups are typically observed early in the fragmentation process, i.e., MS^2 level, it was determined that fragmentation patterns are specific to a given synthetic methodology.[12]

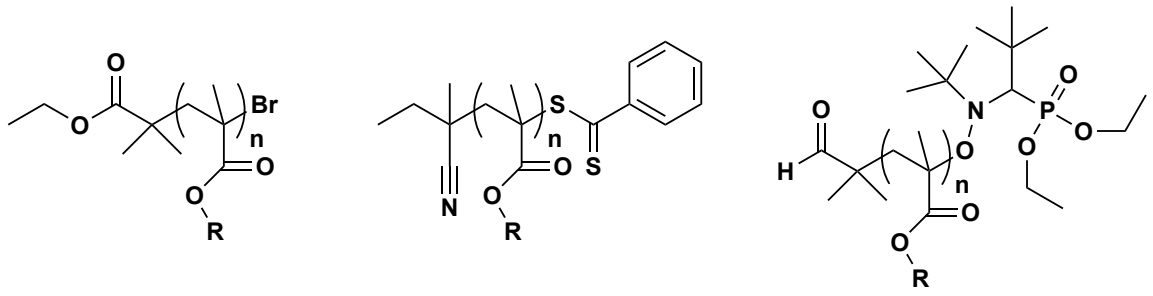

Figure 4.2 Variation of α and ω-end groups obtained via different CRP techniques: ATRP (left), RAFT (middle), NMP (right).

Due to the numerous applications of PHEMA[18-21] and PDMAEMA[22-26] in the biomedical, water remediation, and materials development fields, there is a need for investigations into fragmentation patters of poly(HEMA-ran-DMAEMA). To date, there have been no reports investigating the fragmentation pattern of this random copolymer. Here, poly(HEMA-ran-DMAEMA) was synthesized via photoATRP. Multi-stage mass

spectrometry was implemented to investigate the fragmentation pattern and to elucidate potential structures/sequences of the copolymer.

4.2 Materials

All materials were used as received unless otherwise noted. Alumina, copper (II) bromide ($CuBr_2$), and ethy-2-bromoisobutyrate (EBiB) were purchased from Alfa Aesar (Fisher Scientific, Tewksbury MA). Copper (II) chloride ($CuCl_2$), 2-Hydroxyethyl methacrylate (HEMA) and 2-(dimethylamino)ethyl methacrylate (DMAEMA) were purchased from Sigma Aldrich (St. Louis MO). The monomers were passed through a column of basic alumina to remove inhibitor and were stored at 4^0C prior to use. Optima grade methanol (MeOH) and optimal grade formic acid were purchased from Fisher Scientific (Pittsburgh PA). The highly active ligand, Me_6-TREN, was synthesized according to a previously reported method.[27-28]

4.3 Methods

4.3.1 Polymer Synthesis

The synthesis of PHEMA, PDMAEMA, and poly(HEMA-ran-DMAEMA), was achieved via photoATRP using a modified literature procedure.[29] Briefly, the polymerization of poly(HEMA-ran-DMAEMA) is described below. First, a solution containing a ratio of 1:1:2 (v/v) HEMA:DMAEMA:MeOH was prepared. Catalyst solution (0.082 M, 500 μL) was then added to the reaction vial. Lastly, the initiator, EBiB (30 μL, 0.2 mmol) was added to the mixture to give a final ratio of $[HEMA]_0:[DMAEMA]_0:[I]_0:[Cu^{II}]_0:[Me\text{-}_6TREN]_0 = [10]:[10]:[1]:[0.02]:[0.12]$. The vial

was capped with a septum, sealed with electrical tape, and purged with nitrogen for 10 minutes. To begin polymerization, the reaction vial was placed in a UV nail curing lamp ($\lambda_{max} \approx 360$ nm, 4x9 W bulbs), which was set on a magnetic stir plate for a predetermined amount of time.

4.3.2 Mass Spectrometry

High-resolution MS and MS/MS experiments were performed using an Agilent 6530 Accurate Mass QTOF LC/MS (Agilent, Santa Clara CA) equipped with an electrospray ionization source and operated in the positive mode. MeOH w/0.1% formic acid was used as mobile phase. The capillary voltage, skimmer voltage, and fragmentor voltage were optimized at 3 kV, 65 V, and 250 V, respectively. Drying and sheath gas temperatures were set at 350 ^{0}C. Crude polymer was dissolved in MeOH to a concentration of 1 mg mL^{-1}. The sample was introduced into the ionization source via flow injection analysis at a flow rate of 0.5 mL min^{-1} for PHEMA and 1.0 mL min^{-1} for both PDMAEMA and poly(HEMA-ran-DMAEMA). For MS/MS experiments nitrogen was used as the collision gas. Data processing was carried out using MassHunter (Agilent, Santa Clara CA). Multi-stage (MS^n) experiments were carried out using a Thermo LTQ-XL Linear Ion Trap Mass Spectrometer (Thermo Fisher Scientific, Pittsburgh PA) equipped with an ESI source and operated in the positive mode. MeOH w/0.1% formic acid was used as mobile phase and argon as the collision gas. The spray voltage, capillary voltage, and tube lens voltage were optimized at 4.2 kV, 40 V, and 100 V, respectively. The capillary temperature was set at 250 ^{0}C and the sheath and sweep gases set to 12 and 3 arbitrary units, respectively. The normalized collision energy was

optimized for each precursor ion during fragmentation analysis and ranged from 20-35 arbitrary units. Crude polymer was dissolved in MeOH to a concentration of 1 mg mL^{-1}. The sample was introduced into the ionization source at a flow rate of 5 μL min^{-1} via a syringe pump. Data processing was carried out using Xcalibur (Thermo Fisher Scientific, Pittsburgh PA).

4.4 Results and Discussion

4.4.1 Fragmentation Pattern Analysis of PHEMA and PDMAEMA Oligomers Using Tandem Mass Spectrometry

In order to perform fragmentation pattern analysis of copolymers, it is of fundamental importance to understand these patterns of the respective homopolymers that comprise the copolymer. Therefore, fragmentation pattern analysis was performed on both PHEMA and PDMAEMA. There have been few reports on the fragmentation analysis of PHEMA[30-31]. Because different synthetic methods, i.e. RAFT and NMP, produce polymers with different end-groups, the information provided below gives insight into the fragmentation of PHEMA synthesized using ATRP.

Initially, MS/MS was performed on PHEMA oligomers ranging in degree of polymerization (DP) from 3 to 9 using the Agilent 6530 Accurate Mass QTOF LC/MS. Figure 4.3 is representative spectra for all DPs examined. At a collision energy of 20 eV, the primary loss was 80 Da (HBr) giving rise to the product ion at m/z 657. The small peak at m/z 635 represents a second product ion and the loss of 102 Da, which was assigned NaBr. As the CE was increased to 40 eV, the product ion at 613 m/z becomes more intense and represents a loss of 44 Da, vinyl alcohol arising from the pendent arm

of HEMA. As CE was increased to 60 eV, the precursor ion became non-observable. The product ion peaks at m/z 657 and m/z 613 have reduced in intensity and the low to mid m/z range became more convoluted hence making fragmentation pathway analysis more difficult. Therefore, a linear ion trap mass spectrometer was used to perform MS^n analyses.

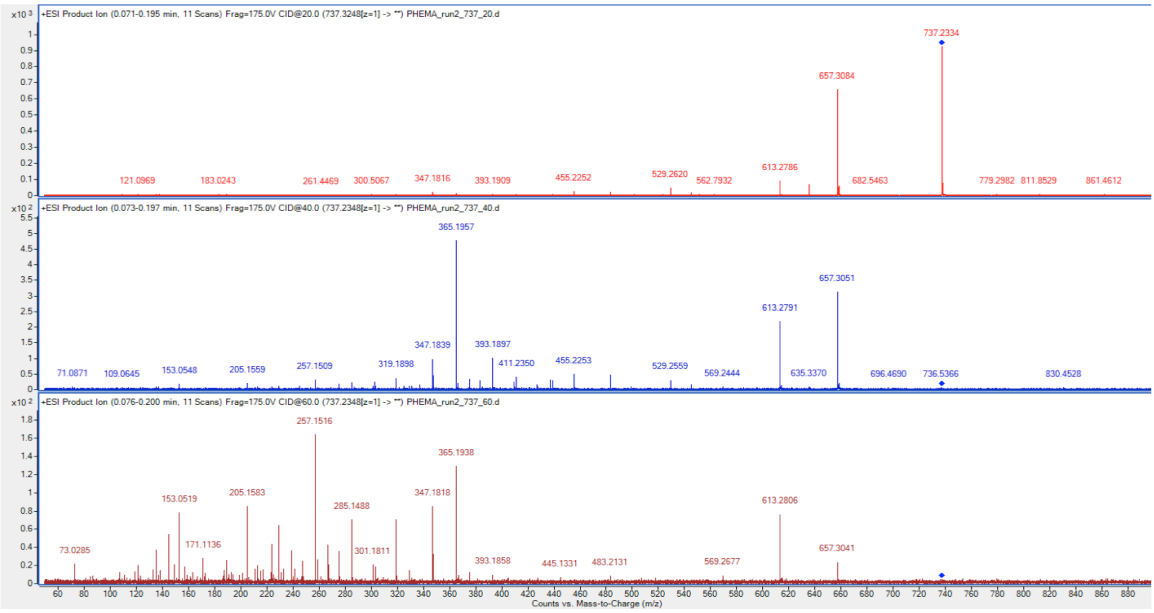

Figure 4.3 MS/MS spectra collected using an Agilent 6530 Accurate Mass QTOF mass spectrometer of PHEMA oligomer (DP = 4) at various collision energies of 20 eV (top), 40 eV (middle), and 60 eV (bottom).

Multi-stage mass spectrometry (MS^n) was carried out using a Thermo LTQ-XL Linear Ion Trap mass spectrometer. Initially, MS^2 was performed on the precursor ion at m/z 737 (DP = 4) and is shown in Figure 4.4. Similar to the data collected using the Agilent 6530 Accurate Mass QTOF mass spectrometer, a primary loss of 80 Da (HBr) was observed in addition to a minor fragmentation pathway showing a loss of 102 Da (NaBr). Additionally in Figure 4.4, two potential structures of the PHEMA oligomer are

shown. One structure possesses a cyclic ω-end group that is formed via an S_n1-type reaction between they hydroxyl group on the pendant arm of PHEMA and bromine. The other structure possesses a vinyl ω-end group formed via β-hydrogen abstraction due to the lability of bromine.[32-34] Both fragmentation pathways involve the loss of 80 Da (HBr).

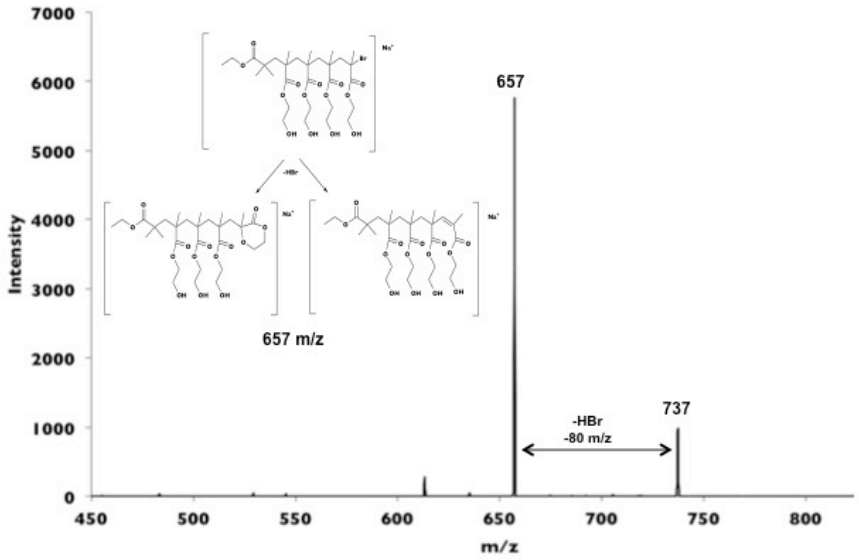

Figure 4.4 MS^2 spectrum of PHEMA oligomer collected using a Thermo LTQ-XL mass spectrometer. The primary fragmentation pathway shows a loss of 80 Da and potential structures that represent m/z 657.

The product ion at m/z 657 was isolated and fragmented for MS^3 analysis and is shown in Figure 4.5. The loss of 44 Da (vinyl alcohol) is observed giving rise to m/z 613. Similar to MS^2 analysis, there are two potential structures each with different ω-end groups. The vinyl alcohol fragment arises from the pendant arm of HEMA monomer and this fragment has been previously reported but the overall fragmentation pathway deviates from the one presented here due to the synthetic methodology implemented.[30]

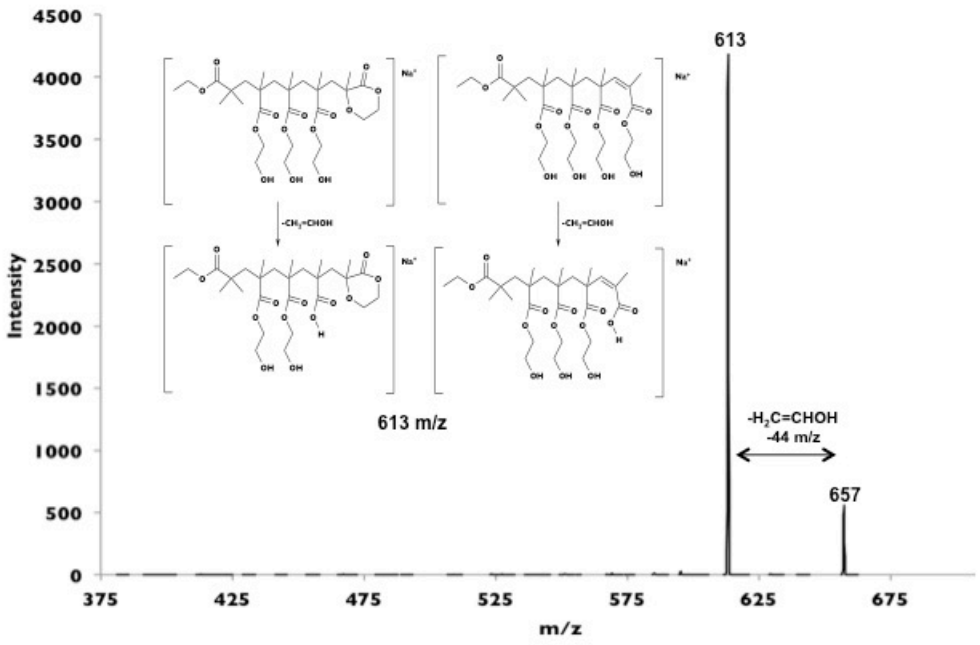

Figure 4.5 MS^3 analysis of PHEMA oligomer showing the loss of 44 Da (vinyl alcohol) as the primary fragmentation pathway, giving rise to two potential structures. Collected using a Thermo LTQ-XL mass spectrometer.

The ion representing m/z 613 was isolated and fragmented for MS^4 analysis and is shown in Figure 4.6. At this level, multiple fragmentation pathways can be observed with the preferred pathway consisting of a loss of 44 Da (vinyl alcohol) giving rise to the product ion peak at m/z 569. Additionally, a loss of 28 Da was observed and assigned as carbon monoxide (CO). This loss is significant in that it suggests that both possible structures at m/z 613 are present. The primary fragmentation pathway is the loss of vinyl alcohol and the secondary pathway is the loss of CO. Cyclic esters can expel CO via carbon-carbon bond scission forming two radicals. Following expulsion of CO, radicals couple forming a new cyclic structure.[32, 35] Additionally, there were two fragmentation pathways showing the loss of 62 Da, which has been assigned as ethylene glycol and is thought to be due to the further fragmentation of the product ions at m/z 585 and m/z 569.

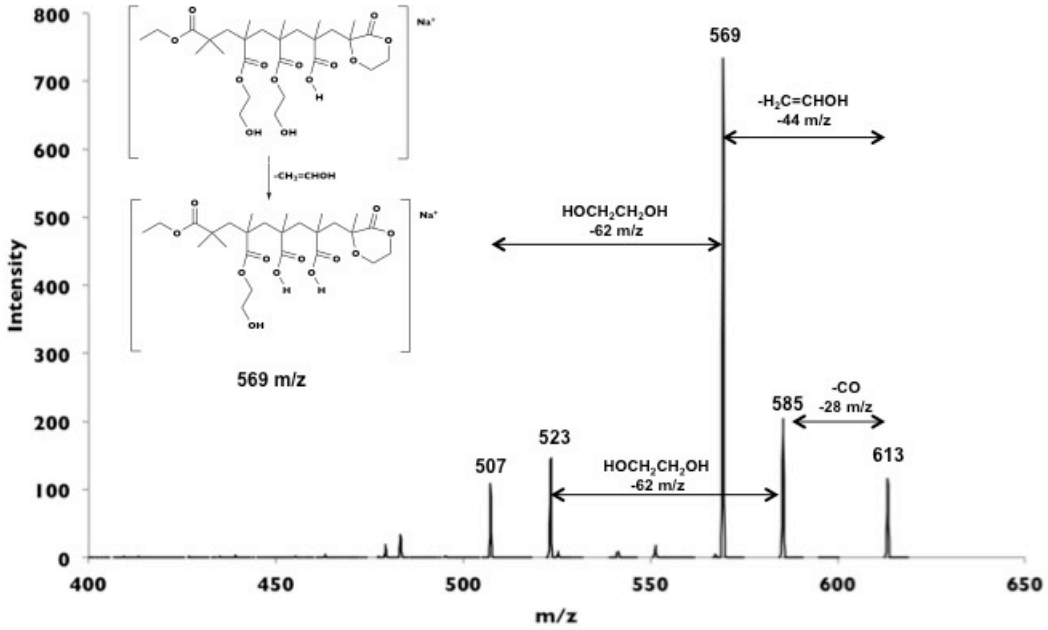

Figure 4.6 MS^4 analysis of PHEMA oligomer showing multiple fragmentation pathways, with the most preferred being the loss of vinyl alcohol (44 Da). Collected using a Thermo LTQ-XL mass spectrometer.

The final isolation/fragmentation step was performed at MS^5 for m/z 569 and is shown in Figure 4.7. The primary fragmentation pathway is the loss of 62 Da (ethylene glycol) giving rise to m/z 507. This fragmentation occurs via the coupling of the pendent arm of HEMA and the carboxylic acid group that is present after the loss of vinyl alcohol from an adjacent HEMA monomer present in the oligomer chain.[30] Further isolation/fragmentation steps could not be performed due to the low abundance of precursor ion. Theoretically, MS^n can be performed but typically falls in the range of approximately n=5-10 due to the eventual low abundance of precursor ions.

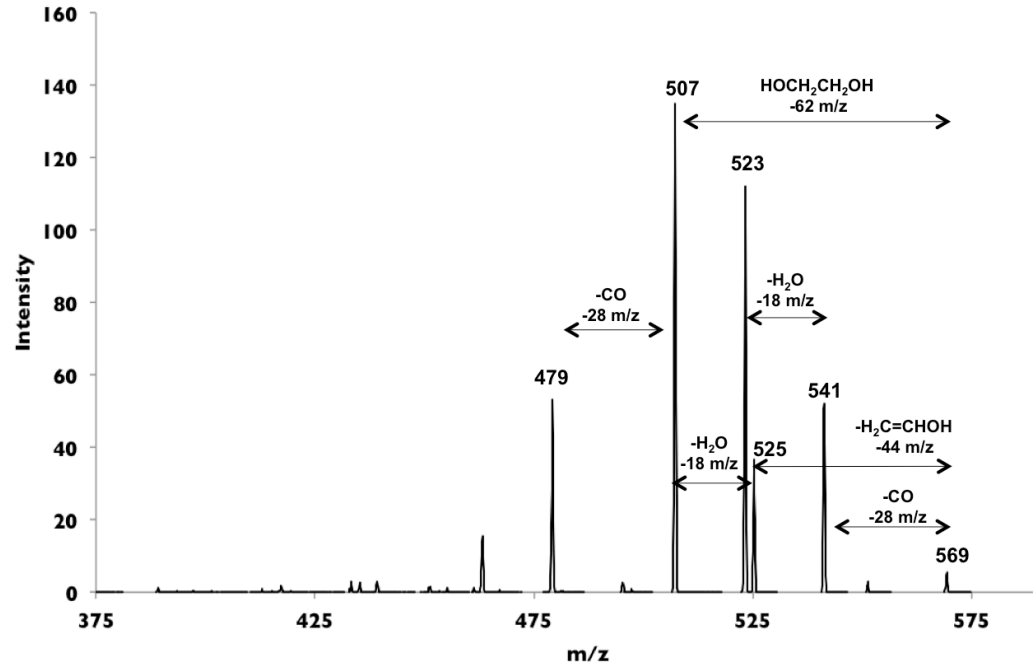

Figure 4.7 MS^5 analysis of PHEMA oligomer showing multiple fragmentation pathways. The most preferred pathway is the loss of ethylene glycol (62 Da) from the precursor ion m/z 569. Collected using a Thermo LTQ-XL mass spectrometer.

Overall, by performing more successive fragmentation-isolation steps, the tandem mass spectra show a more convoluted spectrum and numerous fragmentation pathways. These pathways consist of losing only 5 individual fragments starting with HBr, which is followed by vinyl alcohol, carbon monoxide, ethylene glycol, and water. After the initial loss of hydrogen bromide, the loss of vinyl alcohol always preceded losses of ethylene glycol (62 Da) and carbon monoxide (28 Da), which was expected due to the structure of the PHEMA oligomer. This fragmentation must occur to form the carboxylic acid group that is needed for the losses of ethylene glycol and water. Once numerous vinyl alcohol fragments are lost, the loss of water was also observed. This fragment arises from two adjacent HEMA monomers following fragmentation of their pendant arms leaving carboxylic acid groups, which can couple by expelling water and recombining to form a

cyclic anhydride. The preferred fragmentation pathway of a PHEMA oligomer (DP = 4) is shown in Scheme 4.1

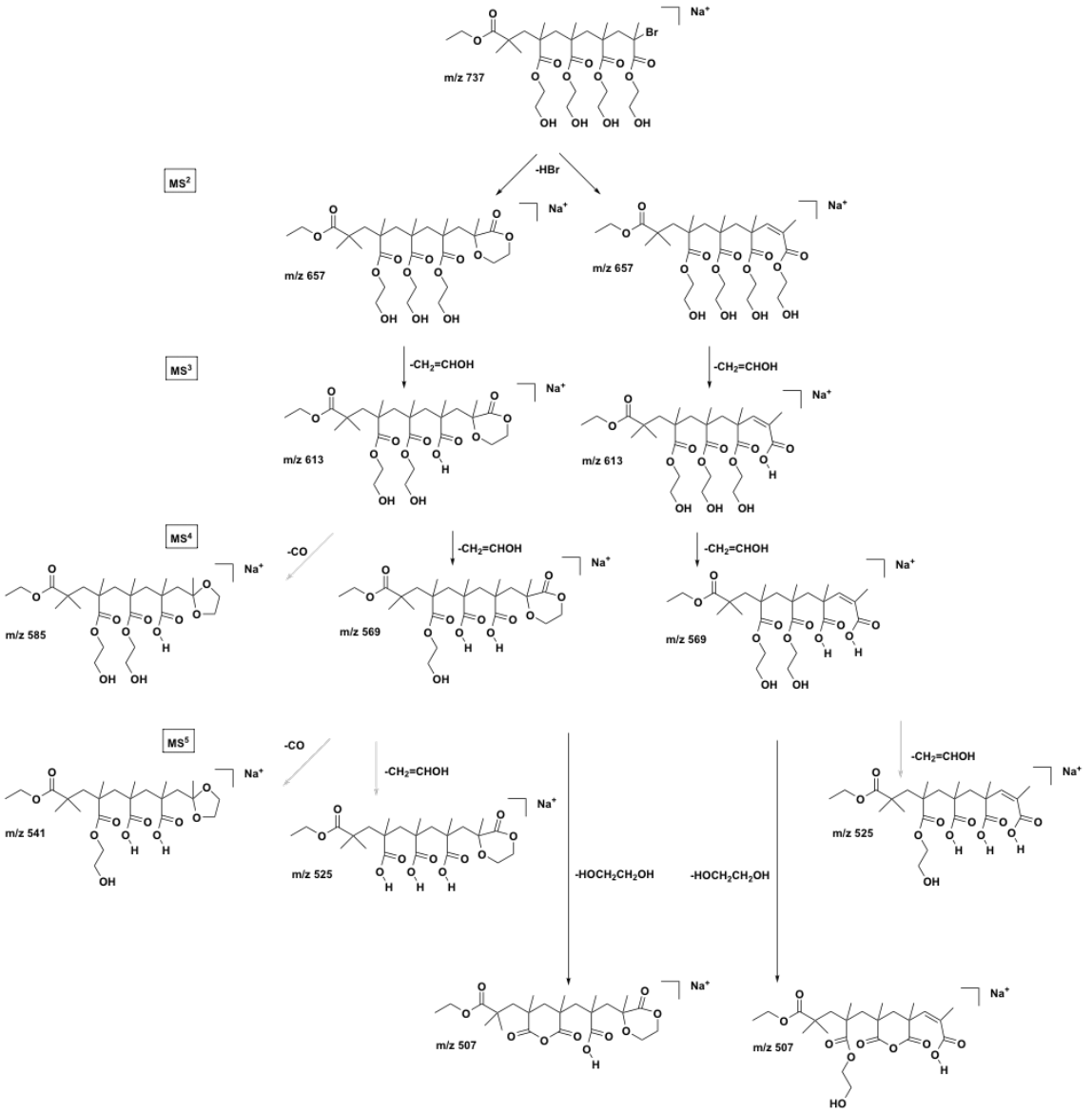

Scheme 4.1 Fragmentation pattern of PHEMA oligomer showing multiple pathways with the preferred marked using bold arrows. Additionally, different levels of sequential isolation/fragmentation (MS^n) are given on the left side of the image.

Similar to PHEMA, initially MS/MS of PDMAEMA oligomers (DP of 3 to 9) was performed using the Agilent 6530 Accurate Mass QTOF mass spectrometer. In contrast to the PHEMA MS/MS spectra, the data for PDMAEMA only shows relatively

few product ions and as the CE is increased the spectra do not become convoluted in the mid to low m/z range as shown in Figure 4.8. Initially, as the CE was increased stepwise from 5 to 40 eV, the precursor ion at m/z 823 became non-observable as the product ion at m/z 72 became more intense and was assigned as protonated vinyl amine. This is indicative of the fragmentation of the pendant arms of PDMAEMA, which retain the charge. Two additional product ions are observed at m/z 743 and m/z 672, which represent losses of 80 Da (HBr) and 71 Da (vinyl amine), respectively. The loss of HBr was expected since the synthetic methodology implemented, i.e., photoATRP, provides a brominated ω-end group. Using the fragmentation data obtained from each homopolymer, tandem mass spectrometry (MS^n) was used to preform fragmentation pathway analysis on the random copolymer, poly(HEMA-ran-DMAEMA).

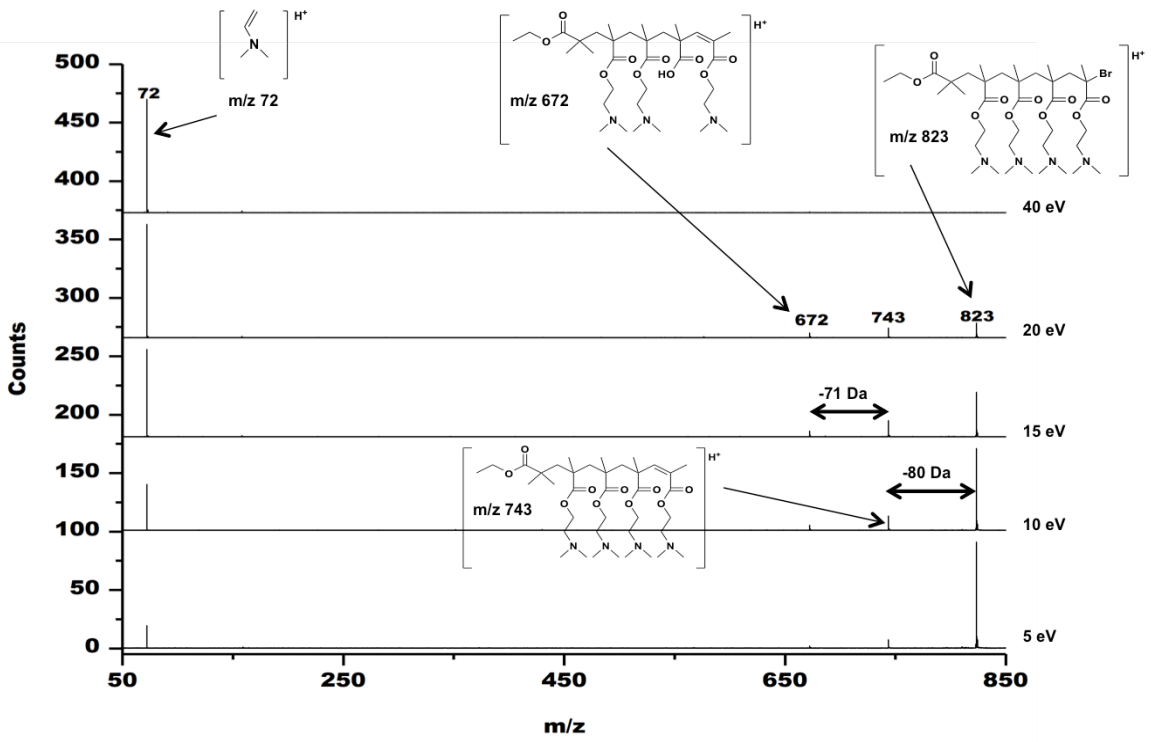

Figure 4.8 MS/MS spectra of PDMAEMA oligomer (DP = 4) at various collision energies, 5, 10, 15, 20, and 40 eV. Losses of 80 Da (HBr) and 71 Da (vinyl amine) were observed and the corresponding structures are shown. Spectra collected with Agilent 6530 Accurate Mass QTOF LC/MS.

4.4.2 Fragmentation Pattern Analysis of poly(HEMA-ran-DMAEMA) Oligomers Using Tandem Mass Spectrometry

The information discussed in the previous section was applied to analysis of the fragmentation pattern of poly(HEMA-*ran*-DMAEMA) providing insight into the sequence/composition of these random copolymers. Tandem mass spectrometry (MS^n) was carried out using a Thermo LTQ-XL Linear Ion Trap mass spectrometer for poly(HEMA-*ran*-DMAEMA) oligomers containing the HEMA:DMAEMA monomer ratios of 2:2 and 3:2.

Using the structure identification chart shown in Chapter 3 (Figure 3.9), the oligomer consisting of two HEMA and two DMAEMA monomers was selected for

fragmentation pattern analysis. During MS^2 analysis, preferred fragmentation pathways for the precursor ion at m/z 769 produced two product ions at m/z 689 and m/z 618 representing losses of 80 Da (HBr) and 71 Da (vinyl amine) as shown in Figure 4.9.

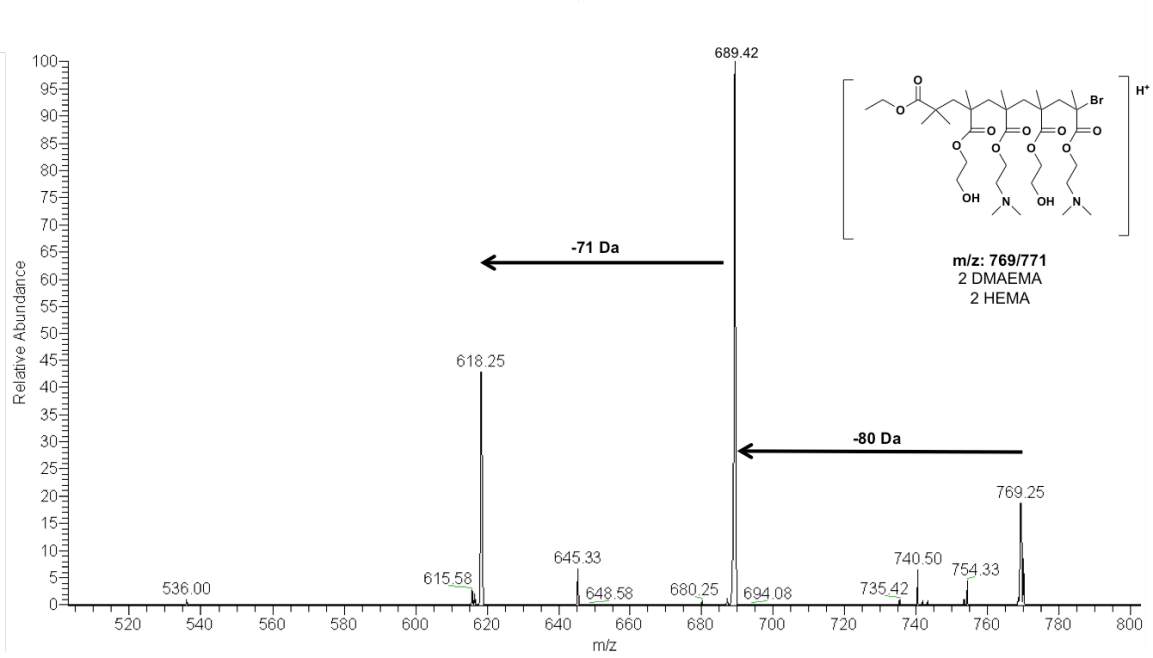

Figure 4.9 MS^2 spectrum of poly(HEMA-*ran*-DMAEMA) oligomer (DP = 4) collected using the Thermo LTQ-XL mass spectrometer. Losses of 80 Da and 71 Da represent HBr and vinyl amine, respectively were observed.

The product ion at m/z 689 was isolated and fragmented for MS^3 analysis producing multiple product ions as shown in Figure 4.10. A loss of 44 Da was observed as the preferred fragmentation pathway, giving rise to the product ion at m/z 645. The secondary fragmentation pathway shows a loss of 89 Da, which was assigned as 2-(dimethylamino)ethanol. This fragment was not observed for the homopolymers and was concluded this fragment arises from the coupling of adjacent DMAEMA and HEMA pendant arms.

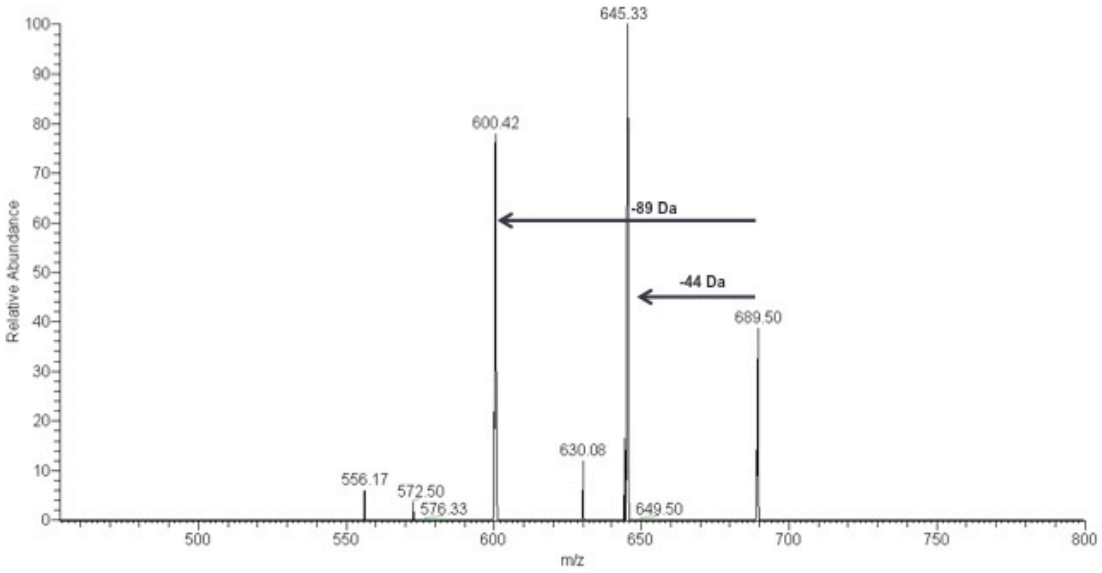

Figure 4.10 MS^3 spectrum of poly(HEMA-*ran*-DMAEMA) oligomer (DP = 4) collected using the Thermo LTQ-XL mass spectrometer. Observed losses of 44 Da and 89 Da represent vinyl alcohol and 2-(dimethylamino)ethanol, respectively.

The fragment at m/z 645 was isolated and fragmented for MS^4 analysis and numerous product ion peaks were observed as shown in Figure 4.11. Fragments lost included vinyl alcohol, 2-(dimethyl)amino ethanol, vinyl amine, and carbon monoxide. Most notably, the loss of 62 Da (ethylene glycol) was not observed. This piece of information is significant for determining the monomer sequence of the oligomer since ethylene glycol can only be observed when HEMA monomers are adjacent along the polymer backbone.

The complete fragmentation pathway is shown in Scheme 4.2. To demonstrate the loss of ethylene glycol could be used to further investigate the sequence of this copolymer, an oligomer containing 3 HEMA and 2 DMAEMA monomers was selected for fragmentation pattern analysis.

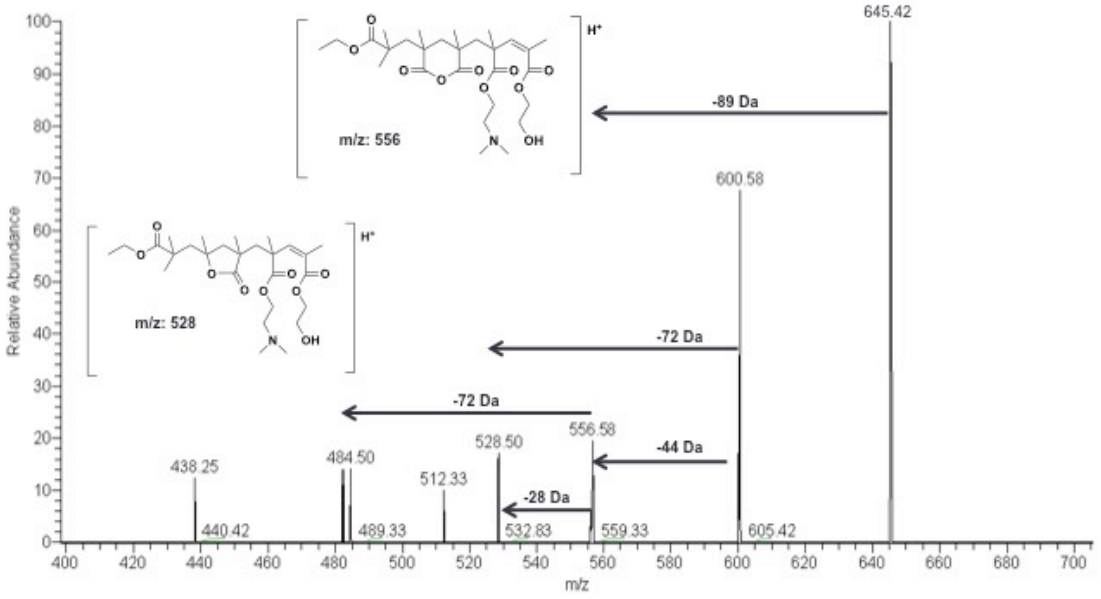

Figure 4.11 MS^4 spectrum of poly(HEMA-*ran*-DMAEMA) oligomer (DP = 4) collected using the Thermo LTQ-XL mass spectrometer. Potential structures for various m/z ratios are shown.

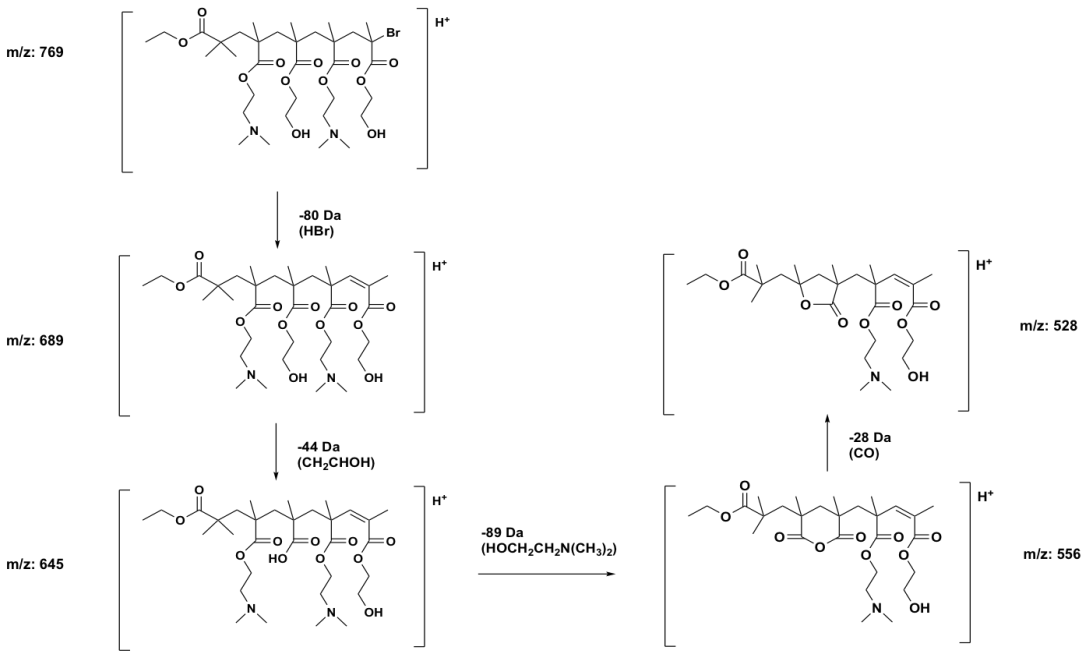

Scheme 4.2 Preferred fragmentation pathway of poly(HEMA-*ran*-DMAEMA) oligomer (DP = 4) showing no loss of ethylene glycol.

An oligomer containing 3 HEMA monomers and 2 DMAEMA monomers represents the precursor ion at m/z 901 was isolated and fragmented for MS^2 analysis. Similar to the oligomer containing a monomer ratio of 2 HEMA : 2 DMAEMA, the most prominent fragment lost was HBr and is shown in Figure 4.12.

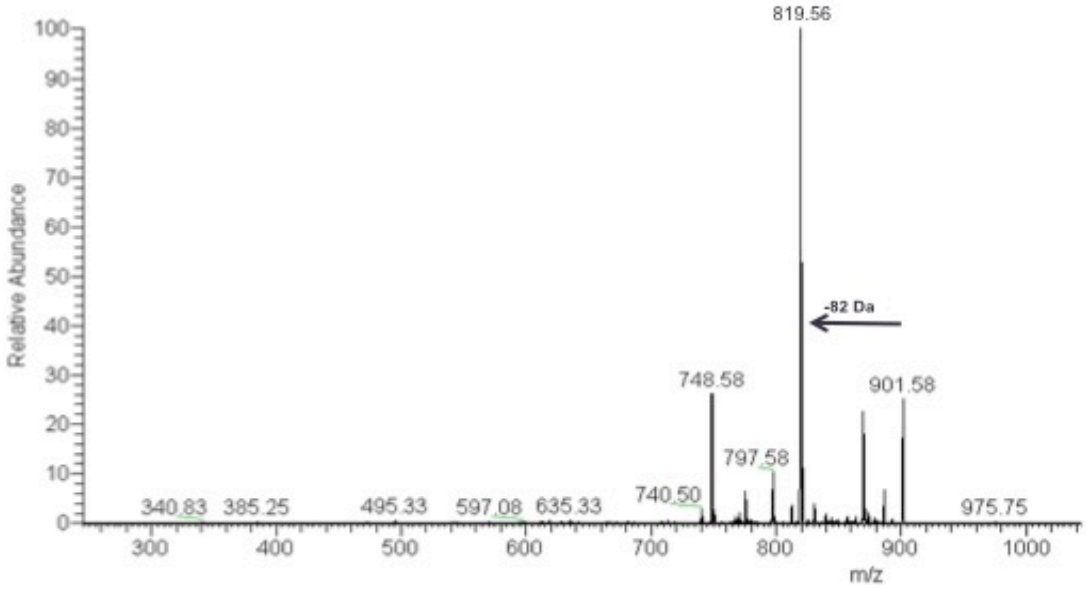

Figure 4.12 MS^2 analysis showing the preferred fragmentation pathway of poly(HEMA-*ran*-DMAEMA) oligomer (DP = 5). The loss of HBr (82 Da) is the preferred fragmentation pathway shown by the bold arrow. Collected using the Thermo LTQ-XL mass spectrometer.

The product ion at m/z 819 was isolated and fragmented for MS^3 analysis producing two peaks at m/z 775 after a loss of 44 Da (vinyl alcohol) and the more prominent one at m/z 730 after a loss of 89 Da (2-dimethylamino)ethanol as shown in Figure 4.13. Following the preferred fragmentation pathway, m/z 730 was isolated and fragmented for MS^4 analysis. The most prominent fragmentation pathway gave rise to m/z 686 after a loss of 44 Da (vinyl alcohol) and is shown if Figure 4.14. Next, m/z 686 was isolated and fragmented for MS^5 analysis. The primary fragmentation pathway was again the loss of 44 Da but the secondary fragmentation pathway involved the loss of 62

Da, which was assigned as ethylene glycol (Figure 4.15). This fragment is significant since it can only arise from two adjacent HEMA monomers in the polymer backbone and thereby provides insight in to the sequence of the oligomer under investigation. Further fragmentation analysis could not be performed due to the low abundance of ions remaining following MS^5 analysis. The preferred fragmentation pathway of an oligomer containing 3 HEMA and 2 DMAEMA monomers is shown in Scheme 4.3. During MS^5 analysis a loss of ethylene glycol was observed which can only occur if two HEMA monomers are adjacent in the polymer backbone.

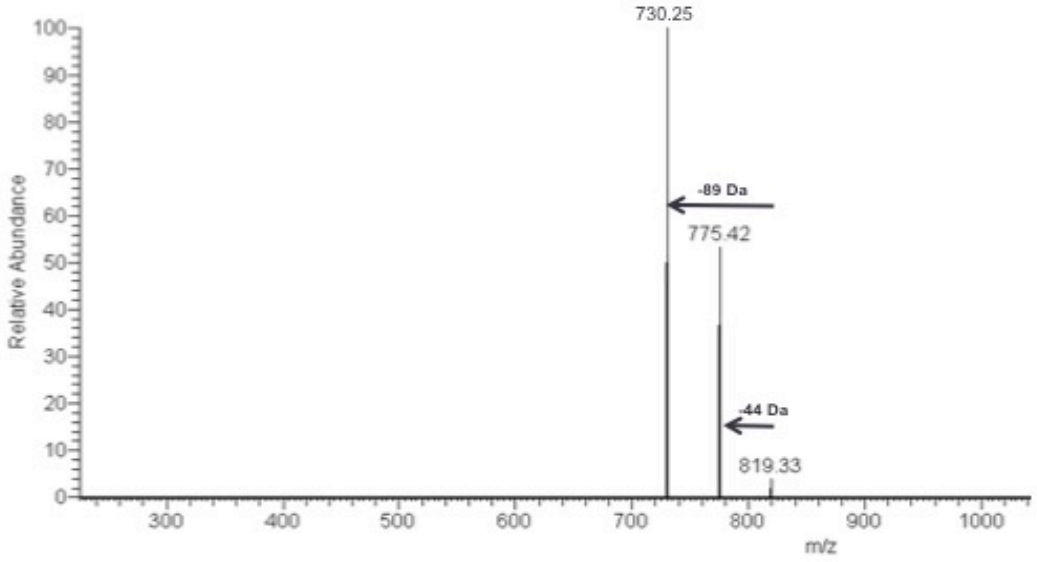

Figure 4.13 MS^3 analysis of poly(HEMA-*ran*-DMAEMA) oligomer (DP = 5) showing losses of 89 Da (preferred) and 44 Da (secondary). Collected using the Thermo LTQ-XL mass spectrometer.

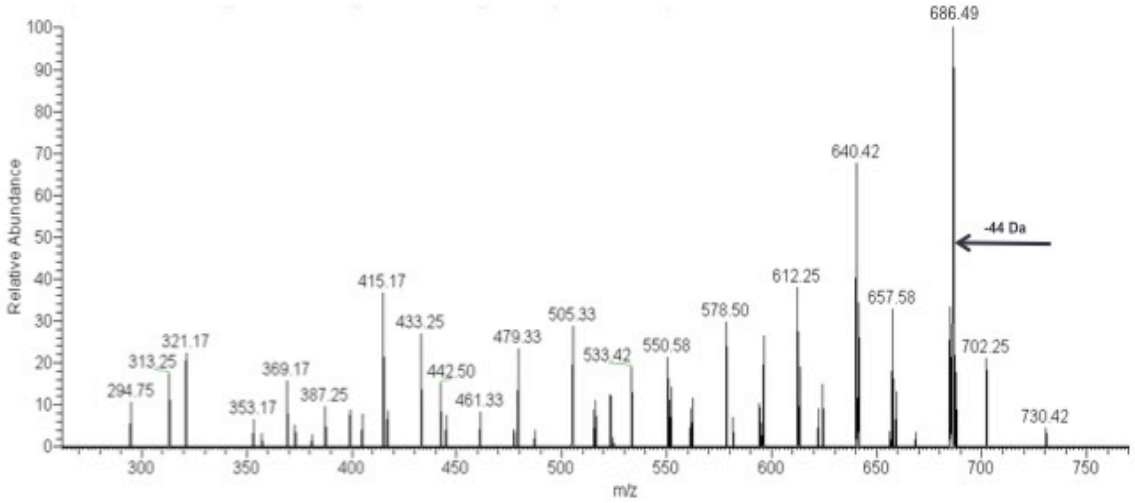

Figure 4.14 MS^4 analysis of poly(HEMA-*ran*-DMAEMA) oligomer (DP = 5) showing a loss of 44 Da as the preferred fragmentation pathway. Collected using the Thermo LTQ-XL mass spectrometer.

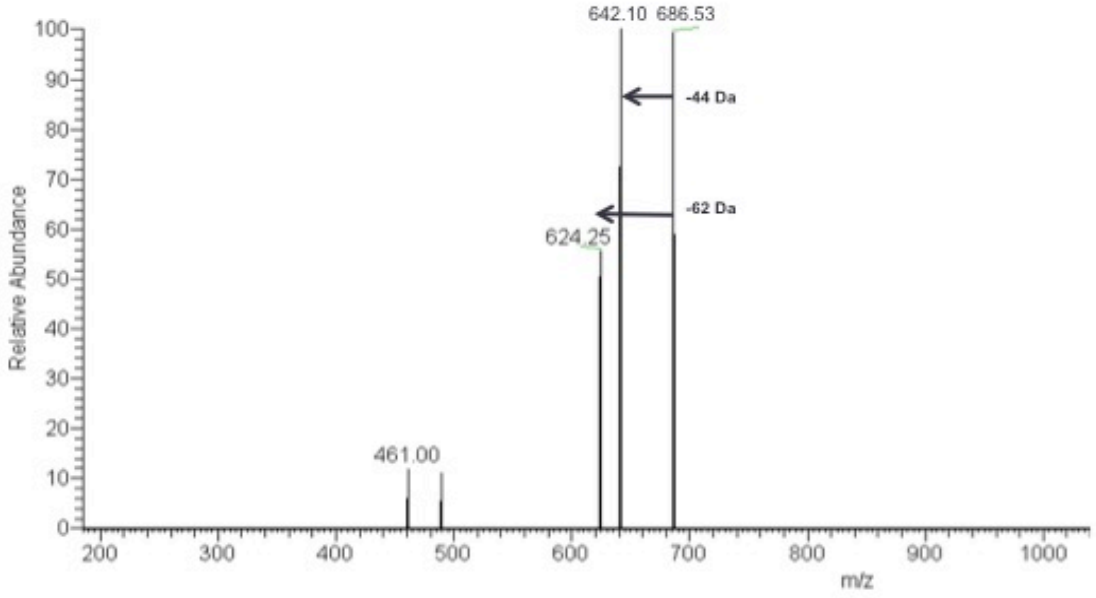

Figure 4.15 MS^5 analysis of poly(HEMA-*ran*-DMAEMA) oligomer (DP = 5) showing a loss of 44 Da as preferred fragmentation pathway and loss of 62 Da representing ethylene glycol which is indicative of two adjacent HEMA monomers. Collected using the Thermo LTQ-XL mass spectrometer.

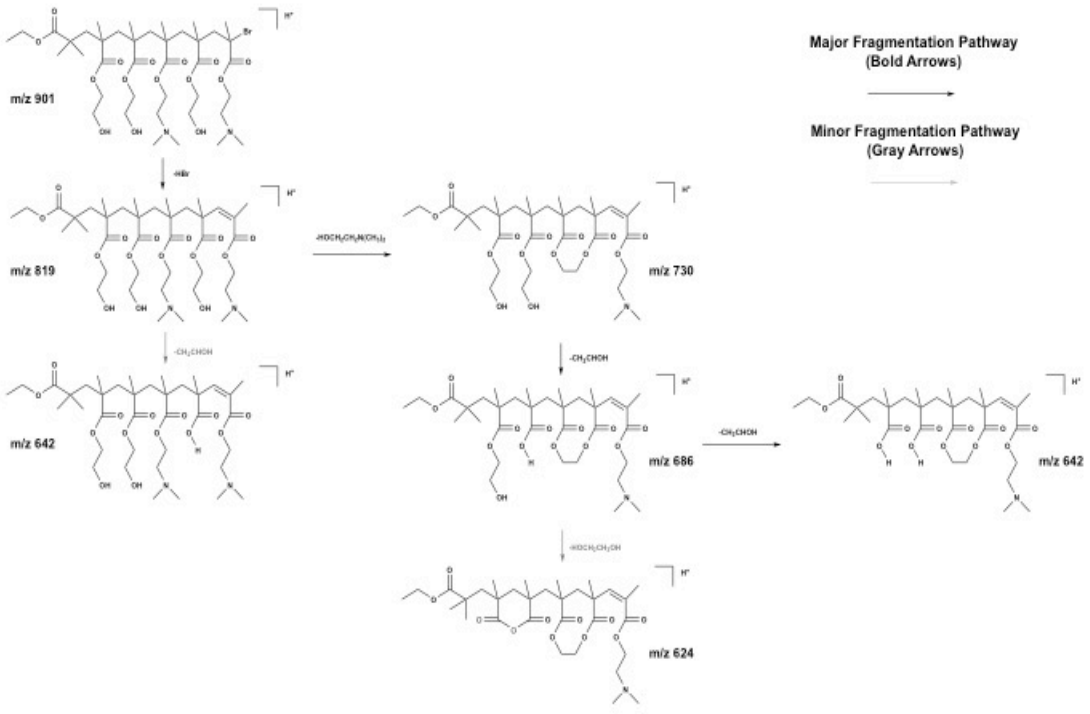

Scheme 4.3 Fragmentation pathways of poly(HEMA-*ran*-DMAEMA) oligomer (DP = 5) showing a loss of 62 Da during MS^5 analysis, which represents ethylene glycol, indicative of two adjacent HEMA monomers in the polymer structure.

4.5 Summary and Conclusions

When performing MS^n analysis of copolymers, it is of fundamental importance to examine the fragmentation patterns of the respective homopolymers comprising the copolymer. Therefore, tandem mass spectrometry was performed on PHEMA and PDMAEMA prior to poly(HEMA-ran-DMAEMA).

The fragmentation pathways of each homopolymer had similarities and differences. Initially, the preferred pathway was the loss of hydrogen bromide for both PHEMA and PDMAEMA. As the collision energy was increased during MS^2 analysis, the fragmentation pathway of PHEMA became convoluted in the low to mid m/z range. Therefore, a linear ion trap was used for MS^n analysis of PHEMA. Four primary

fragments were observed after the initial loss of hydrogen bromide. During MS^3 analysis a loss of vinyl alcohol was observed followed by a loss of carbon monoxide (MS^4). The loss of ethylene glycol was observed during MS^5. This fragment can only be observed if two HEMA monomers are adjacent in the polymer backbone and became significant when examining the fragmentation patterns of copolymers containing HEMA.

In contrast to PHEMA, the fragmentation pattern of PDMAEMA was not convoluted during MS^2 analysis. As CE was increased the primary fragment observed was protonated vinyl amine arising from the pendant arm of PDMAEMA. Using the information collected from the fragmentation pattern analysis of PHEMA and PDMAEMA, the fragmentation pattern analysis of poly(HEMA-ran-DMAEMA) was performed.

Initially, MS^n was performed on a co-oligomer containing 2 HEMA and 2 DMAEMA monomers. Following the loss of hydrogen bromide, losses of vinyl alcohol and 2-(dimethyl)amino ethanol were observed. No loss of ethylene glycol was observed indicating that the two HEMA monomers in the oligomer were not adjacent to each other. It was then hypothesized that ethylene glycol would be observed during fragmentation analysis of a co-oligomer containing 3 HEMA and 2 DMAEMA monomers. The fragmentation data showed similar losses that were observed for the 2 HEMA : 2 DMAEMA co-oligomer when performing MS^2 through MS^4. But as expected during MS^5 analysis, the loss of ethylene glycol was observed indicating that two HEMA monomers were adjacent to one another along the polymer backbone. Therefore, it was concluded that the loss of ethylene glycol during MS^n analysis provides insight into the

composition/sequence of HEMA-containing copolymers and can be applied to investigations focusing on these types of polymeric systems.

4.6 References

1. Matyjaszewski, K. Advanced Materials by Atom Transfer Radical Polymerization. *Advanced Materials* **2018,** *30* (23), 1706441.

2. Hu, J.; Liu, S. Responsive Polymers for Detection and Sensing Applications: Current Status and Future Developments. *Macromolecules* **2010,** *43* (20), 8315-8330.

3. Wang, H.-S.; Song, M.; Hang, T.-J. Functional Interfaces Constructed by Controlled/Living Radical Polymerization for Analytical Chemistry. *ACS Applied Materials & Interfaces* **2016,** *8* (5), 2881-2898.

4. Gao, Y.; Wei, M.; Li, X.; Xu, W.; Ahiabu, A.; Perdiz, J.; Liu, Z.; Serpe, M. J. Stimuli-responsive polymers: Fundamental considerations and applications. *Macromolecular Research* **2017,** *25* (6), 513-527.

5. Altuntaş, E.; Schubert, U. S. "Polymeromics": Mass spectrometry based strategies in polymer science toward complete sequencing approaches: A review. *Analytica Chimica Acta* **2014,** *808*, 56-69.

6. Fournier, D.; Hoogenboom, R.; Thijs, H. M. L.; Paulus, R. M.; Schubert, U. S. Tunable pH- and Temperature-Sensitive Copolymer Libraries by Reversible Addition−Fragmentation Chain Transfer Copolymerizations of Methacrylates. *Macromolecules* **2007,** *40* (4), 915-920.

7. Han, X.; Zhang, X.; Zhu, H.; Yin, Q.; Liu, H.; Hu, Y. Effect of Composition of PDMAEMA-b-PAA Block Copolymers on Their pH- and Temperature-Responsive Behaviors. *Langmuir* **2013,** *29* (4), 1024-1034.

8. Choi, J. W.; Baek, K.-Y.; Cho, K. Y.; Bhattacharjee, N.; Lee, S.-H. Amphiphilic Block Copolymer for adsorption of Organic Contaminants. *Advances in Chemical Engineering and Science* **2011,** *1*, 77-82.

9. Baş, N.; Yakar, A.; Bayramgil, N. P. Removal of cobalt ions from aqueous solutions by using poly(N,N-dimethylaminopropyl methacrylamide/itaconic acid) hydrogels. *Journal of Applied Polymer Science* **2014,** *131* (7).

10. Liu, X.; Guan, J.; Lai, G.; Xu, Q.; Bai, X.; Wang, Z.; Cui, S. Stimuli-responsive adsorption behavior toward heavy metal ions based on comb polymer functionalized magnetic nanoparticles. *Journal of Cleaner Production* **2020,** *253*, 119915.

11. Lee, J. B.; Schlautman, A. M. Effects of Polymer Molecular Weight on Adsorption and Flocculation in Aqueous Kaolinite Suspensions Dosed with Nonionic Polyacrylamides. *Water* **2015,** *7* (11).

12. Altuntaş, E.; Krieg, A.; Baumgaertel, A.; Crecelius, A. C.; Schubert, U. S. ESI, APCI, and MALDI tandem mass spectrometry of poly(methyl acrylate)s: A comparison study for the structural characterization of polymers synthesized via CRP techniques and the software application to analyze MS/MS data. *Journal of Polymer Science Part A: Polymer Chemistry* **2013,** *51* (7), 1595-1605.

13. Wesdemiotis, C. Multidimensional Mass Spectrometry of Synthetic Polymers and Advanced Materials. *Angewandte Chemie International Edition* **2017,** *56* (6), 1452-1464.

14. Crotty, S.; Gerişlioğlu, S.; Endres, K. J.; Wesdemiotis, C.; Schubert, U. S. Polymer architectures via mass spectrometry and hyphenated techniques: A review. *Analytica Chimica Acta* **2016,** *932*, 1-21.

15. Barner-Kowollik, C.; Gruendling, T.; Falkenhagen, J.; Weidner, S.; Barner-Kowollik, C. *Mass Spectrometry in Polymer Chemistry*; John Wiley & Sons, Incorporated: Hoboken, GERMANY, 2012.

16. Gruendling, T.; Weidner, S.; Falkenhagen, J.; Barner-Kowollik, C. Mass spectrometry in polymer chemistry: a state-of-the-art up-date. *Polymer Chemistry* **2010,** *1* (5), 599-617.

17. Miladinović, S. M.; Kaeser, C. J.; Knust, M. M.; Wilkins, C. L. Tandem Fourier transform mass spectrometry of block and random copolymers. *International Journal of Mass Spectrometry* **2011,** *301* (1), 184-194.

18. Zhang, Y.; Chu, D.; Zheng, M.; Kissel, T.; Agarwal, S. Biocompatible and degradable poly(2-hydroxyethyl methacrylate) based polymers for biomedical applications. *Polymer Chemistry* **2012,** *3* (10), 2752-2759.

19. Montheard, J.-P.; Chatzopoulos, M.; Chappard, D. 2-Hydroxyethyl Methacrylate (HEMA): Chemical Properties and Applications in Biomedical Fields. *Journal of Macromolecular Science* **1992,** *Part C: Polymer Reviews*, 1-34.

20. Pereira, A. T.; Henriques, P. C.; Costa, P. C.; Martins, M. C. L.; Magalhães, F. D.; Gonçalves, I. C. Graphene oxide-reinforced poly(2-hydroxyethyl methacrylate) hydrogels with extreme stiffness and high-strength. *Composites Science and Technology* **2019,** *184*, 107819.

21. Gao, H.; Liu, G.; Chen, X.; Hao, Z.; Tong, J.; Lu, L.; Cai, Y.; Long, F.; Zhu, M. Media-Modulated Interchain or Intrachain Coordination of Amphiphilic Block Copolymer Micelles. *Macromolecules* **2010,** *43* (14), 6156-6165.

22. Pan, Y.; Cai, P.; Farmahini-Farahani, M.; Li, Y.; Hou, X.; Xiao, H. Amino-functionalized alkaline clay with cationic star-shaped polymer as adsorbents for removal of Cr(VI) in aqueous solution. *Applied Surface Science* **2016,** *385*, 333-340.

23. Yoshida, E. Preparation of giant vesicles containing quaternary ammonium salt of 2-(dimethylamino)ethyl methacrylate through photo nitroxide-mediated controlled/living radical polymerization-induced self-assembly. *Journal of Polymer Research* **2018,** *25* (5), 109.

24. Kuila, A.; Chatterjee, D. P.; Maity, N.; Nandi, A. K. Multi-functional poly(vinylidene fluoride) graft copolymers. *Journal of Polymer Science Part A: Polymer Chemistry* **2017,** *55* (16), 2569-2584.

25. Saha, A.; Jana, S.; Bose, A.; Mandal, T. K. Peptide-poly(2-(dimethylamino)ethyl methacrylate) conjugates: Synthesis and aqueous/nonaqueous self-aggregation into nanostructures of dendritic and spherical morphologies. *Journal of Polymer Science Part A: Polymer Chemistry* **2017,** *55* (19), 3286-3297.

26. Asamoto, H.; Kimura, Y.; Ishiguro, Y.; Minamisawa, H.; Yamada, K. Use of polyethylene films photografted with 2-(dimethylamino)ethyl methacrylate as a potential adsorbent for removal of chromium (VI) from aqueous medium. *Journal of Applied Polymer Science* **2016,** *133* (18), n/a-n/a.

27. Ciampolini, M.; Nardi, N. Five-Coordinated High-Spin Complexes of Bivalent Cobalt, Nickel, andCopper with Tris(2-dimethylaminoethyl)amine. *Inorganic Chemistry* **1966,** *5* (1), 41-44.

28. Cohen, N. A.; Tillman, E. S.; Thakur, S.; Smith, J. R.; Eckenhoff, W. T.; Pintauer, T. Effect of the Ligand in Atom Transfer Radical Polymerization Reactions Initiated by Photodimers of 9-Bromoanthracene. *Macromolecular Chemistry and Physics* **2009,** *210* (3-4), 263-268.

29. Anastasaki, A.; Nikolaou, V.; Simula, A.; Godfrey, J.; Li, M.; Nurumbetov, G.; Wilson, P.; Haddleton, D. M. Expanding the Scope of the Photoinduced Living Radical Polymerization of Acrylates in the Presence of CuBr2 and Me6-Tren. *Macromolecules* **2014,** *47* (12), 3852-3859.

30. Jackson, A. T.; Thalassinos, K.; John, R. O.; McGuire, N.; Freeman, D.; Scrivens, J. H. Characterisation of end groups in poly(2-hydroxyethyl methacrylate) by means of electrospray ionisation-mass spectrometry/mass spectrometry (ESI-MS/MS). *Polymer* **2010,** *51* (6), 1418-1424.

31. Hearn, M. J.; Briggs, D. Analysis of polymer surfaces by SIMS. 12. On the fragmentation of acrylic and methacrylic homopolymers and the interpretation of their positive and negative ion spectra. *Surface and Interface Analysis* **1988,** *11* (4), 198-213.

32. Wesdemiotis, C.; Solak, N.; Polce, M. J.; Dabney, D. E.; Chaicharoen, K.; Katzenmeyer, B. C. Fragmentation pathways of polymer ions. *Mass Spectrometry Reviews* **2011,** *30* (4), 523-559.

33. Town, J. S.; Jones, G. R.; Hancox, E.; Shegiwal, A.; Haddleton, D. M. Tandem Mass Spectrometry for Polymeric Structure Analysis: A Comparison of Two Common MALDI–ToF/ToF Techniques. *Macromolecular Rapid Communications* **2019,** *40* (13), 1900088.

34. Nyström, F.; Soeriyadi, A. H.; Boyer, C.; Zetterlund, P. B.; Whittaker, M. R. End-group fidelity of copper(0)-meditated radical polymerization at high monomer conversion: an ESI-MS investigation. *Journal of Polymer Science Part A: Polymer Chemistry* **2011,** *49* (24), 5313-5321.

35. Maurer, J. J.; Eustace, D. J.; Ratcliffe, C. T. Thermal characterization of poly(acrylic acid). *Macromolecules* **1987,** *20* (1), 196-202.

Chapter 5

Project Impact and Future Directions

5.1 Project Impact

5.1.1 Development of Novel Highly Active Catalysts for Atom Transfer Radical Processes

Hybrid ligands, 2-(dimethylamino)ethyl-bis-[2-(pyridylmethyl)amine] (M1-T2) and bis[2-(dimethylamino)ethyl]-2-(pyridylmethyl)amine (M2-T1), were successfully synthesized and complexed to copper centers to use as catalysts for atom transfer radical processes, i.e. ATRA and ATRP. The hybrid ligands contain different numbers of tris[2-(dimethylamino)ethyl]amine (Me_6TREN) and tris(2-pyridylmethyl)amine (TPMA) arms, which are known to be two of the most highly active ligands for these types of reactions.[1] Typically, Me_6TREN complexes outperform TPMA complexes in ATRA and ATRP reactions. The one exception is when performing ARGET ATRA utilizing ascorbic acid as the reducing agent. Upon the formation of dehydroascorbic acid, a strong acid is produced. Me_6TREN is more susceptible to protonation than TPMA and this attribute of Me_6TREN ultimately renders the catalyst inactive. Hence, TPMA is a better choice for ARGET ATRA reactions but is not as active as Me_6TREN when utilized in other protocols. The novel hybrid ligands discussed in this work maintain high activity in ARGET ATRA systems and are less susceptible to protonation, allowing them to outperform TPMA complexes in reactions of this type. The data suggest that it is possible to create hybrid ligands based off of known highly active species allowing for novel ligand scaffolds to be developed, ultimately increasing catalyst activity and reducing the amount of heavy metal waste produced.

5.1.2 Fragmentation Pattern analysis of PHEMA, PDMAEMA, and Poly(HEMA-ran-DMAEMA)

Poly(2-hydroxyethyl methacrylate) (PHEMA) and poly(2-dimethylamino)ethyl methacrylate (PDMAEMA) are two important polymers having applications in numerous areas.[2-5] PHEMA is hydrophilic due to the hydroxyl functionalities on its pendent arms making it useful for biomedical applications such as contact lenses and the fabrication of biocompatible materials. PDMAEMA is a stimuli-responsive polymer and possesses pH-tunability due to the tertiary amine functionalities on its pendent arms. Therefore (co)polymers containing HEMA and/or DMAEMA can form amphiphilic materials and stimuli-responsive hydrogels for drug release applications, microfluidic devices, and tissue engineering.[6-8] Additionally, due to the advent of controlled radical polymerization methodologies, (co)polymers can be engineered to have complex architectures, predetermined molecular weights, and narrow polydispersity indices (PDI).[9-10] Therefore there exists a need to investigate the structures and compositions of (co)polymers containing HEMA and/or DMAEMA. In the work presented here, PHEMA and PDMAEMA were synthesized utilizing a photoATRP technique and their fragmentation patterns examined using tandem mass spectrometry (MS/MS). The data collected provided insight into the species formed during fragmentation. It was determined the number of ethylene glycol losses during multi-stage mass spectrometry (MS^n) analysis can provide information as to how many adjacent HEMA monomers are present in a random copolymer. This aspect is of interest since the amount of a given monomer in copolymers can influence characteristics such as architecture, volume of hydrogels, and lower critical solution temperature (LCST).[11-12]

5.1.3 Removal of Pb^{2+} From Aqueous Systems Using Polymeric Adsorbents (Preliminary Data)

Heavy metal ions are highly toxic for aquatic and terrestrial life, including humans. Three heavy metals e.g. Cd, Hg, and Pb are on the World Health Organization's top ten list for pollutants of major health concern.[13] Therefore, it is of utmost importance to develop methodologies that can efficiently remove them from hazardous industrial wastewater prior to being released into the environment. The polymeric materials discussed in the Chapter 5 Appendix, PHEMA and poly(AAm-*co*-AAc), address this problem by removing these pollutants via adsorption processes. Preliminary data suggests that they have the ability to remove Pb^{2+} from aqueous systems. Due to the development of controlled radical processes, it is believed that copolymers can be specifically tailored for wastewater produced by the industrial sector.

5.2 Future Directions

5.2.1 Polymer Synthesis and Mass Spectrometry Characterization

Due to the applicability of (co)polymers containing HEMA and/or DMAEMA there exists an interest to understand and predict the properties of these types of materials. A variety of different architectures and compositions can be realized due to controlled radical polymerizations such as ATRP, RAFT, and NMP. Since the development of soft ionization sources, e.g. ESI and MALDI, mass spectrometry has become a powerful tool for examining polymer architectures, compositions, and sequences.[14] It is envisioned that the information obtained in this work may allow for the elucidation of compositions and architectures of (co)polymers containing HEMA and/or

DMAEMA. For example, fragmentation data obtained could be used to examine the degree of polymerization of the PHEMA block of an A-B-A block copolymer as shown in Figure 5.1. Additionally, due to the advancement of an emerging field termed polymeromics, software has been designed to predict fragmentation patterns of polymers.[15] This software could be implemented to support or refute experimental data and assist in determination of fragmentation patterns of (co)polymers.

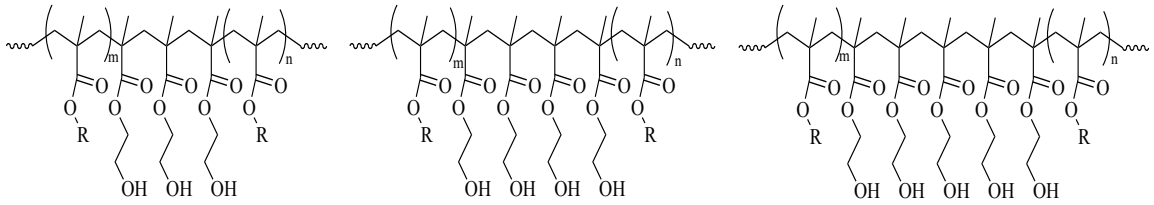

Figure 5.1 Utilizing MS^n, the number of HEMA monomers in an A-B-A block copolymer can be determined.

5.2.2 Removal of Heavy Metals From Aqueous Systems Using Polymeric Adsorbents

To examine the adsorption capabilities of various polymer motifs, different types of monomers possessing different attributes, e.g., chelating functionalities and pendant arm lengths could be polymerized using ATRP methodologies. Employing different monomers, shown in Figure 5.2, could provide insight into relationships between chelator identity/pendant arm length and adsorption capacity. Additionally, it would provide details on the selectivity of different polymer functionalities towards various heavy metal ions. Soft chelating functionalities are expected to more efficiently adsorb softer metals while hard chelating groups will more efficiently adsorb hard metals. All monomers shown in Figure 6.2 are commercially available with the exception of (7), which would be synthesized and polymerized according to a previously reported method shown in

Scheme 5.1.[16] Lastly, since all monomers are comprised of the methacrylate functionality, methyl methacrylate (MMA) could be implemented as the spacer monomer (8) since it is expected to have a comparable polymerization rate as the other monomers.[17]

There have been few reports describing the relationship between molecular weight (MW) and adsorption capabilities.[18] By synthesizing polymers using a controlled radical method such as ATRP, correlations could be made for this relationship. Additionally, ATRP allows for a finely tuned degree of polymerization (DP) and narrow PDI values, which are directly related to the molecular weight. These values for controlled radical polymerizations typically range from 1.05-1.5 in contrast with traditional radical or condensation techniques, which have PDI values > 2. Hence, it is difficult to establish a correlation between molecular weight and adsorption capacity if using the latter polymerization methods since there is a large variation of MW for the polymeric chains. Therefore, metal adsorbing polymers with narrow PDIs and predetermined degrees of polymerization can be synthesized via ATRP and correlations made between MW and adsorption capacity.

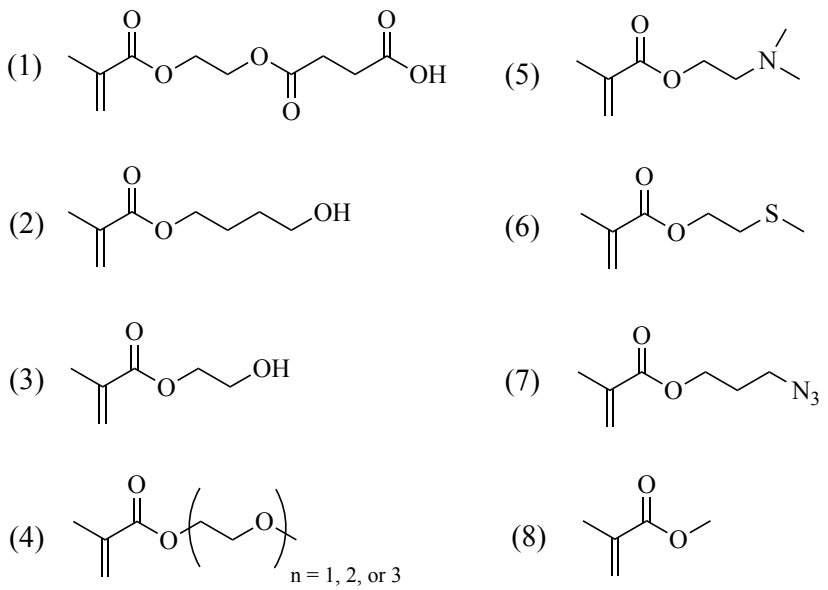

Figure 5.2 Functional monomers polymerized via ATRP producing polymers with different chelating species and pendent arm lengths. (1) mono-2-(methacryloyloxy)ethyl succinate, (2) 4-hydroxybutyl methacrylate, (3) 2-hydroxyethyl methacrylate, (4) (di)(tri)ethylene glycol methyl ether methacrylate, (5) 2-(dimethylamino)ethyl methacrylate, (6) 2-(methylthio)ethyl methacrylate, (7) 3-azidopropyl methacrylate, (8) methyl methacrylate.

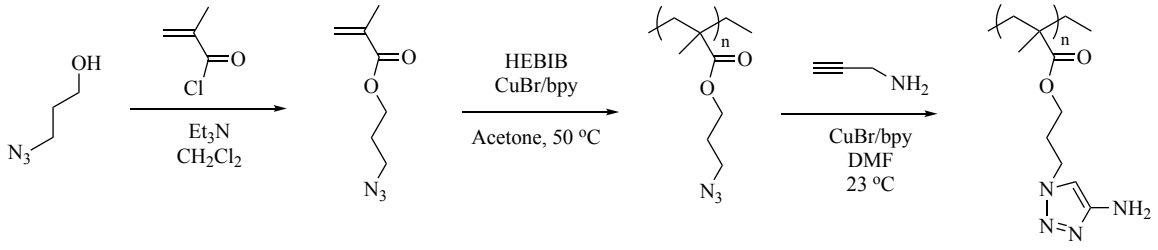

Scheme 5.1 Synthetic route for monomer (7) and the corresponding polymer containing the triazole chelating group.

The architecture or morphology of the polymer plays a role with regards to their heavy metal adsorption properties. Polymer architecture involves characteristics such as chelator density, i.e., spacing between chelating monomers, and length of pendent arms. The different sections of polymers are shown in Figure 5.3 and include the backbone (A), pendent arms (B), and chelating functional groups (C). The most important aspects

influencing adsorption capacity and selectivity for one metal over another are the pendent arms and chelating functionalities. The primary advantage of synthetic polymers synthesized via controlled radical polymerizations is the ability to fine-tune these aspects.

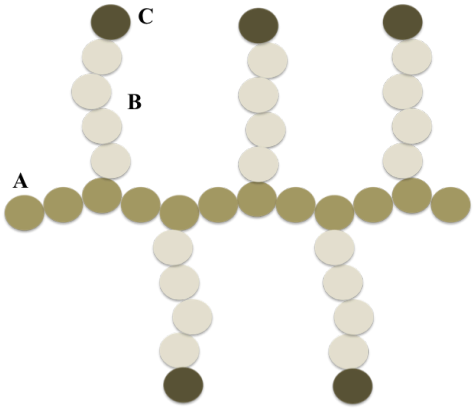

Figure 5.3 Architecture of a polymeric adsorbent. The polymer backbone (A), pendant arm (B), and chelating moiety (C) are shown.

The most direct way to prepare a functional polymer is to polymerize monomers that contain the desired pendant arm length and functionality. Since ATRP is tolerant of various functional groups, a wide range of structural motifs can be accessed.[1, 19] The differences between monomers will lie in their chelator composition and pendant arm lengths. It has been reported that longer, more flexible pendent arms can accommodate more coordination geometries of metals, thereby aiding in chelation.[20] To the best of our knowledge, there have been no reports addressing the relationship between the spacing of chelating monomers and adsorption capacity. Chelating functionalities that are too close in proximity to one another may impede the adsorption process due to steric hindrance therefore investigations into the effect of "spacer" monomers on adsorption capacity are warranted. An increase in chain length and the introduction of spacer monomers would

be expected to increase the adsorption capacity of the polymer by providing more flexibility to the pendent arms and reducing steric hindrance between chelating groups.

Due to the versatility of ATRP, various types of copolymers, e.g. block, random, statistical can be realized by the introduction of second and third monomers during polymerization. Hence, controlled radical polymerizations allow for the production of block copolymers, which could be specifically tailored for industrial wastewaters containing a variety of heavy metals. Due to the chain-end functionality of polymers synthesized using controlled radical methods, block copolymers can be prepared by adding each desired monomer to the reaction mixture in a specified sequence.

In addition to the removal of heavy metal ions from hazardous wastewater, there is a growing interest for developing chemical sensors for these pollutants. It is envisioned that methodologies developed and knowledge gained could aid in creating the next generation of sensors for heavy metal ions, which has become an area of interest due to the ever-increasing need for their detection.[21-23] Therefore, the synthetic protocols developed may find applications beyond the field described here. Ultimately, this work will help in creating a healthier and safer environment for all species affected by heavy metal pollution.

5.3 References

1. Matyjaszewski, K. Atom Transfer Radical Polymerization (ATRP): Current Status and Future Perspectives. *Macromolecules* **2012,** *45* (10), 4015-4039.

2. Samsonova, O.; Christian, P.; Hellmund, M.; Merkel, O.; Kissel, T. Low molecular weight pDMAEMA-block-pHEMA block-copolymers synthesized via RAFT-polymerization: Potential non-viral gene delivery agents. *Polymers* **2011,** *3*, 693-718.

3. Anastasaki, A.; Nikolaou, V.; Nurumbetov, G.; Wilson, P.; Kempe, K.; Quinn, J. F.; Davis, T. P.; Whittaker, M. R.; Haddleton, D. M. Cu(0)-Mediated Living Radical Polymerization: A Versatile Tool for Materials Synthesis. *Chemical Reviews* **2016,** *116* (3), 835-877.

4. Guice, K. B.; Loo, Y.-L. Azeotropic Atom Transfer Radical Polymerization of Hydroxyethyl Methacrylate and (Dimethylamino)ethyl Methacrylate Statistical Copolymers and Block Copolymers with Polystyrene. *Macromolecules* **2006,** *39* (7), 2474-2480.

5. Cao, P.; Mangadlao, J.; Advincula, R. *Stimuli-Responsive Polymers and their Potential Applications in Oil-Gas Industry* 2015; Vol. 55. p 706-733.

6. Teoh, R. L.; Guice, K. B.; Loo, Y.-L. Atom Transfer Radical Copolymerization of Hydroxyethyl Methacrylate and Dimethylaminoethyl Methacrylate in Polar Solvents. *Macromolecules* **2006,** *39* (25), 8609-8615.

7. Benjamin, C. C.; Craven, R. J.; Crone, W. C.; Lakes, R. S. Viscoelastic characterization of pH-sensitive 2-hydroxyethyl methacrylate (2-dimethylamino) ethyl methacrylate HEMA-DMAEMA hydrogels. *Polymer Testing* **2018,** *72*, 372-376.

8. Barbey, R.; Lavanant, L.; Paripovic, D.; Schüwer, N.; Sugnaux, C.; Tugulu, S.; Klok, H.-A. Polymer Brushes via Surface-Initiated Controlled Radical Polymerization: Synthesis, Characterization, Properties, and Applications. *Chemical Reviews* **2009,** *109* (11), 5437-5527.

9. Matyjaszewski, K.; Xia, J. Atom Transfer Radical Polymerization. *Chemical Reviews* **2001,** *101* (9), 2921-2990.

10. Matyjaszewski, K.; Tsarevsky, N. V. Macromolecular Engineering by Atom Transfer Radical Polymerization. *Journal of the American Chemical Society* **2014,** *136* (18), 6513-6533.

11. Kuila, A.; Chatterjee, D. P.; Maity, N.; Nandi, A. K. Multi-functional poly(vinylidene fluoride) graft copolymers. *Journal of Polymer Science Part A: Polymer Chemistry* **2017,** *55* (16), 2569-2584.

12. Fournier, D.; Hoogenboom, R.; Thijs, H. M. L.; Paulus, R. M.; Schubert, U. S. Tunable pH- and Temperature-Sensitive Copolymer Libraries by Reversible Addition−Fragmentation Chain Transfer Copolymerizations of Methacrylates. *Macromolecules* **2007,** *40* (4), 915-920.

13. World Health Organization. http://www.who.int/ipcs/assessment/public_health/chemicals_phc/en/ (accessed 01/14/2017).

14. Wesdemiotis, C.; Solak, N.; Polce, M. J.; Dabney, D. E.; Chaicharoen, K.; Katzenmeyer, B. C. Fragmentation pathways of polymer ions. *Mass Spectrometry Reviews* **2011,** *30* (4), 523-559.

15. Altuntaş, E.; Schubert, U. S. "Polymeromics": Mass spectrometry based strategies in polymer science toward complete sequencing approaches: A review. *Analytica Chimica Acta* **2014,** *808*, 56-69.

16. Sumerlin, B. S.; Tsarevsky, N. V.; Louche, G.; Lee, R. Y.; Matyjaszewski, K. Highly Efficient "Click" Functionalization of Poly(3-azidopropyl methacrylate) Prepared by ATRP. *Macromolecules* **2005,** *38* (18), 7540-7545.

17. Dolinski, N. D.; Page, Z. A.; Discekici, E. H.; Meis, D.; Lee, I.-H.; Jones, G. R.; Whitfield, R.; Pan, X.; McCarthy, B. G.; Shanmugam, S.; Kottisch, V.; Fors, B. P.; Boyer, C.; Miyake, G. M.; Matyjaszewski, K.; Haddleton, D. M.; Alaniz, J. R.; Anastasaki, A.; Hawker, C. J. What happens in the dark? Assessing the temporal control of photo-mediated controlled radical polymerizations. *Journal of Polymer Science Part A: Polymer Chemistry* **2018,** *0* (0).

18. Lee, J. B.; Schlautman, A. M. Effects of Polymer Molecular Weight on Adsorption and Flocculation in Aqueous Kaolinite Suspensions Dosed with Nonionic Polyacrylamides. *Water* **2015,** *7* (11).

19. Shannon, R. W.; Brad, J. D.; Nicolay, V. T. Selecting the Optimal Reaction Conditions for Copper-Mediated Atom Transfer Radical Polymerization at Low Catalyst Concentration. In *Progress in Controlled Radical Polymerization: Mechanisms and Techniques*; American Chemical Society, 2012; Vol. 1100, pp 99-113.

20. Cegłowski, M.; Schroeder, G. Removal of heavy metal ions with the use of chelating polymers obtained by grafting pyridine–pyrazole ligands onto polymethylhydrosiloxane. *Chemical Engineering Journal* **2015,** *259*, 885-893.

21. Tayade, K. C.; Kuwar, A. S.; Fegade, U. A.; Sharma, H.; Singh, N.; Patil, U. D.; Attarde, S. B. Design and Synthesis of a Pyridine Based Chemosensor: Highly Selective Fluorescent Probe For Pb2+. *Journal of Fluorescence* **2014,** *24* (1), 19-26.

22. Banjoko, V.; Xu, Y.; Mintz, E.; Pang, Y. Synthesis of terpyridine-functionalized poly(phenylenevinylene)s: The role of meta-phenylene linkage on the Cu2+ and Zn2+ chemosensors. *Polymer* **2009,** *50* (9), 2001-2009.

23. Feng, X. J.; Tian, P. Z.; Xu, Z.; Chen, S. F.; Wong, M. S. Fluorescence-Enhanced Chemosensor for Metal Cation Detection Based on Pyridine and Carbazole. *The Journal of Organic Chemistry* **2013,** *78* (22), 11318-11325.

Chapter 2 Appendix

Table A.2.1 Summary of crystallographic data for [Cu^{II}(M2-T1)Br][Br].

Crystal Data	
Chemical formula	$C_{14}H_{28}Br_2CuN_4O$
M_r	491.76
Crystal system, space group	Monoclinic, $P2_1/c$
Temperature (K)	150 (2)
a, b, c (Å)	14.039 (3), 7.977 (2), 17.188 (3)
β (°)	99.14 (3)
V (Å^3)	1900.5 (7)
Z	4
Radiation type	Mo Kα
μ (mm^{-1})	5.360
Crystal size (mm)	0.45 x 0.26 x 0.15
Data Collection	
Diffractometer	Bruker Smart ApexIII
Absorption correction	Multi-scan, *SADABS* (Sheldrick, 2002)
No. of measured, independent and observed [$I > 2\sigma(I)$] reflections	23444, 6197, 4360
R_{int}	0.053
Refinement	
$R[F^2 > 2\sigma(F^2)]$, $wR(F^2)$, S	0.048, 0.154, 0.942
No. of reflections	6197
No. of parameters	211
H-atom treatment	H atoms treated by a mixture of independent and restrained confinement and refined using riding model
$\Delta\rho_{max}$, $\Delta\rho_{min}$ (e Å^{-3})	1.411, -1.714

Table A.2.2 Summary of crystallographic data for $[Cu^{II}(M1\text{-}T2)Br][Br]$.

Crystal Data	
Chemical formula	$C_{16}H_{22}Br_2CuN_4$
M_r	495.75
Crystal system, space group	Triclinic, P -1
Temperature (K)	150 (2)
a, b, c (Å)	9.1184 (4), 14.3804 (6), 14.8561 (7)
β (°)	88.9990 (10)
V (Å^3)	1930.36 (15)
Z	4
Radiation type	Mo Kα
μ (mm^{-1})	5.275
Crystal size (mm)	0.18 x 0.11 x 0.07
Data Collection	
Diffractometer	Bruker Smart ApexIII
Absorption correction	Multi-scan, *SADABS* (Sheldrick, 2002)
No. of measured, independent and observed [$I > 2\sigma(I)$] reflections	27334, 13810, 9691
R_{int}	0.032
Refinement	
$R[F^2 > 2\sigma(F^2)]$, $wR(F^2)$, S	0.072, 0.246, 1.532
No. of reflections	13810
No. of parameters	419
H-atom treatment	H atoms treated by a mixture of independent and restrained confinement and refined using riding model
$\Delta\rho_{max}$, $\Delta\rho_{min}$ (e Å^{-3})	12.103, -0.945

Table A.2.3 Summary of crystallographic data for Cu^{I}(M1-T2)Br.

Crystal Data	
Chemical formula	$C_{16}H_{22}BrCuN_4$
M_r	413.82
Crystal system, space group	Monoclinic, P21/n
Temperature (K)	149 (2)
a, b, c (Å)	10.8566 (8), 25.0396 (17), 12.6159 (8)
β (°)	90.652 (4)
V (Å^3)	3429.3 (4)
Z	8
Radiation type	Mo Kα
μ (mm^{-1})	3.606
Crystal size (mm)	1.687, 0.499, 0.448
Data Collection	
Diffractometer	Bruker Smart ApexIII
Absorption correction	Multi-scan, *SADABS* (Sheldrick, 2002)
No. of measured, independent and observed [$I > 2\sigma(I)$] reflections	31443, 5530, 4562
R_{int}	0.054
Refinement	
$R[F^2 > 2\sigma(F^2)]$, $wR(F^2)$, S	0.032, 0.113, 0.864
No. of reflections	5530
No. of parameters	401
H-atom treatment	H atoms treated by a mixture of independent and restrained confinement and refined using riding model
$\Delta\rho_{max}$, $\Delta\rho_{min}$ (e Å^{-3})	0.521, -0.524

Chapter 5 Appendix

Preliminary Data for the Removal of Heavy Metals From Aqueous Solutions Using Polymeric Adsorbents

A.5.1 Introduction

Anthropogenic heavy metal pollution is of major environmental concern due to the rapid development of various industries such as battery manufacturing, iron/steel, semi-conductor, metal plating, and textile.[1-4] The World Health Organization (WHO) lists lead, cadmium, and mercury as three of their top ten environmental pollutants of major public health concern due to their toxicity and prevalence in the environment.[5] The most effective way to prevent introduction of toxic heavy metals into the environment is to remove them from effluent industrial hazardous wastewater prior to its release. Adsorption is a facile methodology that has been utilized for this purpose and is advantageous over other protocols due to efficient heavy metal removal, potential for metal recovery, reusability, and metal selectivity.[2, 6-7] Various adsorbents exist such as activated carbon and polymers but the latter has been gaining attention in the scientific community due to fundamental advantages such as their adjustable surface chemistries and architectures, which provide increased adsorption capacities.[2, 8]

When employing synthetic polymers for remediation of wastewater containing heavy metals, conditions such as pH and contact time in addition to polymer composition and architecture e.g., molecular weight and chelator functionalities, affect adsorption capacities of polymeric adsorbents.[9-10]

A critical factor governing the adsorption of heavy metals is pH of the aqueous system. It has been reported that metal adsorption typically increases with pH until it plateaus and remains relatively unchanged.[11-14] Chelating functionalities typically consist of oxygen and nitrogen hence they can become protonated at low pH values i.e. acidic conditions. Not only does this protonation promote competition between protons and heavy metal cations for adsorption sites, it also leads to accumulation of positive charge and ultimately hinders adsorption capacity due to electronic repulsion.[15] Adsorption processes are not performed under basic conditions, pH > 8, since heavy metal ions will become hydrolyzed and precipitate.

The process of adsorption is similar to other types of chemical reactions in that a dynamic equilibrium is reached after a given amount of time.[16] When implementing the Langmuir isotherm model to determine maximum adsorption capacities, equilibrium adsorption capacities and equilibrium metal concentrations are needed. Therefore, it is critical to allow sufficient time for equilibrium to be reached. Similar to the relationship between adsorption capacity and pH, heavy metal adsorption will increase with contact time until a plateau is reached indicating equilibrium has been established.[17]

The selectivity of polymeric adsorbents is critical for successful wastewater remediation since various types of heavy metal ions are usually present. The identity of the chelating atoms is often associated with the preference to bind one metal species over another. Oxygen, nitrogen, or sulfur atoms are well-known metal chelators and are typically present in the functionalities of metal-adsorbing polymers. Their chelating capacity arises from Lewis base characteristics and the ability to donate a lone pair to Lewis acids, e.g., heavy metal ions.[10, 18-19] This idea is related to Pearson's hard soft acid

base theory (HSAB).[20-21] Therefore, soft bases will preferentially adsorb soft metals and hard bases prefer hard metals. Ceglowski and coworkers reported an adsorption capacity of 253 mg/g for Pb^{2+} using nitrogen and oxygen chelators,[12] whereas Bozbas and coworkers reported an adsorption capacity of 165 mg/g using oxygen-only based chelators.[13] This data is consistent with HSAB theory in terms of selectivity. Preliminary experiments were performed to investigate the efficiency of two hydrophilic polymers for the removal of Pb^{2+} from aqueous systems.

A.5.2 Materials

All materials were used as received unless otherwise noted. High molecular weight poly(2-hydroxyethyl methacrylate) (PHEMA) (M_v = 1,000,000) and Poly(acrylamide-*co*-acrylic acid) (poly(AAm-*co*-AAc) (M_n = 150,000 and M_w = 520,000) were purchased from Sigma Aldrich (St. Louis MO). Trace metal grade nitric acid was purchased from Fischer Scientific (Pittsburgh PA). Lead (II) nitrate was purchased from Acros Organics. Metal-free 50 mL centrifuge tubes were purchased from Globe Scientific.

A.5.3 Methods and Instrumentation

A.5.3.1 Lead Adsorption Experiments

A solution containing the polymer adsorbent (20 mg) and 20 mL of Pb^{2+} stock solution (20,000 ppb) was prepared in a 50 mL centrifuge tube using 18.2 MΩ deionized water and placed on a stir plate at 21.3 ^{o}C. After 3.75 hours aliquots were taken for inductively coupled plasma mass spectrometry (ICP-MS) analysis.

A.5.3.2 Quantitation of Pb^{2+} Removal Using Inductively Coupled Plasma Mass Spectrometry (ICP-MS)

Utilizing an Agilent 7700 Series ICP-MS (Agilent, Santa Clara CA), a calibration curve was prepared using a Pb^{2+} standard solutions (50 ppb, 200 ppb, 400 ppb, 800 ppb, and 1,000 ppb) w/1% HNO_3. Following adsorption experiments, samples were analyzed to determine Pb^{2+} concentrations. Samples were prepared by diluting 1 mL of the reaction mixture to 20 mL using 1% HNO_3 solution. The diluted solutions were then filtered using a 0.45 μm PTFE filter prior to analysis.

A.5.3.3 Determination of pH

The pH of solutions was measured using a Thermo Scientific Orion 2 Star benchtop pH meter (Thermo Fisher, Pittsburgh PA).

A.5.4 Preliminary Results and Discussion

A.5.4.1 Removal of Pb^{2+} From Aqueous Systems Using Polymeric Adsorbents

Preliminary experiments utilizing two hydrophilic polymers, PHEMA and poly(AAm-*co*-AAc) as adsorbents for the removal of Pb^{2+} from aqueous systems were performed. The polymers contain known metal chelators, oxygen and nitrogen shown if Figure A.5.1. These chelating species typically donate both electrons forming coordination bonds with heavy metals allowing for their removal from aqueous systems.

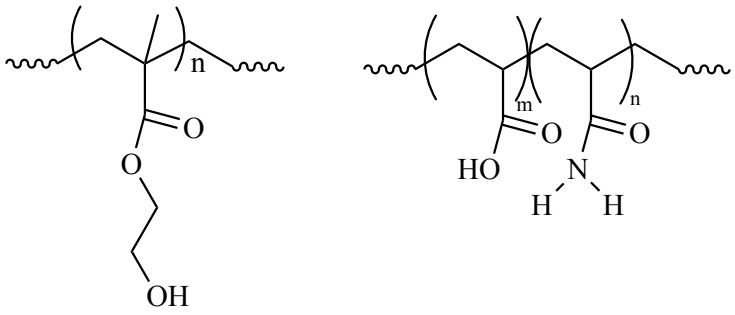

Figure A.5.1 Polymeric adsorbents used for the removal of Pb^{2+} from aqueous systems. PHEMA (left) and poly(AAm-*co*-AAc) (right).

The experimental setup is shown in Figure A.5.2 and consists of a Pb^{2+} solution to which the polymeric adsorbent was added. Following stirring of the reaction mixture for a predetermined amount of time, a 1 mL aliquot was removed, diluted to 20 mL, and filtered prior to ICP-MS analysis.

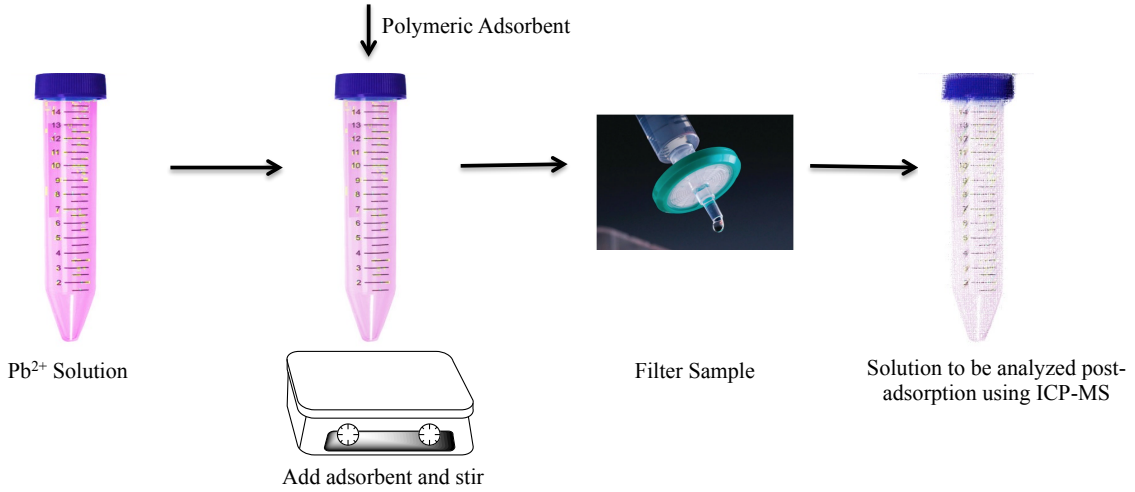

Figure A.5.2 Experimental setup for Pb^{2+} adsorption experiments.

The calibration curve and post-adsorption Pb^{2+} concentrations are shown in Figure A.5.3. This data was collected after a contact time of 3.75 hours at a pH = 2.1. As indicated in the figure, the polymeric adsorbents were effective for the removal of Pb^{2+}.

The $[Pb^{2+}]$ following adsorption was 4.3 +/- 17.9 ppb and 790.4 +/- 15.0 ppb for PHEMA and poly(AAm-*co*-AAc), respectively. The propagation of uncertainty associated with a calibration curve was calculated using the LINEST function in Excel providing the error associated with the aforementioned Pb^{2+} concentrations following adsorption. The relatively large standard deviation for PHEMA is due to the extrapolation of the $[Pb^{2+}]$ outside of the calibration curve.

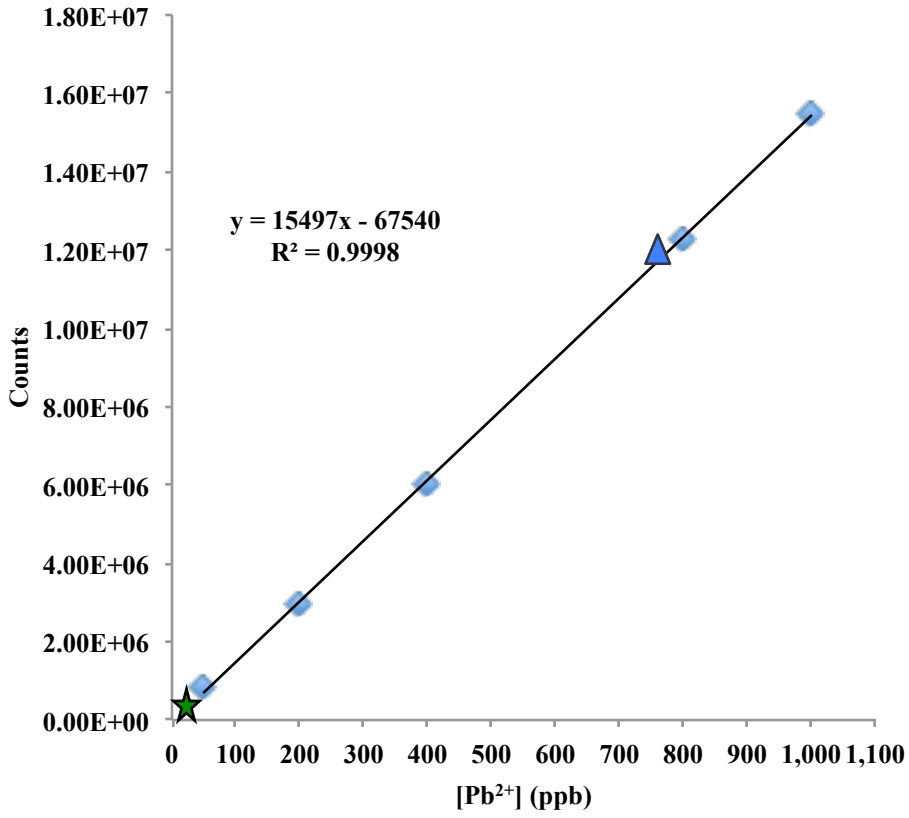

Figure A.5.3 Calibration curve and Pb^{2+} concentrations post-adsorption for PHEMA (star) and poly(AAm-*co*-AAc) (triangle).

To calculate the amount of Pb^{2+} adsorbed by the polymers (q_e), Equation A.5.1 was utilized where q_e = adsorption capacity in units of mg of Pb^{2+} adsorbed/g adsorbent,

C_o = initial $[Pb^{2+}]$, C_e = equilibrium $[Pb^{2+}]$, V = volume of solution, and m = mass of polymeric adsorbent.[22-23] A summary of values is shown in Table A.5.1. The adsorption capacities of PHEMA and poly(AAm-*co*-AAc) were calculated to be 19.91 mg/g and 3.99 mg/g, respectively.

(Eq. A.5.1) $$q_e = (C_o - C_e)\, V / m$$

	PHEMA	**Poly(AAm-*co*-AAc)**
m (g)	0.020	0.021
V (L)	0.020	0.020
C_o (mg/L)	20	20
C_e (mg/L)	0.087	15.81
q_e (mg/g)	19.91	3.99

Table A.5.1 Summary of adsorption data for PHEMA and poly(AAm-*co*-AAc) after a contact time of 3.75 hours at pH = 2.1.

A few key observations were made following the adsorption experiments. It was surprising that $[Pb^{2+}]$ was below 50 ppm following adsorption when using PHEMA. This concentration was comparable to that of the blank sample, which was determined to be 4.4 ppb. Additionally, from the ICP-MS data, both polymeric adsorbents were able to remove Pb^{2+} from the aqueous system even at an acidic pH of 2.1.

A.5.5 Summary and Conclusions

Preliminary data indicates that the two hydrophilic polymers, PHEMA and poly(AAm-*co*-AAc), can effectively remove Pb^{2+} from aqueous systems at low pH values. Adsorption capacities were calculated to be 19.91 mg/g and 3.99 mg/g for

PHEMA and poly(AAm-*co*-AAc), respectively. Additionally, the values reported in Figure 5.3 represent 21% Pb^{2+} removal utilizing poly(AAm-*co*-AAc) and 99% Pb^{2+} removal when using PHEMA adsorbent. These results were unexpected due to the fact that the adsorption experiments were performed at a low pH (pH = 2.1). Although the results were unexpected, they did indicate that these polymeric adsorbents possess the ability to remove Pb^{2+} from aqueous systems and have potential to be utilized for water remediation applications.

A.5.6 References

1. Tchounwou, P. B.; Yedjou, C. G.; Patlolla, A. K.; Sutton, D. J. Heavy Metal Toxicity and the Environment. In *Molecular, Clinical and Environmental Toxicology: Volume 3: Environmental Toxicology*, Luch, A., Ed.; Springer Basel: Basel, 2012, pp 133-164.

2. Tripathi A, R. M. Heavy Metal Removal from Wastewater Using Low Cost Adsorbents. *Journal of Bioremediation and Biodegredation* **2015,** *6* (6).

3. Fu, F.; Wang, Q. Removal of heavy metal ions from wastewaters: A review. *Journal of Environmental Management* **2011,** *92* (3), 407-418.

4. Bailey, S. E.; Olin, T. J.; Bricka, R. M.; Adrian, D. D. A review of potentially low-cost sorbents for heavy metals. *Water Research* **1999,** *33* (11), 2469-2479.

5. World Health Organization. http://www.who.int/ipcs/assessment/public_health/chemicals_phc/en/ (accessed 01/14/2017).

6. Cegłowski, M.; Schroeder, G. Removal of heavy metal ions with the use of chelating polymers obtained by grafting pyridine–pyrazole ligands onto polymethylhydrosiloxane. *Chemical Engineering Journal* **2015,** *259*, 885-893.

7. Kyzas, G. Z.; Siafaka, P. I.; Lambropoulou, D. A.; Lazaridis, N. K.; Bikiaris, D. N. Poly(itaconic acid)-Grafted Chitosan Adsorbents with Different Cross-Linking for Pb(II) and Cd(II) Uptake. *Langmuir* **2014,** *30* (1), 120-131.

8. Pan, B.; Pan, B.; Zhang, W.; Lv, L.; Zhang, Q.; Zheng, S. Development of polymeric and polymer-based hybrid adsorbents for pollutants removal from waters. *Chemical Engineering Journal* **2009,** *151* (1–3), 19-29.

9. Lee, J. B.; Schlautman, A. M. Effects of Polymer Molecular Weight on Adsorption and Flocculation in Aqueous Kaolinite Suspensions Dosed with Nonionic Polyacrylamides. *Water* **2015,** *7* (11).

10. Juang, R.-S.; Chen, M.-N. Measurement of Binding Constants of Poly(ethylenimine) with Metal Ions and Metal Chelates in Aqueous Media by Ultrafiltration. *Industrial & Engineering Chemistry Research* **1996,** *35* (6), 1935-1943.

11. Liu, P.; Jiang, L.; Zhu, L.; Wang, A. Attapulgite/Poly(acrylic acid) Nanocomposite (ATP/PAA) Hydrogels with Multifunctionalized Attapulgite (org-ATP) Nanorods as Unique Cross-linker: Preparation Optimization and Selective Adsorption of Pb(II) Ion. *ACS Sustainable Chemistry & Engineering* **2014,** *2* (4), 643-651.

12. Gierczyk, B.; Schroeder, G.; Cegłowski, M. New polymeric metal ion scavengers with polyamine podand moieties. *Reactive and Functional Polymers* **2011,** *71* (4), 463-479.

13. Bozbas, S. K. A., Umit; Kayan, Asgar. Novel Inorganic-Organic Hybrid Polymers to Remove Heavy Metals from Aqueous Solution. *Desalination and Water Treatment* **2013,** *51*, 7208-7215.

14. Zalloum, R. M.; Mubarak, M. S. Chelation properties of poly(2-hydroxy-4-acryloyloxybenzophenone) resins toward some divalent metal ions. *Journal of Applied Polymer Science* **2008,** *109* (5), 3180-3184.

15. Niu, Y.; Qu, R.; Sun, C.; Wang, C.; Chen, H.; Ji, C.; Zhang, Y.; Shao, X.; Bu, F. Adsorption of Pb(II) from aqueous solution by silica-gel supported hyperbranched polyamidoamine dendrimers. *Journal of Hazardous Materials* **2013,** *244–245*, 276-286.

16. Mittal, H.; Maity, A.; Sinha Ray, S. The Adsorption of Pb2+ and Cu2+ onto Gum Ghatti-Grafted Poly(acrylamide-co-acrylonitrile) Biodegradable Hydrogel: Isotherms and Kinetic Models. *The Journal of Physical Chemistry B* **2015,** *119* (5), 2026-2039.

17. Foo, K. Y.; Hameed, B. H. Insights into the modeling of adsorption isotherm systems. *Chemical Engineering Journal* **2010,** *156* (1), 2-10.

18. Zhu, Y.; Millan, E.; Sengupta, A. K. Toward separation of toxic metal(II) cations by chelating polymers: Some noteworthy observations. *Reactive Polymers* **1990,** *13* (3), 241-253.

19. Abd El-Ghaffar, M. A.; Mohamed, M. H.; Elwakeel, K. Z. Adsorption of silver(I) on synthetic chelating polymer derived from 3-amino-1,2,4-triazole-5-thiol and glutaraldehyde. *Chemical Engineering Journal* **2009,** *151* (1–3), 30-38.

20. Pearson, R. G. Hard and Soft Acids and Bases. *Journal of the American Chemical Society* **1963,** *85* (22), 3533-3539.

21. Rivas, B. L.; Maureira, A. Poly(2-acrylamido glycolic acid-co-acryloyl morpholine) and poly(2-acrylamido glycolic acid-co-acrylamide): Synthesis, characterization, and retention properties for environmentally impacting metal ions. *European Polymer Journal* **2008,** *44* (2), 523-533.

22. Gunathilake, C.; Kadanapitiye, M. S.; Dudarko, O.; Huang, S. D.; Jaroniec, M. Adsorption of Lead Ions from Aqueous Phase on Mesoporous Silica with P-Containing Pendant Groups. *ACS Applied Materials & Interfaces* **2015,** *7* (41), 23144-23152.

23. Naseem, K.; Begum, R.; Wu, W.; Usman, M.; Irfan, A.; Al-Sehemi, A. G.; Farooqi, Z. H. Adsorptive removal of heavy metal ions using polystyrene-poly(N-isopropylmethacrylamide-acrylic acid) core/shell gel particles: Adsorption isotherms and kinetic study. *Journal of Molecular Liquids* **2019,** *277*, 522-531.